

**FACIES DISTRIBUTION, FLUVIAL ARCHITECTURE,
PROVENANCE, DIAGENESIS, AND RESERVOIR QUALITY OF
SYNRIFT SUCCESSIONS FROM THE BREAKUP OF PANGEA:
EXAMPLES FROM THE FUNDY BASIN AND ORPHEUS GRABEN**

by

Darragh O'Connor

Submitted in partial fulfillment of the requirements
for the degree of Master of Science

at

Dalhousie University
Halifax, Nova Scotia
August 2016

© Copyright by Darragh O'Connor, 2016

Table of Contents

List of Figures	iv
List of Tables	vii
Abstract	viii
Acknowledgements.....	ix
Chapter 1: Introduction	1
1.1 Thesis Format	9
1.2 Field Mapping and Core Sampling	9
1.2.1 Field Mapping and Sampling.....	9
1.2.2 Core Sampling	13
1.3 Geologic Overview	14
1.3.1 Regional Geologic Setting	15
1.3.1.1 Tectonics and Stratigraphy of the Scotian Basin.....	20
1.3.1.2 Tectonics and Stratigraphy of the Fundy Basin.....	25
1.4 Aeolian Strata at Red Head	28
Chapter 2: Facies and sedimentary architecture of Mesozoic synrift infill – examples from the Fundy Basin and the Orpheus Graben.....	29
2.1 Introduction	29
2.1.1 Study Area and Location	29
2.2 Methods and Data	31
2.2.1 Measured Stratigraphic Sections	31
2.2.2 Measured Core.....	32
2.2.3 Photographs and Panoramic Photopans with Schematic Diagrams.....	32
2.3 Facies and Facies Associations of the Wolfville, Chedabucto, and Eurydice formations	35
2.3.1 Facies and Facies Associations – Definition and Use	35
2.3.2 The Wolfville Formation.....	38
2.3.3 The Chedabucto Formation	45
2.3.4 The Eurydice Formation	51
2.3.5 Summary	54
2.4 Fluvial Architecture and Paleoflow of the Wolfville and Chedabucto Formations.....	59
2.4.1 Architectural elements – Definition and Use.....	59
2.4.2 Wolfville Formation	60
2.4.2.1 Overview	60
2.4.2.2 Architectural Elements.....	62
2.4.2.3 Paleocurrents	63
2.4.3 Chedabucto Formation	68
2.4.3.1 Overview	68
2.4.3.2 Architectural Elements.....	68
2.4.3.3 Paleocurrents	70
2.4.3.4 Palynology	70
2.4.4 Summary	74
2.5 Paleoenvironments.....	76
2.6 Basin Configuration and the Broad Terrane Hypothesis.....	86
2.7 Conclusions	92

Chapter 3: Provenance, diagenesis, and reservoir quality from early Mesozoic synrift infill – examples from the Fundy Basin and Orpheus Graben, Nova Scotia	94
3.1 Introduction	94
3.1.1 Study Area and Location	95
3.2 Methods and Data	100
3.2.1 Sample Collection.....	100
3.2.2 X-Ray Fluorescence	100
3.2.3 Microscopy.....	103
3.2.4 Handheld Permeameter Measurements	104
3.2.5 Handheld Gamma-Ray Spectrometer Measurements.....	107
3.3 Results: X-Ray Fluorescence, Petrography, and Permeability-Porosity Characteristics.....	110
3.3.1 X-Ray Fluorescence	110
3.3.2 Petrography.....	114
3.3.3 Permeability, Porosity, and Gamma Ray Signature	124
3.4 Discussion: Petrography, X-Ray Fluorescence, and Permeability-Porosity Characteristics.....	126
3.4.1 Sandstone Classification, Tectonic Setting, and Sandstone Provenance.....	126
3.4.2 Diagenesis	137
3.4.3 Reservoir Quality.....	139
3.5 Conclusions	143
Chapter 4: Conclusions and Summary.....	146
4.1 Conclusions and Summary	146
4.2 Facies and Architectural Elements.....	146
4.2.1 Lithology.....	146
4.2.2 Facies.....	146
4.2.3 Architectural Elements.....	147
4.3 Provenance, Diagenesis, and Reservoir Quality.....	148
4.3.1 Provenance	148
4.3.2 Reservoir Quality.....	149
4.3.3 Paleocurrents and Basin Analysis.....	150
References	151
Appendix A	157
Appendix B	188
Appendix C	190
Appendix D.....	195

List of Figures

Figure 1.1: Generalized lithostratigraphic chart of the Scotian and Fundy basins	3
Figure 1.2: Satellite map view of Nova Scotia showing the four general locations of study for this project	4
Figure 1.3: A geologic map of the early Mesozoic synrift successions found along the margins of the Minas Basin, NS	5
Figure 1.4: A geologic map of the early Mesozoic synrift successions found along the margins of Chedabucto Bay, NS.....	6
Figure 1.5: (A) Map view of Rainy Cove within the Minas Basin, Nova Scotia	10
Figure 1.6: Satellite location map and field view of the aeolian successions at Red Head, Five Islands Provincial Park.....	11
Figure 1.7: Map location and field view of the Chedabucto Formation at McCaul Island, NS	12
Figure 1.8: Core collected from the Eurydice P-36 well.....	14
Figure 1.9: A paleogeographic map of North America during the Early Triassic (245 Ma)	17
Figure 1.10: A paleogeographic map of North America during the Late Triassic (210 Ma).....	18
Figure 1.11: Major Paleozoic contractional structures, early Mesozoic rift basins (red) of eastern North America, and key tectonic features of the eastern North Atlantic Ocean	19
Figure 2.1: A detailed sedimentary composite-log of the Late Triassic Wolfville Formation section at Rainy Cove, Nova Scotia.	43
Figure 2.2: Representative facies from the Wolfville Formation.....	44
Figure 2.3: A detailed sedimentary log of the Late Triassic Chedabucto Formation section near McCaul Island, Nova Scotia	49
Figure 2.4: Representative facies from the Chedabucto Formation	50
Figure 2.5: A detailed sedimentary log of the Eurydice P-36 core from the offshore Orpheus Graben, Nova Scotia.....	55
Figure 2.6: Representative photographs from facies 10	56
Figure 2.7: Representative photographs from facies 11	57
Figure 2.8: Representative photographs from facies 12	58
Figure 2.9: Map location and field view of the studied Wolfville Formation at Rainy Cove	61
Figure 2.10: Five measured sections from the Wolfville Formation at Rainy Cove	64
Figure 2.11: Field view of the Wolfville Formation at Rainy Cove with sketch showing the facies distribution and architectural elements present within the outcrop.....	65
Figure 2.12: Field view of the Wolfville Formation at Rainy Cove sketch showing the facies distribution and architectural elements present within the outcrop.....	66

Figure 2.13: Examples of architectural elements and associated facies from the Wolfville Formation at Rainy Cove.....	67
Figure 2.14: Map view of McCaul Island the location of the Chedabucto Formation type section.....	70
Figure 2.15: Field view, facies distribution, and architectural elements of the Chedabucto Formation at McCaul Island.....	71
Figure 2.16: Field view, facies distribution, and architectural elements of the Chedabucto Formation at McCaul Island.....	72
Figure 2.17: Field view, facies distribution, and architectural elements of the Chedabucto Formation at McCaul Island.....	73
Figure 2.18: Coastal process classification ternary plot.....	83
Figure 2.19: Representative schematic depositional model of the Eurydice Formation	84
Figure 2.20: Accommodation/sediment supply (A/S) ratio and thickness/sand-to-shale ratio	85
Figure 2.21: Decision tree for prediction of depositional process dominance for clastic coastal systems of the Eurydice Formation	85
Figure 2.22: Field view image from Rainy Cove highlighting the rift onset unconformity	90
Figure 2.23: Geologic map of the Minas Basin showing paleocurrent indicator data gathered from the Minas Basin (left)	91
Figure 3.1: Field view of the studied Triassic Wolfville Formation at Rainy Cove showing the angular unconformity (rift onset unconformity) with the truncated Carboniferous Horton Bluff Formation	96
Figure 3.2: Field view of the studied Wolfville Formation aeolian successions at Red Head in Five Islands Provincial Park	97
Figure 3.3: Field view of the Chedabucto Formation at McCaul Island showing cyclic stacked channels	98
Figure 3.4: View of Eurydice Formation core from the Eurydice P-36 well.....	99
Figure 3.5: Niton™ XL3t 950 X-Ray Fluorescence (XRF) Analyzer	103
Figure 3.6: Photograph of the Olympus BX51 microscope, Basin and Reservoir Laboratory at Dalhousie University.	104
Figure 3.7: Photograph of the TinyPerm II and its associated parts.....	106
Figure 3.8: Permeability calibration chart, from NER, used to correlate TinyPerm II values to permeability values.....	107
Figure 3.9: Photograph of the Exploranium GR-130 miniSPEC scintillometer.....	108
Figure 3.10: Photograph of the GEORADiS GT-40 Multipurpose Gamma Center and associated parts	109
Figure 3.11: Photomicrographs showing the composition, textures, and porosity	115

Figure 3.12: QtFL classification of Folk (1968) for the Wolfville and Chedabucto formations	128
Figure 3.13: Distribution (relative) of detrital grains in the Wolfville and Chedabucto formations.....	129
Figure 3.14: Sandstone chemical classification for the Wolfville and Chedabucto formations plotted on the SandClass scheme of Herron (1988)	130
Figure 3.15: Distribution of major framework groups for the Wolfville and Chedabucto formations plotted on provenance indicator ternary diagrams	133
Figure 3.16: Major element composition plots of sands from the Wolfville and Chedabucto formations.....	136
Figure 3.17: Thin section microphotographs highlighting porosity from each of the study areas.....	141
Figure 3.18: Permeability versus porosity of samples collected from the Chedabucto Formation (McCaul Island) and the Wolfville Formation (Red Head and Rainy Cove).....	142

List of Tables

Table 1.1: Summary of data collected for this work.....	7
Table 2.1: Lithofacies classification (modified from Miall, 1985)	33
Table 2.2: Architectural elements in fluvial and abandoned channel and overbank deposits (modified from Miall, 2016).....	34
Table 2.3: Summary of facies and facies associations from the Wolfville, Chedabucto, and Eurydice formations.....	37
Table 3.1: Major elemental composition of aeolian sands and sandstones of the Chedabucto Formation at McCaul Island, Chedabucto Bay.....	111
Table 3.2: Major elemental composition of aeolian sands and sandstones of the Wolfville Formation at Five Islands Provincial Park, Nova Scotia.	111
Table 3.3: Major elemental composition of alluvial and fluvial sands and sandstones of the Wolfville Formation at Rainy Cove, Nova Scotia.....	112
Table 3.4: Average major element composition of Mesozoic synrift sandstones of the Wolfville and Chedabucto formations from the Fundy Basin and Orpheus Graben, Nova Scotia.	112
Table 3.5: Known values and XRF analyses of known standard Till-4. The mean, standard deviation, % error, and correction factor for each major oxide examined is shown in the right four columns.....	113
Table 3.6: Statistics of point-counting results of the Chedabucto Formation	120
Table 3.7 Statistics of point-counting results of the aeolian Wolfville Formation	121
Table 3.8: Statistics of point-counting results of the fluvial Wolfville Formation	122
Table 3.9: Summary statistics of point-counting	123
Table 3.10: Summary of TinyPerm, permeability values, and gamma ray scintillometer values	125
Table 4.1: Summary table of interpreted facies, architectural elements, and paleoenvironments.....	148
Table 4.2: Summary table of the sandstone classification, tectonic framework, tectonic setting, diagenesis, and reservoir quality	150

Abstract

This study investigates the sedimentology, provenance, diagenesis, and reservoir characteristics of Late Triassic synrift successions from the Wolfville and Chedabucto formations along the margins of the Minas Basin and Chedabucto Bay and the Eurydice Formation in offshore subsurface regions of the Orpheus Graben. The strata were examined in outcrop and with thin section petrography, X-ray fluorescence, and handheld permeability and gamma ray (radioactivity) tools.

Outcrop examination revealed different stages of rifting and fluvial sedimentation deposited in successions at Rainy Cove (early stage rifting) and McCaul Island (early to middle stage rifting). Synrift successions from the Eurydice P-36 well in the Orpheus Graben revealed finer grained successions with evidence suggesting sedimentation occurred within an estuarine environment during the late stages of rifting.

X-ray fluorescence revealed that the fluvial Wolfville Formation (Rainy Cove) samples plot in the 'wacke', 'litharenite', and 'Fe-sand' field, the aeolian Wolfville Formation (Red Head) samples predominantly plot in the 'sublitharenite' field, and the Chedabucto Formation plots predominantly in the 'sublitharenite' and 'litharenite' fields. Major element composition plots of sands discriminate between passive margin, active continental margin, continental arc, and oceanic arc tectonic setting. Points from the fluvial Wolfville Formation are generally spread within or near the active continental margin field. Whereas the aeolian Wolfville Formation generally plot in or near the passive margin field. Points from the Chedabucto Formation are spread but generally can be found in the passive margin to active continental margin fields.

Point count analyses show that the aeolian and fluvial successions from the Wolfville and Chedabucto formations all plot within the recycled orogen fields of the provenance indicator ternary diagrams. QtFL classification after Folk (1968) reveals that the fluvial Wolfville Formation plots in the 'litharenite' to 'feldspathic litharenite' fields, the aeolian successions plot in the 'sublitharenite' field, and the Chedabucto Formation plots in the "sublithic arenite" to 'litharenite' fields.

Thin section microphotographs show porosity and reservoir quality for samples from each of the study areas. The Eurydice Formation is dominated by silt sized grains, contains some large lithic clasts and sand grains, and shows very poor porosity. Within the Chedabucto Formation, sand dominated beds show very-fine to coarse grain size, are moderately sorted, and can be well cemented with no porosity to highly porous with no indication of cementation. The fluvial Wolfville Formation comprises coarse grained, subangular to angular sands that are typically well cemented in a calcite cement. Secondary porosity is from alteration of feldspar grains in the fluvial Wolfville Formation. The aeolian Wolfville Formation comprises very fine to very coarse grained sands, that are subangular to subrounded and show high porosity with sparse calcite and iron oxide cementation.

Acknowledgements

I would like to thank my supervisor, Grant Wach, and thesis committee members, Marcos Zentilli and David E. Brown, for their patience, guidance, and encouragement during all steps taken during the span of this thesis. I often found myself chasing ideas and reading reports that led me away from my final goals, but each of you pointed me in the direction of the finish line.

Grant – your talent while working in the field fares second to none. I hope to take this work ethic into all future projects I undertake.

Marcos – your knowledge on all geologic subject matter seems endless. However, it was your inquisitiveness that made me realize that I wasn't asking that right questions from my data.

David – your “big picture” thoughts and conversations always helped me gain traction after I had fallen off course. I must always remember think in broad strokes, especially when dealing with detailed work.

I would also thank past and present members of the Basin and Reservoir Laboratory. Your help was invaluable during field work and thesis preparation.

Lastly, I would like to thank the Nancy White, Mary Jean Verall, and the entire staff from the CNSOPB's Geoscience Research Centre.

Chapter 1: Introduction

Middle to Late Triassic (Anisian to Norian) sediments from the Fundy Basin and Orpheus Graben (Nova Scotia) (Figure 1.1) reveal synrift successions comprising alluvial-fan, braid-fluvial, aeolian, lacustrine, and estuarine type deposits. Previous studies of the Wolfville, Chedabucto and Eurydice formations have examined their sedimentology and paleoenvironments, e.g. Klein (1960, 1962), Hubert and Mertz (1980, 1984), Tanner and Brown (1999, 2003), and Leleu et al. (2009, 2010) and have shown that the two basins are structurally linked through the Minas Fault Zone (Keppie, 1982; Tanner and Brown 2003; Murphy et al., 2011). However, no continuous outcrop exists between the two basins and an integrated analysis of the synrift successions from each basin remains incomplete. With recent global recognition of synrift (pre-salt) rocks as having huge potential for oil and gas plays (Santos and Campos basins of Brazil), and with scarce outcrop and few offshore well penetrations, the synrift exposures in the Minas Basin and Orpheus Graben offer a window into the sedimentological and stratigraphic characteristics of equivalent offshore subsurface successions in the underexplored Scotian margin (Figure 1.2).

The Fundy Basin is a tripartite basin located on the western margin of Nova Scotia containing three structurally linked rift basins known as the Fundy, Chignecto, and Minas subbasins (Wade et al., 1996). The Orpheus Graben is a rift basin which formed along the eastern margin of Nova Scotia, just south of Cape Breton Island. The northern flanks of both basins contain their respective border faults, which are an individual faults belonging to a larger fault complex known as the Minas Fault Zone (MFZ). In addition to being structurally related, the basins comprise similar synrift sedimentary units (Figure 1.2) (Wade et al., 1996).

This study examines the sedimentology and reservoir characteristics (provenance, diagenesis, and porosity and permeability) of these three formations to provide new insight into

their stratigraphy, stratigraphic relationships, paleoenvironments, and hydrocarbon reservoir potential. The rocks are exposed in cliff faces in the Minas Basin (Figure 1.3) (Rainy Cove and Red Head, Minas Basin), and Orpheus Graben (Figure 1.4) (McCaul Island, Chedabucto Bay), as well as conventional core and cuttings from the Eurydice P-36 offshore well Orpheus Graben. Methods and collected data for the present work have been summarized in Table 1.1.

As noted above, synrift successions along the margins and offshore regions of Nova Scotia have been studied for decades, but questions pertaining to their local and regional development, and their reservoir quality and role as potential reservoir analogues, remain open for discussion. This research contributes to a better understanding of the sedimentological evolution and reservoir characteristics of the synrift units from the Minas Basin and Orpheus Graben, Nova Scotia. The objectives of this research are as follows:

- To develop a local and regional understanding of the distribution of depositional facies and architectural elements of marginal sedimentary successions of active rift basins.
- To better understand the sedimentological evolution and active paleoenvironments during early (Rainy Cove), middle (McCaul Island) and late (Eurydice P-36) active rifting.
- To test the validity of the broad terrane hypothesis of Russell (1880) i.e. once larger sedimentary basins are now smaller remnants due to upheaval and erosion of connecting successions.
- To quantify the reservoir characteristics (provenance, permeability, and porosity) of the variable stages of synrift sedimentation.

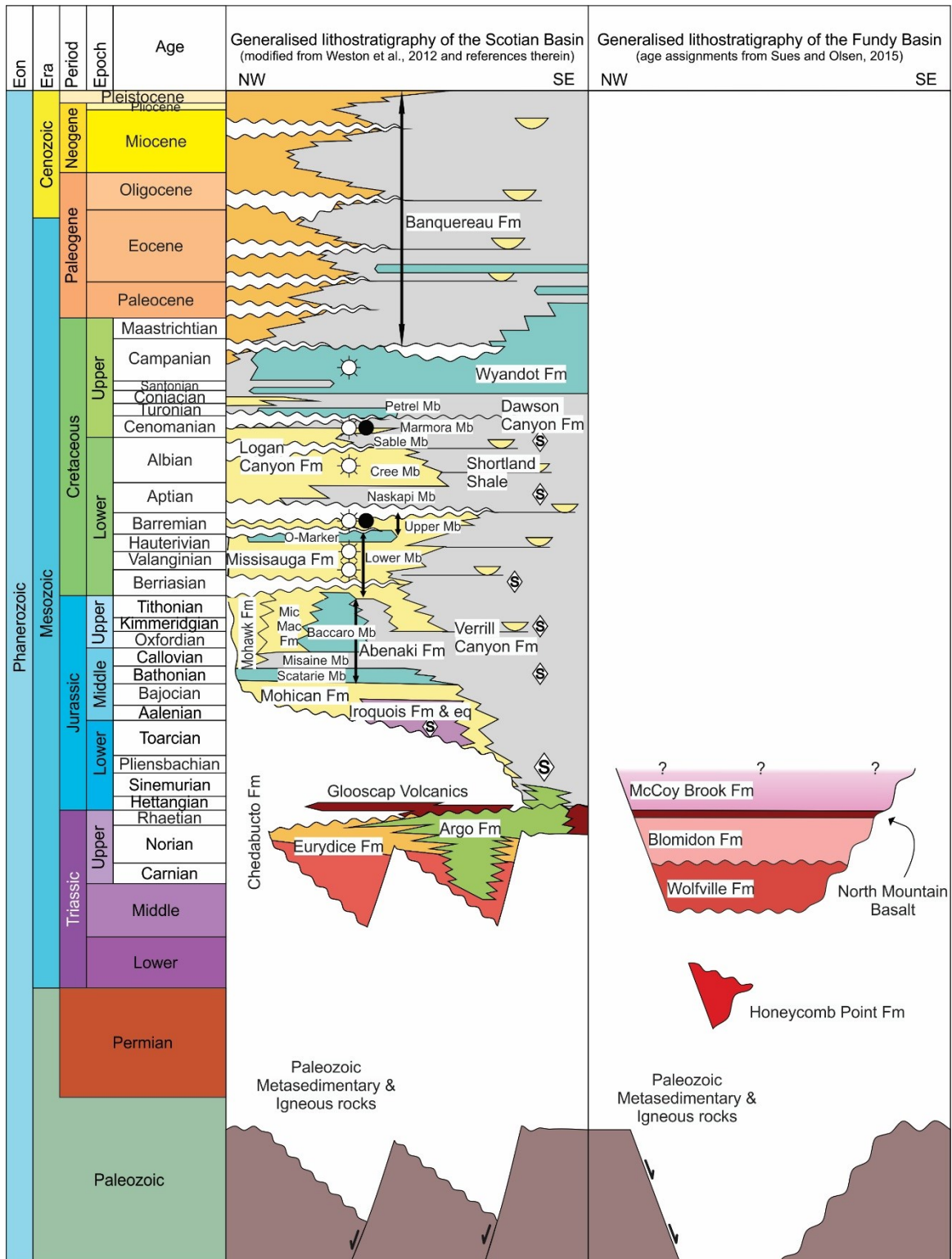


Figure 1.1: Generalized lithostratigraphic chart of the Scotian and Fundy basins (modified from Weston et al., 2012)

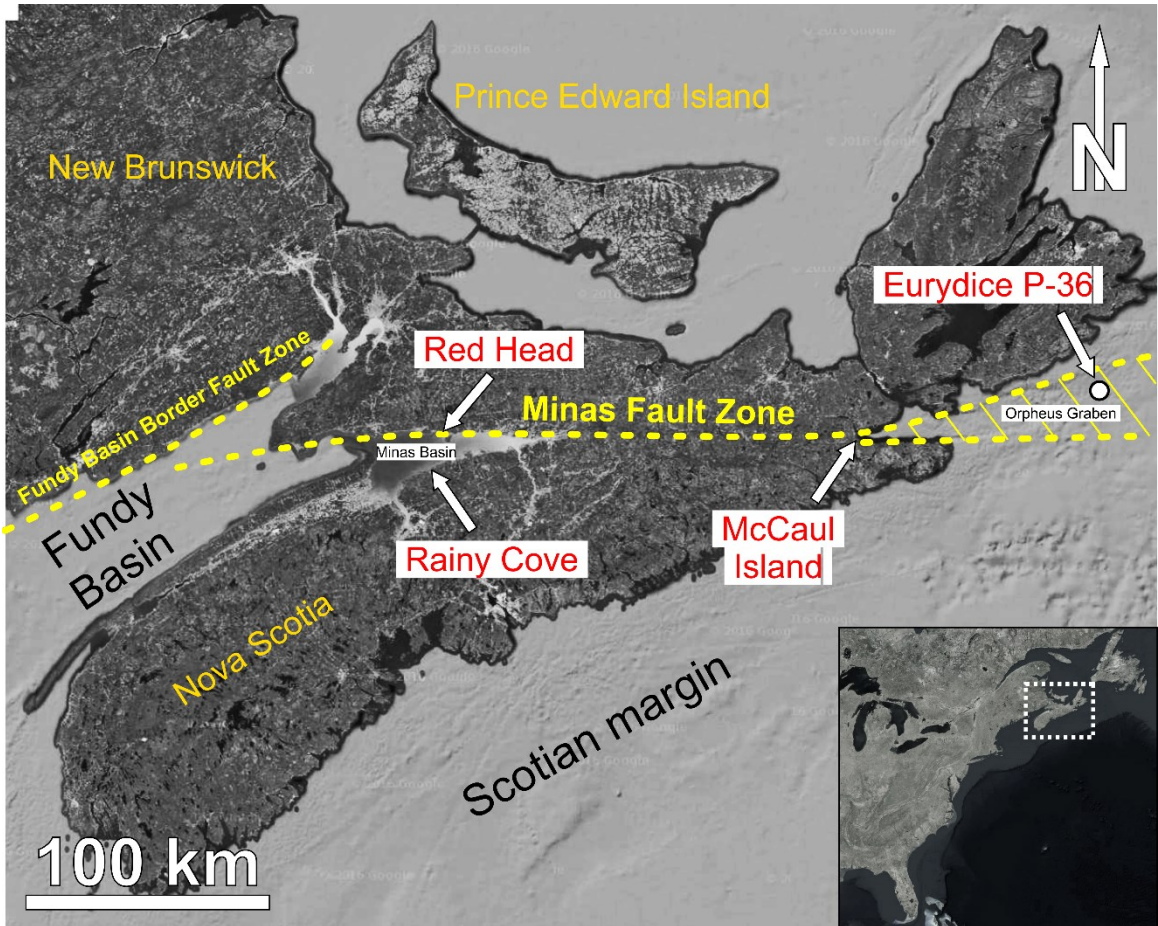


Figure 1.2: Satellite map view of Nova Scotia showing the four general locations of study for this project (Red Head, Rainy Cove, McCaul Island, and the offshore Eurydice P-36 well). All four locations are along strike and are structurally related to the Minas Fault Zone (yellow dashed line in central part of figure). Red Head and Rainy Cove are located in the Minas Basin (west flank) while McCaul Island and Eurydice P-36 well are location in the Orpheus Graben (east flank).

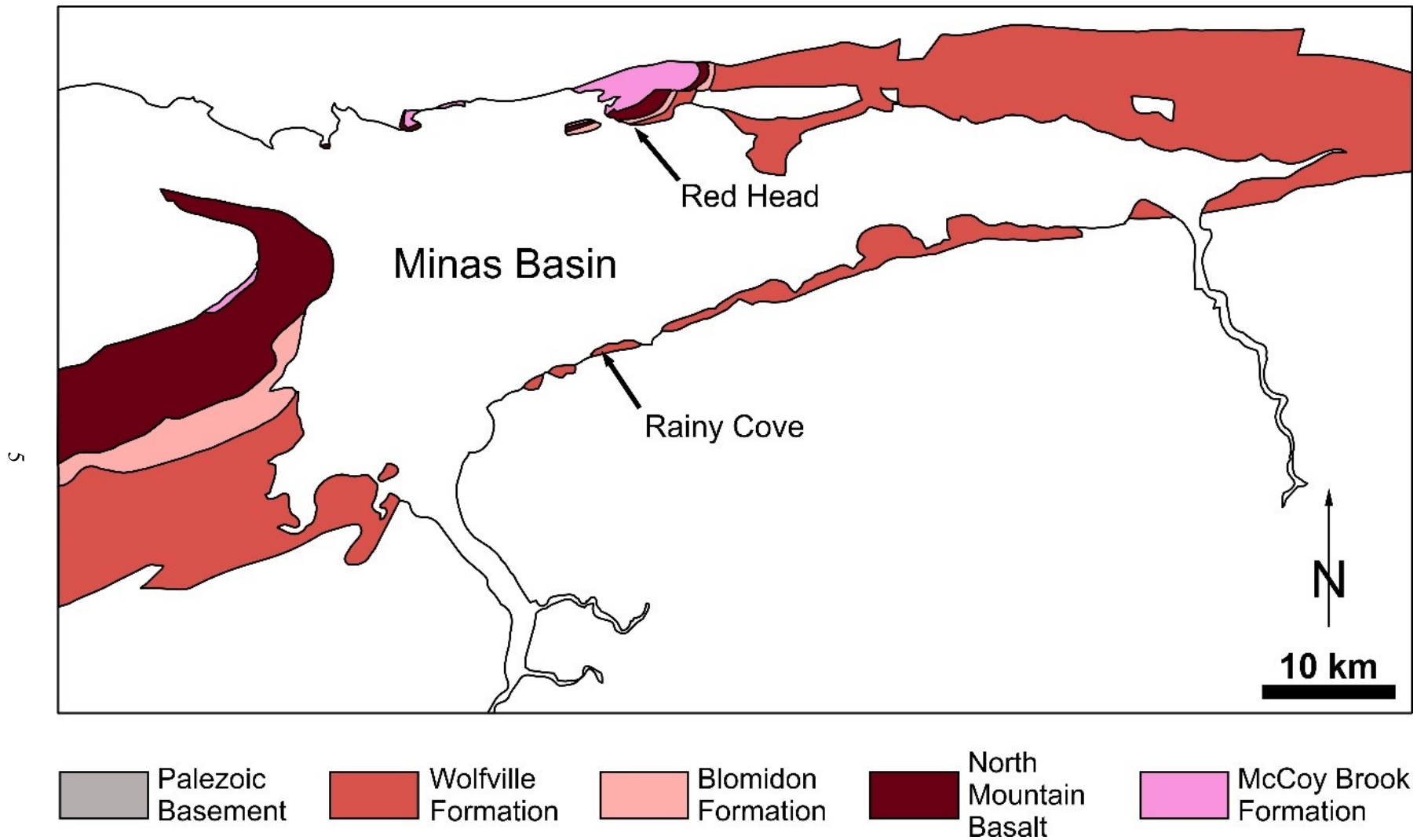


Figure 1.3: A geologic map of the early Mesozoic synrift successions found along the margins of the Minas Basin, NS. The areas of study are shown highlighted by their name and a black arrow.

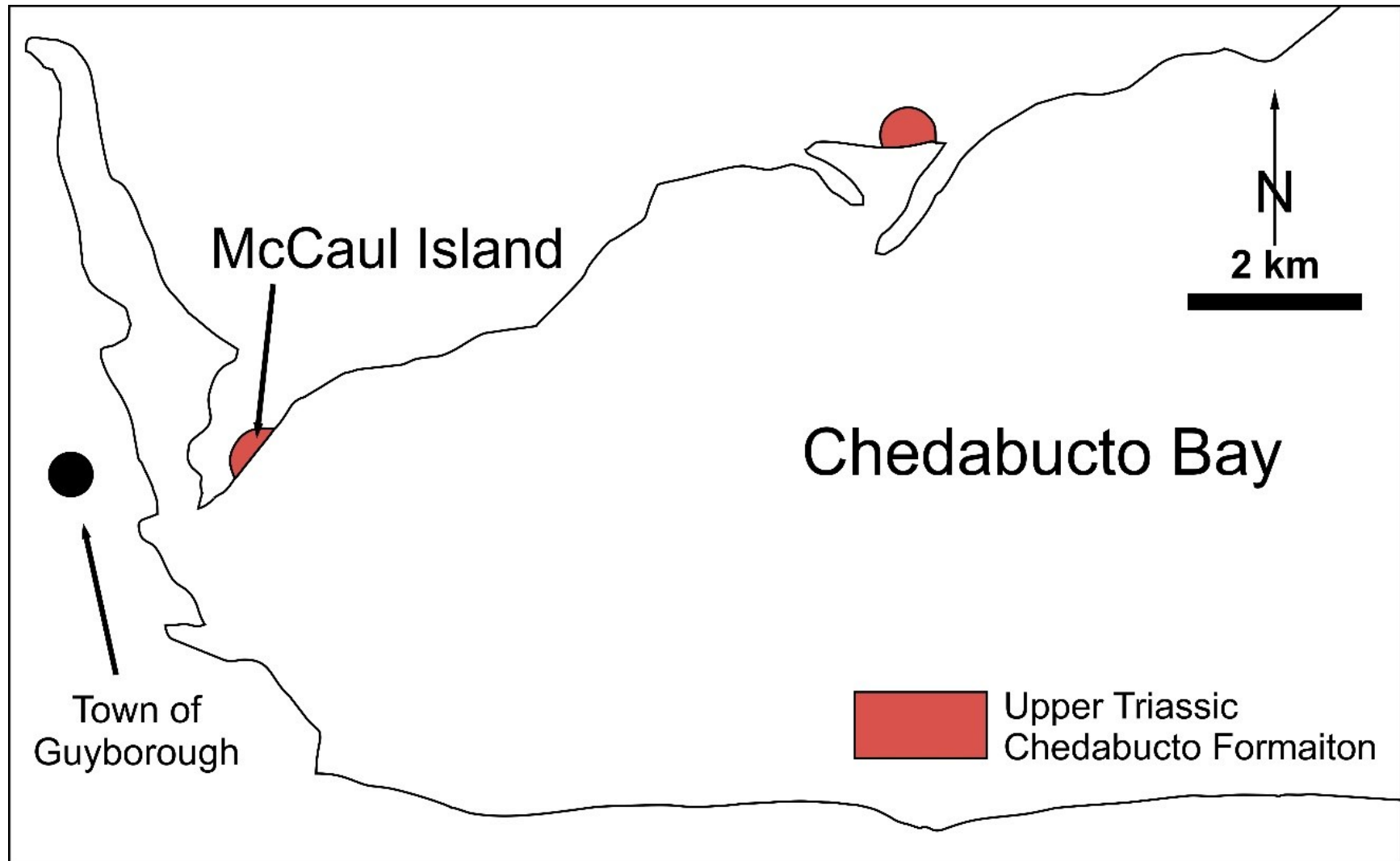


Figure 1.4: A geologic map of the early Mesozoic synrift successions found along the margins of Chedabucto Bay, NS. The area of study is shown highlighted by its name and a black arrow

Table 1.1: Summary of data collected for this work.

Formation	Sample Name	Figure I.D. Number	Field View and Location	Measured Section/Core	Thin Section Point Count	XRF Analysis	TinyPerm Analysis	Scintillometer Analysis
Eurydice Formation (Eurydice P-36, Orpheus Graben)	Multiple analyses from Eurydice P-36 core (CNSOPB)	-	Figure 1.2	Figure 2.5	-		Table 3.10	Table 3.10
		-			-			
		-			-			
		-			-			
		-			-			
Chedabucto (McCaul Island, Orpheus Graben)	GW-301-2012	1	Figure 1.7	Figure 2.3	Table 3.6	Table 3.1	Table 3.10	Table 3.10
	GW-302-2012	2						
	GW-303-2012	3						
	GW-304-2012	4						
	GW-305-2012	5						
	GW-306-2012	6						
	GW-307-2012	7						
	GW-308-2012	8						
GW-309-2012	9							
Wolfville Formation (Top) (Red Head, Minas Basin)	RHP-Base	1	Figure 1.6	-	Table 3.7	Table 3.2	Table 3.10	Table 3.10
	RHP-1	2						
	RHP-2	3						
	RHP-3	4						
	RHP-4	5						
	RHP-5	6						
	RHP-7	7						
	RHP-8	8						

**Wolville
Formation**
(Rainy Cove,
Minas Basin)

GW-02-RC	1
GW-03-RC	2
GW-06-RC	3
GW-08-RC	4
GW-04-RC	5
GW-07-RC	6
GW-05-RC	7
GW-09-RC	8
01-GW-RC-2015	9
02-GW-RC-2015	10
03-GW-RC-2015	11
04-GW-RC-2015	12
05-GW-RC-2015	13
06-GW-RC-2015	14
07-GW-RC-2015	15
RC-DO-2014	16

Figure 1.5

Figure 2.1

Table 3.8

Table 3.3

Table 3.10

Table 3.10

1.1 Thesis Format

This thesis consists of the integration of two projects, related through their study of early Mesozoic synrift successions from the Fundy Basin and the Orpheus Graben, Nova Scotia. Each produces new contributions to the understanding of regional synrift paleoenvironments and reservoir characteristics, and are an examination at two scales; (1) the basin scale examining facies and architecture of fluvial and estuarine deposits in outcrop and core and (2) the grain scale, examining reservoir characteristics (porosity and permeability) and provenance of collected samples from outcrop and core. Both projects use well known sedimentological and geochemical techniques and integrate regional data into a single document.

1.2 Field Mapping and Core Sampling

This section covers the specific areas chosen for field mapping and sampling, and core sampling for this work. See Appendix A for summary descriptions of each of the collected samples and thin sections.

1.2.1 Field Mapping and Sampling

Field mapping and rock sampling was completed on synrift cliff exposures in the Minas Basin areas of Rainy Cove (Figure 1.5) and Red Head (Figure 1.6) and along the western margin of Chedabucto Bay near McCaul Island (Figure 1.7). Measured sections and facies analysis were completed for the Rainy Cove and McCaul Island locations while rock samples were collected from all three locations.

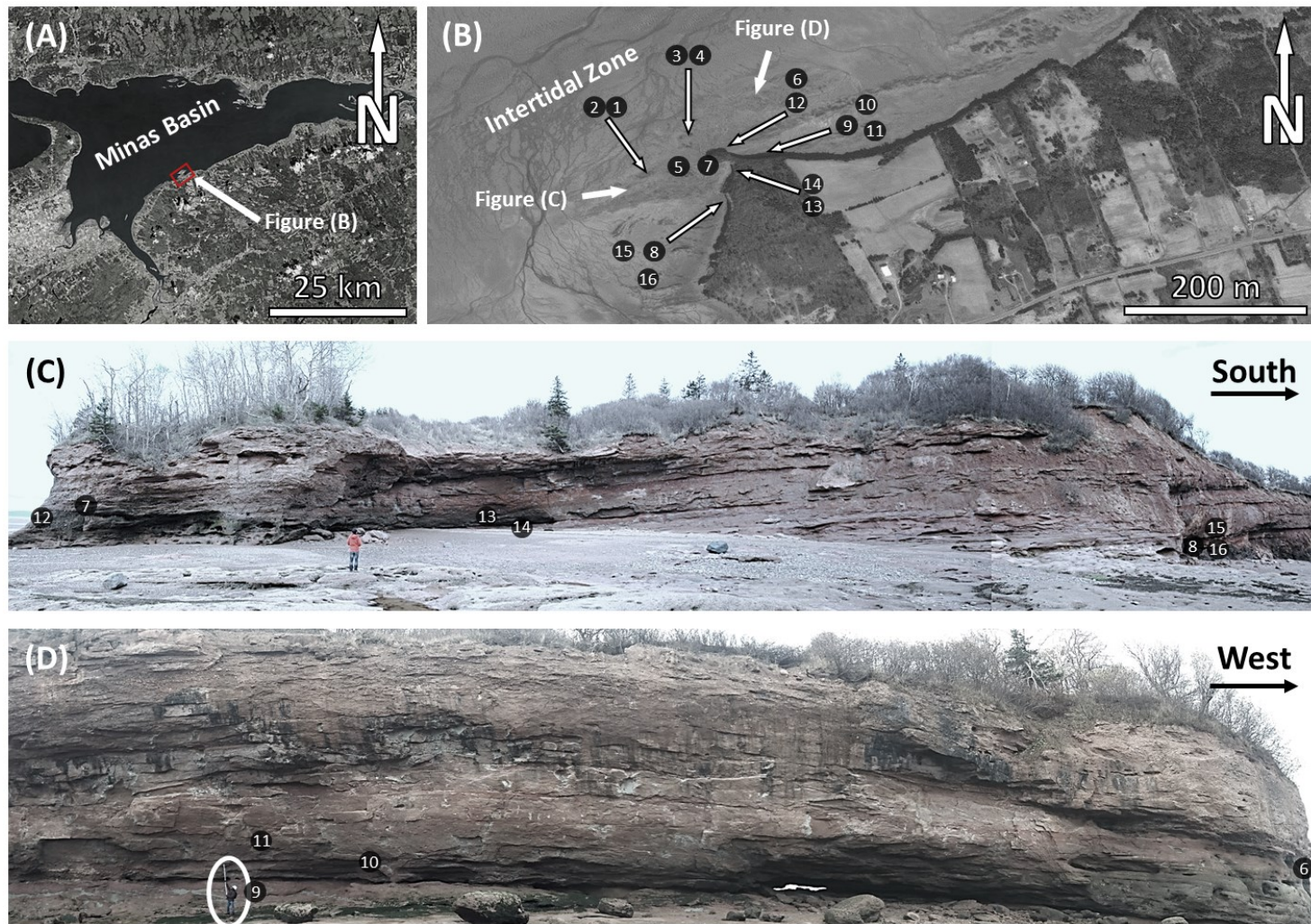


Figure 1.5: (A) Map view of Rainy Cove within the Minas Basin, Nova Scotia. (B) Satellite map view of the study area at Rainy Cove. Arrows show the location and orientation of photographs of field view images. (C & D) Field view of the studied Wolfville Formation at Rainy Cove and site of the samples taken for analysis. (C) Southwestern side of the promontory (D) Northeastern side of the promontory. Noted the circled geologist (1.7 m height) for scale.

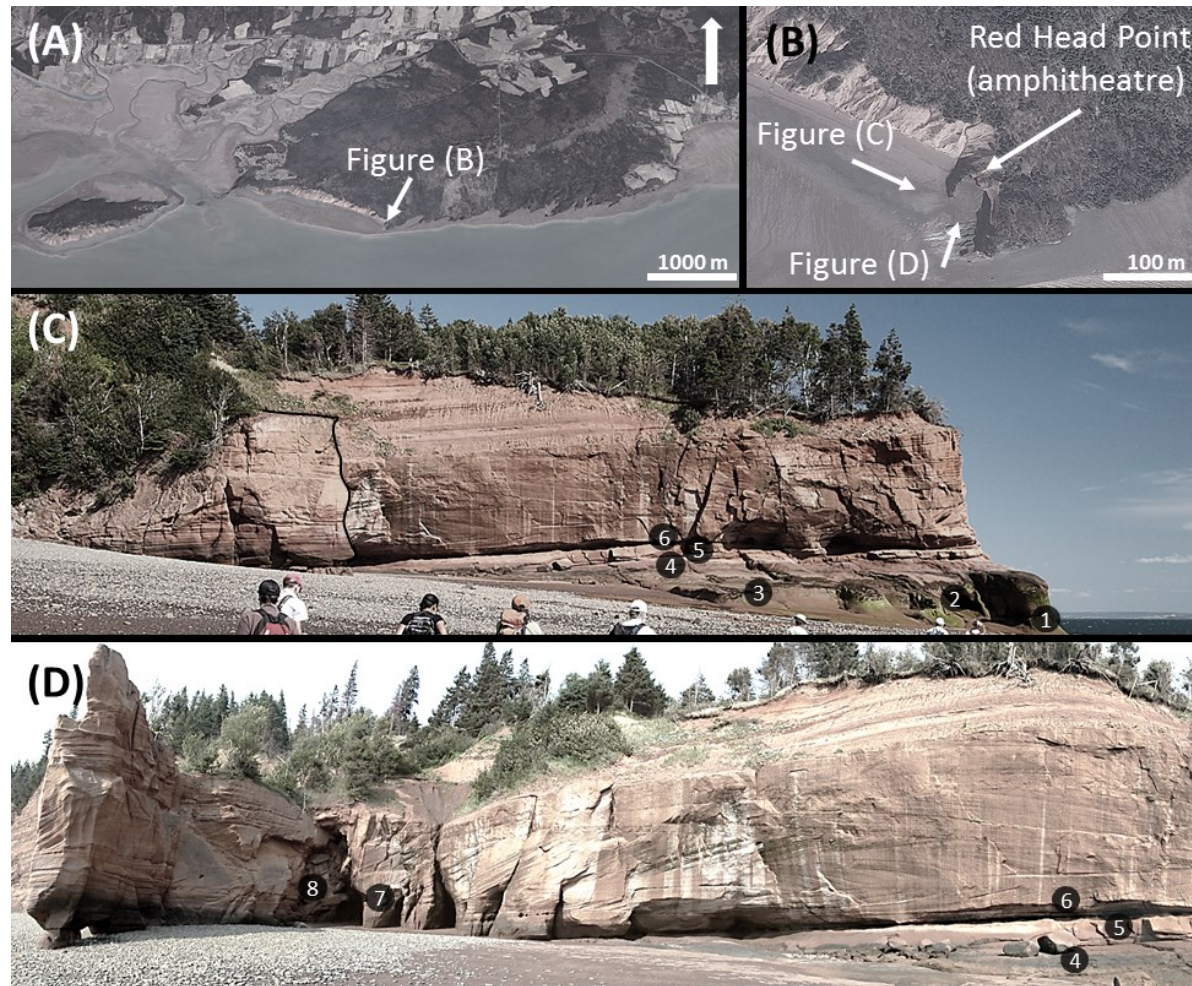


Figure 1.6: Satellite location map and field view of the aeolian successions at Red Head, Five Islands Provincial Park. (A) Map view showing Five Islands Provincial Park. (B) Map view of the study area at Five Islands. The bottom of the image shows the intertidal zone which was traversed to gain access to the cliff face. (C & D) Field view of the studied aeolian successions and location of the eight samples taken for analysis. Image (C) captures the western side of the amphitheatre and image (D) captures the interior of the amphitheatre from the south.

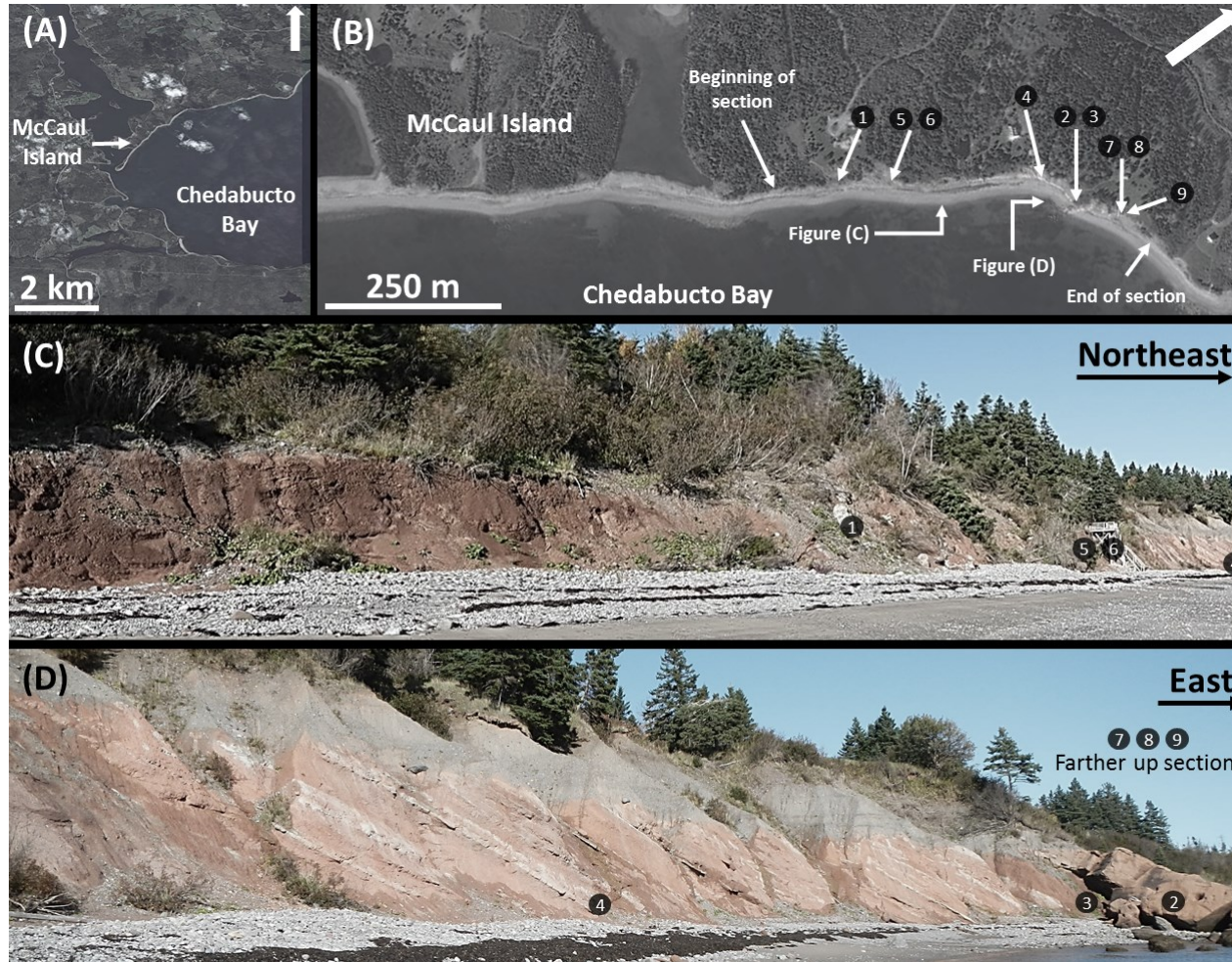


Figure 1.7: Map location and field view of the Chedabucto Formation at McCaul Island, NS. (A) Map view showing the general location of McCaul Island in the western margin of Chedabucto Bay. (B) Map view of the study area just north of McCaul Island. The bottom of the image shows the intertidal zone which was traversed to gain access to the cliff face. The numbered circles identify the locations of nine rock samples gathered for this study. (C & D) Field view of the studied Chedabucto Formation and location of the nine rock samples taken for analysis. Image (C) captures successions from the beginning of the outcrop and image (D) captures successions of stacked fine and coarse grained sandstone higher in the section.

1.2.2 Core Sampling

Core sampling was completed on the Eurydice P-36 well from the Orpheus Graben at the Canada-Nova Scotia Offshore Petroleum Board's Geoscience Research Centre (CNSOPB GRC) in Dartmouth, Nova Scotia. This well drilled approximately 2965 m (9728 ft) of Late Triassic evaporites and redbeds, with the basal 572 representing the Eurydice Formation type section (Williams et al, 1985). Approximately 8.8 m (28.8 ft) of core was collected at the base of the well between 2956 – 2965 m (9698 – 9728 ft) composed of fine grained, red and yellow consolidated sands and silts that was described (Figure 1.8).

Box 1 & 2



Box 3 & 4



Box 5 & 6



Box 7 & 8



Figure 1.8: Core collected from the Eurydice P-36 well. A total of eight boxes of core are shown and labeled. A meter scale is placed between the two boxes in each image for scale. The core can be viewed at the CNSOPB's GRC in Dartmouth, NS. The top of the core is at the top-left and base at the bottom-right. **Geologic Overview**

1.3.1 Regional Geologic Setting

During the early Mesozoic, likely the Early to Middle Triassic, the Pangean supercontinent began to fracture as a massive rift zone formed within its interior (Figure 1.9). Rifting was underway throughout the entire supercontinent by the Late Triassic (Figure 1.10) (Olsen, 1997). Rifting ultimately led to the breakup of Pangea and the formation of the continental configuration as seen today along the margins of the North and South Atlantic. Remnants of the massive rift zone now remain along the conjugate margins of the Atlantic Ocean (Olsen, 1997). The rift remnant preserved along the western margin of the North Atlantic is known as the eastern North American rift system (Olsen, 1997; Roberts and Bally, 2012), which comprises a series of interconnected, buried and exposed rift basins extending nearly 3000 km from Florida (USA) to offshore Newfoundland (Canada) (Olsen, 1997) (Figure 1.11).

The eastern North American rift zone can be divided geographically into the southern, central, and northern segments based on the age of preserved synrift strata (Withjack and Schlische, 2005). By the Late Triassic, rifting was underway within all three segments. However, the end of rifting and beginning of drifting occurred in the southern segment at the end of the Triassic, in the central segment during the Early to Middle Jurassic, and in the northern segment during the Early Cretaceous (Withjack and Schlische, 2005). During the transition from rifting to drifting, the southern and central segments underwent basin inversion in which the original basin geometry and stratigraphy was significantly altered (Withjack et al. 1995; Withjack and Schlische, 2005; Withjack et al. 2009).

Rift basins within the eastern North American rift system developed along pre-existing compressional structures from Paleozoic and older orogenic belts, causing thrust faults to be reactivated as normal and strike slips basin border faults during rifting (Swanson, 1986; Withjack

et al., 1998). Most of the rift basins developed as asymmetric half-grabens striking generally northeast-southwest with gentle to moderate normal dips along their border faults. However, if the pre-existing structures were oriented obliquely to the forces of extension, half-grabens with steep dipping strike slip border faults developed (e.g. the northern boundary of the Fundy Basin) (Olsen and Schlische, 1990; Schlische, 2003, Withjack et al., 2009).

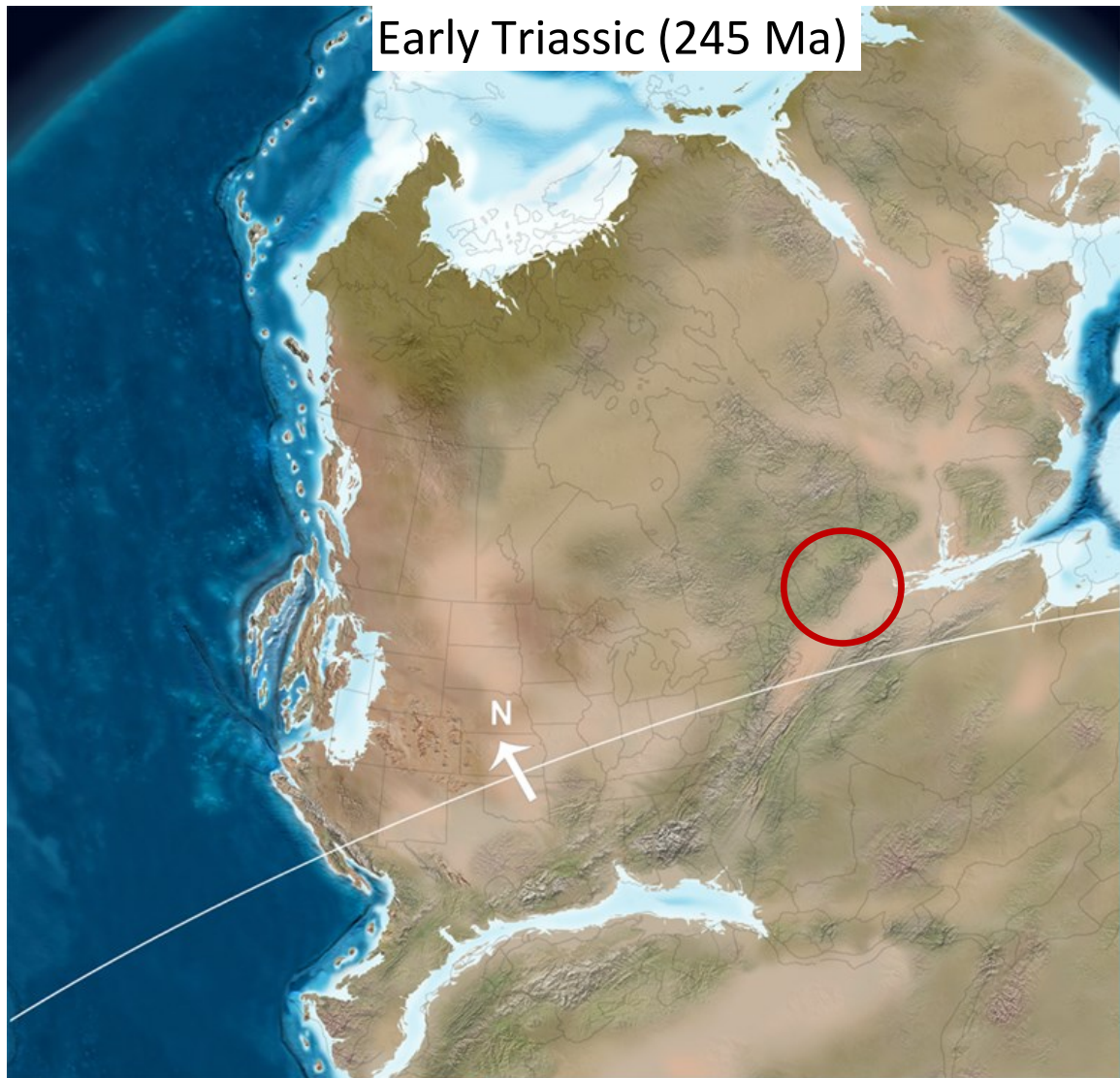


Figure 1.9: A paleogeographic map of North America during the Early Triassic (245 Ma). The white line indicates the paleo-equator and the red circle indicates the paleo-location of Nova Scotia. Rifting was underway and incursion of marine waters from the east is occurring during this time (© 2014 Colorado Plateau Geosystems Inc., used with permission).

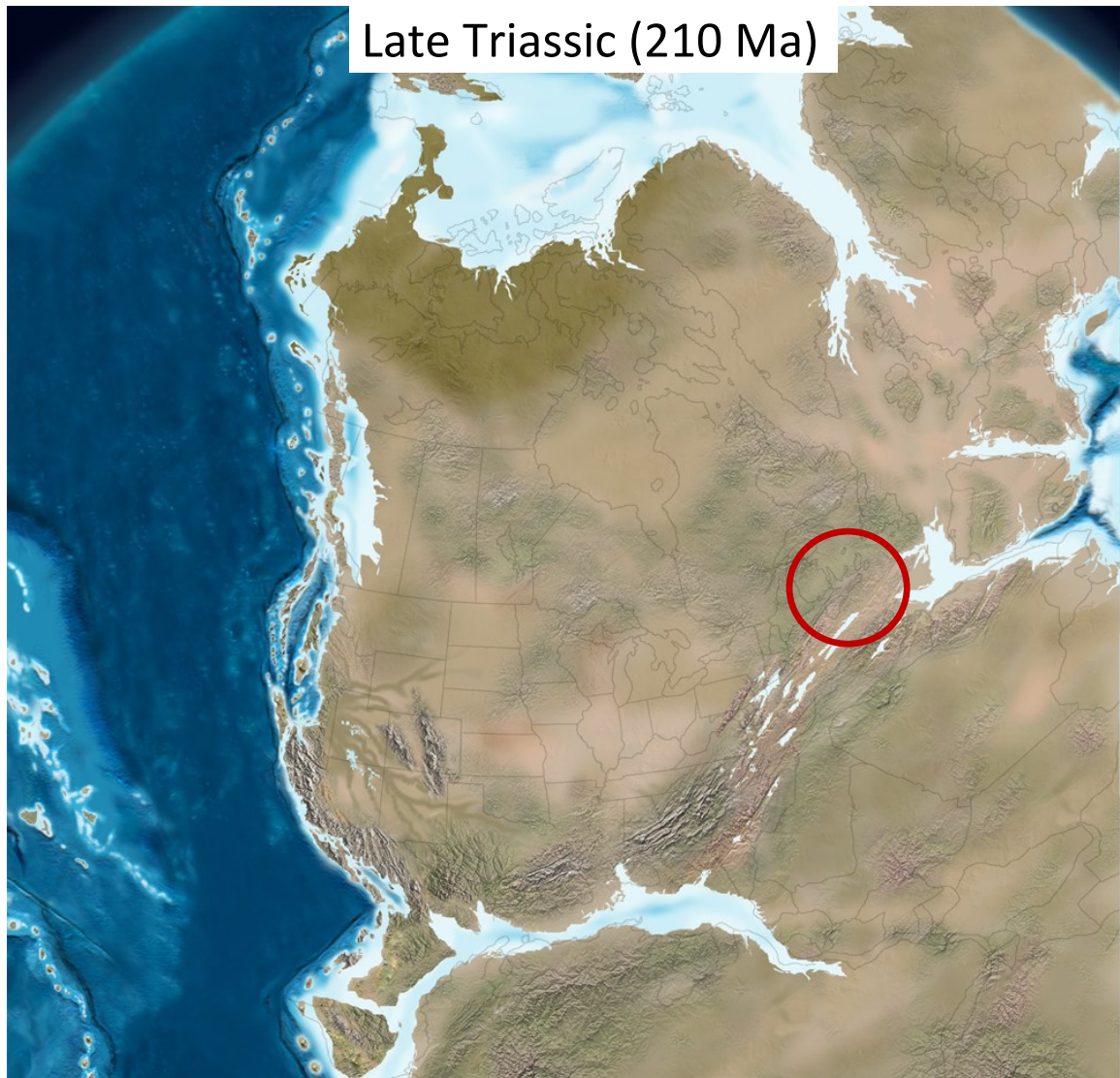


Figure 1.10: A paleogeographic map of North America during the Late Triassic (210 Ma). The red circle indicates the paleo-location of Nova Scotia. Rifting of the Pangean supercontinent is still underway and incursion of marine waters from the east is occurring. Endorheic basins, separated from marine waters and from one another by regional highlands, are well developed within the interior of the Pangean supercontinent (© 2014 Colorado Plateau Geosystems Inc., used with permission).

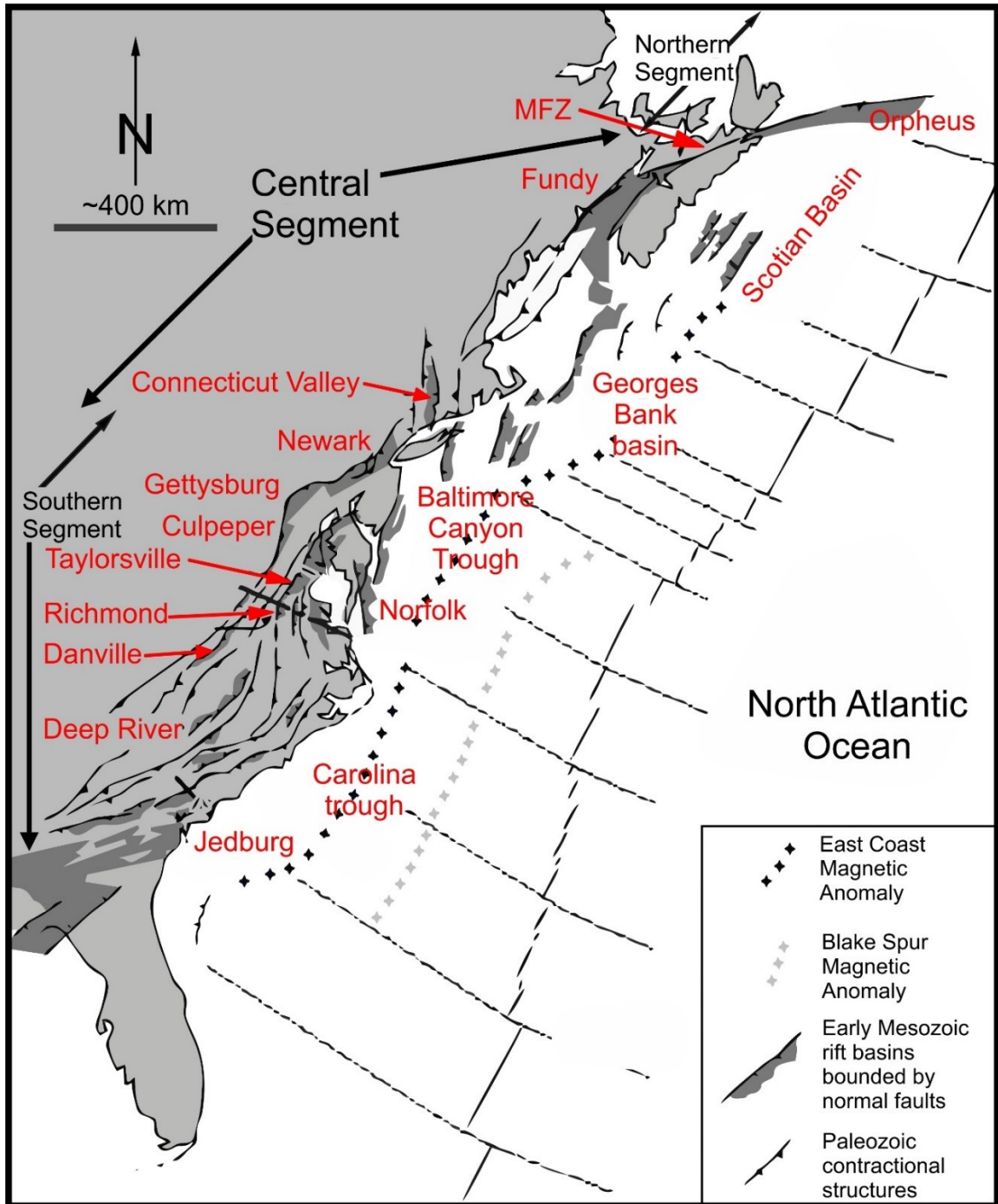


Figure 1.11: Major Paleozoic contractional structures, early Mesozoic rift basins (red) of eastern North America, and key tectonic features of the eastern North Atlantic Ocean (modified from Withjack et al., 1998).

1.3.1.1 Tectonics and Stratigraphy of the Scotian Basin

Tectonics and Basin Setting

The Scotian Basin is a submarine rift to passive margin basin that extends from the eastern flanks of Georges Bank to the central Grand Banks, covering a distance of 1200 km and an area of nearly 300,000 km² (Wade and MacLean, 1990). The basin formed during rifting of the Pangean supercontinent and now lies along the northern most part of the central segment within the eastern North American rift system (Roberts and Bally, 2012). The basin is described as an accreted wedge of Mesozoic-Cenozoic sediment collected in a series of interconnected subbasin depocenters which are flanked by large basement features in the northeast, northwest, and southwest (Jansa and Wade, 1975; Wade and MacLean, 1990). The subbasins strike southwest-northeast and, from the south to north, are known as the Shelburne Subbasin, LaHave Platform, Mohican Graben Complex, Sable and Abenaki subbasins, Banquereau Platform, and Laurentian Subbasin. The west-east trending Orpheus Graben is Chedabucto subbasin located between the Canso Ridge and Burin Platform along the northern flank of the Scotian Basin (Tanner and Brown, 1999; Wade and MacLean, 1990).

Regional data from the Scotian Basin suggests that rifting and synrift sedimentation began sometime in the Middle Triassic manifested as a northeast-trending complex of grabens and half grabens. Similar to other basins of the eastern North American rift system, border faults of these graben and half graben rift basins formed through the reactivation and reversal of Paleozoic compressional structures during regional northwest-southeast extension with the basins filled with synrift siliciclastics, evaporites, and volcanics (Wade and MacLean, 1990). During the rift-to-drift transition the rift basins were peneplaned in response to basin inversion and marine regression, resulting in erosion of the upper synrift strata and the formation of the

Breakup Unconformity (Wade and MacLean, 1990). During drifting, the basins intermittently subsided due to increased sediment influx and loading, and a passive margin began to evolve. This process resulted in thick accumulations of sediments in the Shelburne, Sable, Abenaki, and Laurentian subbasins, with more than 12 km of strata deposited and a maximum of 18 km in the Laurentian (Wade and MacLean, 1990). The LaHave Platform and Canso Ridge have considerably thinner strata not exceeding 4 km due to their relative positive relief through geologic time. The basement surface within the platform and ridge is broken into a series of half graben basins bounded by major counter-regional faults along their south margins and filled with synrift sediments and evaporites. The northern Burin Platform offshore Newfoundland contains even less strata of only 2 km in thickness, though its synrift faulting and sedimentation history is less well understood due to limited datasets (Wade and MacLean, 1990).

The Mohican Graben Complex and the Orpheus Graben are two similar but distinct rift depocenters that formed in the Scotian Basin. The Mohican Graben Complex is a southwest-plunging series of southerly-bounded large half-grabens within the central LaHave Platform. Sediments dip toward the south and generally comprise synrift siliciclastics and salt and are capped by basaltic flows (Wade and MacLean, 1990). The Orpheus Graben is a narrow, elongate fault-bounded easterly-plunging rift basin located between the Canso and Scatarie ridges. It is in response to extensional reactivation along the eastern flank of the Minas Fault Zone (MFZ) comprising some combination of normal and strike-slip movement along this border fault system (Keppie, 1982; Murphy et al., 2011; Wade and MacLean, 1990). Seismic and well data suggest the graben contains up to 10 km of Lower Jurassic and Upper Triassic strata, with approximately 3 km of synrift redbeds and 5 km of evaporite facies (Jansa and Wade, 1975; Wade and MacLean, 1990). Along its western flank and along the southern side of the MFZ are a series of redbed outcrops presumed to be of Late Triassic age (Tanner and Brown, 1999). Although it is

clear these redbeds were deposited during rifting the synrift phase, their origin and relation to the other synrift equivalents within the Scotian Basin remains enigmatic. It is thought these successions may be lateral / marginal equivalents to the deepest (oldest) Orpheus Graben redbeds, or instead were deposited in a juxtaposed mini-basin named the Chedabucto Subbasin (Tanner and Brown, 1999).

Stratigraphy

Stratigraphy of the Scotian Basin comprises up to 16 km of Mesozoic-Cenozoic successions overlying a crystalline basement of early to middle Paleozoic schists, phyllites, quartzites of the Meguma Supergroup and plutonic granites of the South Mountain Batholith. The oldest sediments within the basin are the Norian to Hettangian-Sinemurian continental redbeds of the Eurydice and Chedabucto formations and evaporites of the Argo Formation (Wade and MacLean, 1990). Rift deposition ceased sometime in the Early Jurassic (Sinemurian?) and was succeeded by coeval deposition of continental clastics and shallow water evaporitic dolostones of the Mohican and Iroquois formations. As the Atlantic Ocean widened, a passive margin setting evolved with the deposition of fluvial and shallow marine clastics of the Mohawk and Mic Mac formations, and establishment of the Abenaki Formation carbonate reef margin along the basin margin hingeline, and in deep water. Thick fluvial-deltaic deposits of the Missisauga and Logan Canyon formations characterized the Early Cretaceous prograding across the margin followed in the Late Cretaceous by transgressive marine shales, minor limestones, chalk, and marls of the Dawson Canyon and Wyandot formations. The mudstones, sandstones, and conglomerates of the Banquereau Formation comprise the latest Cretaceous to Neogene sediments within the Scotian Basin (Wade and MacLean, 1990). The following paragraphs will focus the stratigraphy of the synrift successions of Late Triassic to Early Jurassic age.

The oldest dated strata from the Scotian Basin is Norian to Hettangian-Sinemurian synrift successions of the Eurydice and Chedabucto formations composed of continental siliciclastics and evaporites of the Argo Formation (Williams et al., 1985). Due to the limited regional stratigraphic control within the basin depocenters, some authors (e.g. Kent et al., 2000; Olsen et al., 2000) have suggested synrift successions may have deposited as early as the Permian. These successions were deposited synchronously with rifted grabens and half grabens under seasonally arid to semi-arid climatic conditions in fluvial, lacustrine, aeolian, and coastal marine to sabkha environments (Klein, 1962; Jansa and Wade, 1975; Wade and MacLean, 1990). Synrift successions are separated from overlying postrift sediments by the breakup unconformity. Stratigraphically, the Chedabucto Formation is thought to be equivalent to the oldest Eurydice Formation successions within the deepest parts of the Orpheus Graben while the Argo Formation deposited synchronously with youngest Eurydice Formation sediments (Tanner and Brown, 1999). The type section for all three of these formations is found within the Orpheus Graben (Williams, 1985; Wade and MacLean, 1990; Tanner and Brown, 1999).

The type section for the Eurydice Formation is found in the Eurydice P-36 well between the depths of 2393-2965 m (Williams et al., 1985). The Eurydice Formation is dated palynologically as Rhaetian-early Hettangian to late Hettangian-early Sinemurian and consists of reddish shales and siltstones with some feldspathic sandstones deposited under seasonally arid continental conditions. Williams et al. (1985) identifies the formation comprising primarily of shale (96%) with minor siltstone and sandstone (4%) with a clay matrix stained by iron oxide. Wade and MacLean (1990) suggest the formation consists of 45% red, silty shale, 45% sandstone and siltstone, and a 10% mixture of limestone, evaporites, and green shale. In other offshore penetrations of the Eurydice Formation, most notably from the Sambro I-29 well in the Mohican Graben Complex, the synrift strata comprise a much coarser material comprising 37% fine- to

medium-grained sandstone, 28% red siltstone, and 35% red shale (Wade and MacLean, 1990). These strata significantly differ from the Eurydice Formation and future study may determine that they should exist as a separate lithostratigraphic unit. Seismic data from the Scotian Basin suggests the Eurydice Formation and successions of similar age are widespread with variable thickness along the margin, with approximately 3 km of strata within the Orpheus Graben, 1600 m within the Mohican Graben Complex, and thousands of meters within tilted blocks along the hinge zone of the LaHave Platform (Wade and MacLean, 1990). Overall the regional stratigraphic control of the Eurydice Formation is limited, which is evident as the thickness, areal extent, and lithology are often reported as estimations or have significant variability (Wade and MacLean, 1990).

The Chedabucto Formation crops out along the western coastline of Chedabucto Bay, Nova Scotia (Klein, 1962; Williams, 1985; Tanner and Brown, 1999). The formation comprises a series of noncyclic brown to red shale, siltstones, sandstones, conglomerates, and agglomerates which strike northeast at 030° to 050°, and dip to the southeast at 20° to 40°, thus obscuring lateral facies relationships (Williams et al., 1985; Tanner and Brown, 1999). The lower part of the section contains several small reverse faults, with meters of offset, and gentle anticlinal folding (Tanner and Brown, 1999). The type section, which outcrops along McCaul Island, has a minimum thickness of 65 m and was originally identified by Klein (1962) but was never formally described. Tanner and Brown (1999) were the first to formally describe the Chedabucto Formation and interpreted the type section as consisting of nine interbedded, but noncyclic, facies consisting of featureless, fining upward, and clast supported sandstones (82%), reddish-brown mudstones containing desiccation cracks and root traces (10%), claystone with slickensides (5%), and fining-upward clast-supported conglomerates (3%) (Figure 2.7). These

sediments are interpreted to have deposited in sand-rich braided stream system flowing eastward into the Orpheus Graben (Tanner and Brown, 1999).

The Argo Formation is coeval with and overlies the Eurydice Formation (Wade and MacLean, 1990). The type section is found in the Shell F-38 well drilled in the Orpheus Graben, between 2305-3085 m depth and is dated as Rhaetian to early Hettangian (Williams et al., 1985). The formation consists of finely crystalline dolomite and massive beds of coarsely crystalline salt which are separated by zones of red shale and occasional anhydrite, both of which become more frequent near the top of the unit (Williams et al., 1985; Wade and MacLean, 1990). The thickness of the formation varies considerably within the Scotian Basin. In the type well the formation is 780 m thick but, due to halokinesis over time, the unit may be absent or exceed 1830 m locally along the basin (Jansa and Wade, 1975; Williams et al., 1985).

1.3.1.2 Tectonics and Stratigraphy of the Fundy Basin

Tectonics and Basin Setting

The Fundy Basin is an offset Mesozoic rift basin formed within the northern part of the eastern North American rift system central segment, located between the provinces of Nova Scotia and New Brunswick covering an area of roughly 16,000km² (Wade et al., 1996; Chenin and Beaumont, 2013). Similar to the Scotian Basin, the Fundy Basin developed during rifting of the Pangean supercontinent as a series of interconnected and structurally related half-graben rift basins known as the Fundy, Chignecto, and Minas subbasins (Olsen and Schlische, 1990; Withjack et al., 1995; Wade et al., 1996). The main Fundy Basin is bounded along its northwest margins by low-angle, NE-striking normal extensional faults that was originally compressive during the middle to late Paleozoic (Wade et al., 1996). Its northern extension, the Chignecto Subbasin, is bounded by a left-lateral strike-slip extensional fault. Likewise, the Minas Subbasin

with its northern margin defined by E- to ENE-striking steeply dipping normal and left-lateral strike-slip extensional faults that together form a border fault system and make up the western extension of the Minas Fault Zone (Withjack et al., 1995; Wade et al., 1996; Withjack et al., 2009).

Age control taken from synrift successions within the Fundy Basin suggest that rifting was underway throughout the entire basin by the Middle Triassic, however some data suggests rifting may have started as early as the Permian (Withjack et al., 1995; Olsen et al., 2000). The associated depocenters were filled with non-marine fluvial and lacustrine sedimentary rocks and basalt flows. Rifting ceased in the Early to Middle Jurassic during continental breakup and the onset of seafloor spreading (Withjack et al., 1998). During the transition from continental rifting to drifting, reverse movement along the border fault system led to post depositional basin inversion with significant alteration to the structure and stratigraphy of the Fundy Basin. In addition to numerous large-scale folds and faults that formed during inversion, approximately 2 km of the uppermost Early to Middle(?) synrift playa-lacustrine strata of the McCoy Brook Formation was later eroded and removed from the basin (Wade et al., 1996; Withjack et al., 2009).

Stratigraphy

Synrift successions of the Fundy Basin lie unconformably on Carboniferous and older metasediments and igneous rocks of the Meguma and Avalon Terranes, and in ascending order the Wolfville, Blomidon, North Mountain, and McCoy Brook formations. These successions were deposited in a variety of depositional environments within an endorheic (land-locked) basin under semiarid to subhumid climatic conditions.

The Wolfville Formation comprises stratified coarse- to medium-grained arenites and arkose, subarkose, and orthoquartzites, usually characterized by large scale cross-stratification. At the base of the formation are pebbly and conglomeratic units with extrabasinal clasts derived from nearby metamorphic and granitic highlands and from material eroded from Lower Carboniferous metasedimentary strata (Williams et al., 1985). These were deposited as alluvial-fan sandstones, fluvial sandstones, aeolian dune sediments (Williams, 1985; Leleu et al., 2009). Based on seismic datasets of the Fundy Basin, Wade et al. (1996) suggest that the Wolfville has a laterally equivalent lacustrine succession in the basin depocenter. Based on gathered remains of mollusks, reptiles, and amphibians, the Wolfville Formation has been age dated as Anisian to Carnian (Sues and Olsen, 2015) (Figure 1.1). The Wolfville Formation unconformably overlies the Cambrian to Ordovician Meguma Supergroup, the Middle Devonian South Mountain Batholith, the Lower Carboniferous Horton and Windsor groups, and the Upper Carboniferous Canso (Mabou) Group within the Fundy Basin (Williams et al., 1985). The formation reaches a maximum thickness of up to 3000 m within the Fundy Subbasin and intermittently extends laterally for nearly 240 km from the Fundy Subbasin to the Minas Subbasin (Wade et al., 1996), of which 27 km of laterally continuous strata have been described along the southeastern flank of the Minas Subbasin along the shoreline of Minas Basin (Leleu et al., 2009).

The type section for the Blomidon Formation was designated by Klein (1962) as the section exposed between Cape Blomidon and Paddy Island, within the Minas Subbasin. Here, the Blomidon Formation is described as evenly bedded red shales, claystones, and siltstones predominantly deposited as lacustrine sediments in an endorheic basin under arid climatic conditions (Williams et al., 1985). The formation was deposited during the Late Triassic (Norian to Rhaetian) based on studies of palynomorphs and tetrapod remains (Sues and Olsen, 2015). The formation comfortably to unconformably overlies the Upper Wolfville Formation and

underlies the tholeiitic basalts of Lower Jurassic North Mountain Formation throughout the region. Within the Minas Subbasin, the Wolfville and Blomidon formations may locally interfinger, and the Blomidon Formation may be in fault contact with the Lower Carboniferous basement rocks (Williams et al., 1985).

1.4 Aeolian Strata at Red Head

In this work the aeolian strata located at Red Head in Five Islands Provincial Park are considered part of the upper limits of the Wolfville Formation. These successions have been informally named by Hubert and Mertz (1984), Olsen (1997), and Olsen et al. (2003) and were considered to be either part of the upper Wolfville Formation or the lower Blomidon Formation. Sues and Olsen (2015) defined these successions as the Red Head Member of the Blomidon Formation in accordance with the North American Stratigraphic Code. They maintain variations in lithology and grain size drastically differ from the Wolfville Formation and that these aeolian successions outcrop directly on Carboniferous strata with the complete absence of the Wolfville Formation, as their evidence that the aeolian strata at Red Head are part of the lower Blomidon Formation. However, these authors, as well as Leleu et al. (2010), recognize increasing levels of aeolian sandstone layers within the fluvial and alluvial strata of the Economy Member of the Wolfville Formation, speculating that reworking of the fluvial Wolfville Formation by winds produced overlying aeolian strata. At Red Head, we see exactly this relationship, a series of aeolian successions deposited above a conglomeratic, fluvial succession. In contrast, I believe that the aeolian strata at Red Head are part of the upper Wolfville Formation conglomeratic fluvial strata which have been reworked by wind.

Chapter 2: Facies and sedimentary architecture of Mesozoic synrift infill – examples from the Fundy Basin and the Orpheus Graben

2.1 Introduction

Recent sedimentological work on the Nova Scotian Early Mesozoic synrift successions has largely focused on the lithological description of individual basins within the offshore and onshore margin areas examining the large and small scale lithological and architectural elements distribution and paleoenvironments (Tanner and Brown, 1999, Leleu et al., 2009; Leleu and Hartley, 2010; Broom, 2015). This study will test the broad terrane hypothesis (Russell, 1880) which states that adjacent basins are remnants of a once larger connected basin which underwent upheaval and erosion. I will test this hypothesis by examining the sedimentological nature and distribution of facies and architectural elements along the margins and off shore areas of the Minas Basin and Orpheus Graben (Figure 1.2, Figure 1.3, and Figure 1.4).

This study involves the characterization of facies and architectural elements from Middle to Late Triassic synrift successions from three locations onshore and one offshore Nova Scotia, Canada. Facies from the Wolfville and Chedabucto formations were classified using a modified version of Miall's (1978) facies classification system, while the Eurydice Formation was classified using the clastic coastal ternary diagram from Ainsworth et al. (2011).

2.1.1 Study Area and Location

The study areas for this paper are located within and along the margins of the Minas Subbasin and the Orpheus Graben. Locations of each area can be found in Chapter 1 of this project. The following describes in detail the location and access to each of the study areas:

- 1) The marine Minas Basin is a northeastern extensional arm of the Bay of Fundy and is located approximately 100 km northwest of Halifax. The study area is located along the southwest margin at Rainy Cove where laterally continuous outcrop is exposed in 20+ m high coastline cliffs which are accessed only by traverse along a rocky beach.
- 2) Chedabucto Bay is located along the eastern margin of Nova Scotia near the community of Guysborough, approximately 200 km northeast of Halifax. The study area is located 75 m north of McCaul Island along the western margin of Chedabucto Bay. Outcrop is exposed along 5+ m high cliff faces for approximately 500 m. The outcrop is seasonally accessible (summer only) through a privately owned property located on the south side of Parker Hart Road.
- 3) The Eurydice P-36 well is located offshore Nova Scotia in the Orpheus Graben (45.42981, -60.07972). The well was drilled by Shell Canada in September of 1971 as an exploratory well to test a salt- and basement-related structural closure on the northern Scotian margin (MacLean and Wade, 1993). Core collected during drilling was accessed through the Canadian Nova Scotia Offshore Petroleum Board's (CNSOPB) Geoscience Research Centre (GRC) in Dartmouth and well files and data through the CNSOPB's online Data Management Center (DMC).

2.2 Methods and Data

The lowermost Wolfville Formation and the Chedabucto Formation are described here from coastal outcrops. Within the Wolfville, numerous intra-Triassic unconformities are mapped that represent laterally continuous minor and significant erosional events (Leleu et al. 2009). Within the Chedabucto Formation, stacked sequences can be mapped but their lateral distribution is obscured due to the high dip in the beds along the outcrops (Tanner and Brown 1999). The Eurydice Formation is constrained to a single well core from the Eurydice P-36 well. The core is 9 m in length and provides visual information on the physical and biogenic sedimentological features.

Collected data from these field sites and core, used to address the research objectives include: (1) measured stratigraphic sections and sample collection, (2) measured core, and (3) photographs and panoramic photopans with schematic diagrams.

2.2.1 Measured Stratigraphic Sections

Stratigraphic sections were measured at the Rainy Cove and McCaul Island field locations. Descriptions for each bed were completed by analyzing grain size, sedimentary structures, contacts between beds, bioturbation, and any other stratigraphic features. The measured sections were used to document facies and facies associations within the channel belt successions. At Rainy Cove, five representative sections, between 10 to 20 m in height, were measured and used to create a composite section of the lowermost Wolfville Formation outcrop. At McCaul Island, one representative section was measured on the Chedabucto Formation outcrop through 80 m of strata. Paleo-flow measurements were recorded at both outcrop locations and measured from trough bed axes directions when present.

2.2.2 Measured Core

Core analyzed for this work was accessed through the Canada-Nova Scotia Offshore Petroleum Board's Geoscience Research Centre (CNSOPB GRC) located at 201 Brownlow Avenue, Suite 27 Dartmouth, Nova Scotia. Core from the Eurydice P-36 well comprises a total of eight boxes which were put on rolling rack display at the GRC. The core was described and photographed using a Nikon DSLR camera. Core description consisted of examining grain size, lithology, physical sedimentary structures, biogenic sedimentary structures, and all surfaces or boundaries following the methodology present in Appendix D. Core notes were recorded and digitized using CorelDraw® and were made into a digital core section. Photographs of representative lithologies and sedimentary structures were captured using a high zoom macro lens attached to a Nikon DSLR camera attached to a tripod.

2.2.3 Photographs and Panoramic Photopans with Schematic Diagrams

At Rainy Cove and McCaul Island, a detailed photographs were captured using a Nikon DSLR camera. These photographs were merged into panoramic image using Microsoft ICE™. The panoramic images were used define interpreted facies, architectural and structural elements, and bounding surfaces of the architectural elements of the Wolfville and Chedabucto formation outcrops. CorelDraw® was used in the digitization of each of the photopans to make schematic diagrams upon which were applied the lithofacies, architectural elements, and bounding surfaces defined on the photo pans. Designated lithofacies and architectural elements used here were modified from works by Miall (1978, 1985, 1996) and can be found in Table 2.1 and Table 2.2. Bounding surfaces of the channel belts were modified from work completed by Leleu et al. (2009).

Table 2.1: Lithofacies classification (modified from Miall, 1985)

Lithofacies classification for the Wolfville and Chedabucto formations			
Facies Code	Lithofacies	Sedimentary Structures	Interpretation
Gmm	Matrix-supported, massive gravel	Weak grading	Plastic debris flow (high-strength)
Gcm	Clast-supported massive gravel	-	Pseudoplastic debris flow (inertial bedload, turbulent flow)
Gh	Clast-supported, crudely bedded gravel	Horizontal bedding, imbrication	Longitudinal bedforms, lag deposits, sieve deposits
Gt	Gravel, stratified	Trough crossbeds	Minor channel fills
Gp	Gravel, stratified	Planar crossbeds	Transverse bedforms, deltaic growths from older bar remnants
St	Sand, fine to v. coarse, may be pebbly	Solitary or grouped trough crossbeds	Sinuuous-crested and linguoid (3-D) dunes
Sh	Sand, fine to v. coarse, may be pebbly	Horizontal lamination	Plane bed flow (super critical flow)
Ss	Sand, fine to v. coarse, may be pebbly	Broad shallow scours	Scour fill
Sm	Sand, fine to coarse	Massive or faint laminations	Sediment gravity-flow deposits
P	Paleosol carbonate	Paleosol carbonate	Paleosol carbonate
Fl	Sand, silt, mud	Fine laminations, small ripples	Overbank, abandoned channel, or waning flood deposits
Fsm	Silt, mud	Massive	Back-swamp or abandoned channel deposits
Fr	Mud, silt	Massive, roots	Root bed, incipient soil

Table 2.2: Architectural elements in fluvial and abandoned channel and overbank deposits (modified from Miall, 2016)

Channel and overbank architectural elements			
Element	Symbol	Principle facies	Geometry and relationships
Channels	CH	Any combination of facies	Finger, lens, sheet; scale and shape highly variable
Gravel bars and bedforms	GB	Gcm, Gh, Gt, Gp	Lens, blanket
Sandy bedforms	SB	St, Ss	Lens, sheet, blanket, wedge
Downstream accretion macroforms	DA	Gt, Gp, St	Lens resting on flat or channelized base and an upper bounding surface. Accretion surfaces orientated downstream
Sediment gravity flows	SG	Gmm, Sm	Lobe, sheet
Laminated sand sheet	LS	Sh	Sheet, blanket
Floodplain fines or abandoned channel	FF	Sm, Fsm, Fr	Extensive lateral dimensions. Up to 9 m thick.

2.3 Facies and Facies Associations of the Wolfville, Chedabucto, and Eurydice formations

This chapter summarizes the synrift stratigraphy of the lowermost Wolfville Formation in the Minas Subbasin, and the Chedabucto and Eurydice formations in the Orpheus Graben. The stratigraphic analyses and interpretations rely on facies and architectural element analysis.

2.3.1 Facies and Facies Associations – Definition and Use

The term facies is attributed to Gressly (1838) and Reading (1996) subsequently defined facies as “a body of rock, which may include a single bed or a group of multiple beds, with a specific set of characteristics reflecting a particular process, set of conditions, or environment”. A facies may be defined on the basis of colour, bedding, composition, texture, sedimentary structures, and fossils. Depending which primary feature is used to define the rock facies, different prefixes may be used on the term facies. When placing emphasis on the physical and chemical structures, the term *lithofacies* is used. When placing emphasis on the fossil content, the term *biofacies* is used. When using thin section to identify rock characteristics, the term *microfacies* should be used. In addition to a descriptive type facies, a geologist may choose to use an interpretive type facies nomenclature. These are often based on interpretations of processes (e.g. turbidite facies), environments (e.g. fluvial facies), or tectonic settings (e.g. post-orogenic facies) (Reading, 1996).

The grouping of facies into genetically or environmentally related assemblages produces *facies associations*. Reading (1996) recognized that individual facies have limited interpretive value as, for example, a cross stratified sandstone bed may belong to one of many depositional environments. By collectively grouping adjacent and genetically related facies into facies associations, evidence for depositional environment interpretations is made easier and holds

more argumentative strength compared to when considering individual facies in isolation (Reading, 1996).

Within the stratigraphic successions under investigation, thirteen facies were defined. Each facies is described based on its physical and biogenic sedimentary structures, mean bed thickness, and other defining characteristics. These descriptions, and interpretations on their formation, are found below and are summarized in Table 2.3. The facies are then related to architectural elements in the following section.

Table 2.3: Summary of facies and facies associations from the Wolfville, Chedabucto, and Eurydice formations. A total of twelve facies were identified; five (F1 to F5) in the lowermost Wolfville Formation, four (F6 to F9) in the Chedabucto Formation, and three (F10 to F12) in the Eurydice Formation.

Facies and facies associations from the Wolfville, Chedabucto, and Eurydice formations						
Formation	Facies Name	Facies code	Lithology	Description	Interpretation	Facies association
Wolfville	F1	Gmm	Matrix supported intrabasinal-clastic breccia	Weakly stratified to completely chaotic, 0.75 m (average) thick beds comprising poorly sorted, angular to sub-angular, 1 to 10 cm metasedimentary clasts in a red, silty fine- to coarse-grained sandstone matrix. Gray redox spotting, small (cm scale) reddish-white nodules, and sub-rounded pebbles are present in the upper portion of this facies.	The matrix supported breccia was deposited by low strength, viscous debris flows	Alluvial fan
	F2	Gcm, Gh	Clast- to matrix-supported, crudely stratified conglomerate	Crudely visible trough and planar cross-stratified, 1 to 3 m thick beds comprising poorly sorted, pebble to cobble, rounded to sub-angular clasts of variable lithology in a fine- to coarse-grained red silty-sandstone matrix. Clast content typically decrease upward.	The clast- to matrix-supported conglomerate deposited in mixed sheet floods and debris flows representing synchronous alluvial and fluvial deposits.	Alluvial fan to fluvial
	F3	Gh, Gt	Matrix supported conglomerate	Horizontal to trough cross stratified, 0.5 to 1 m thick beds comprising poorly sorted, angular to rounded, pebble to cobble sized clasts of variable lithology in a silty fine to coarse-grained sandstone matrix. Beds typically show normal grading with bedding-parallel clast fabrics.	Matrix-supported conglomerate deposited by sheet floods representing fluvial deposition	Fluvial
	F4	St, Ss, Sh	Pebbly to clean sandstone	Near-horizontal planar cross-stratified, 0.5 to 5 m thick beds comprising angular to round, mixed lithology pebbles in a yellowish-red, medium- to very coarse-grained fining upward sandstone matrix. Pebbles may comprise up to 20% of the unit.	Pebbly to clean sandstones represent bedload and suspension deposits formed in a braided channel system	Fluvial
	F5	P	Carbonate-nodule-rich paleosol	Featureless 0.5 m thick beds comprising a series of carbonaceous nodules in a mottled, silty-sandstone matrix. The nodules increase in size and number upwards until passing into a thick (5 cm) carbonate crust of coalesced nodules.	Mature paleosol	Fluvial
Chedabucto	F6	Gh, Gp	Matrix supported conglomerate	Featureless to vaguely laminated, 0.05 to 1 m thick beds comprising quartzitic to mafic, angular to subrounded, randomly oriented, 1 to 10 cm clasts hosted in a fine to coarse grained silty sandstone.	Traction current bedload or debris flow deposits related to a braided river system	Alluvial fan to fluvial
	F7	St and Sp	Fine to coarse grained pebbly sandstone	Planar to trough cross stratified, 0.2 to 1.2 m thick beds comprising rounded to sub-rounded, granular to pebbly clasts in a yellow-brown or greenish-gray, fine lower to coarse upper sandstone.	Bedload deposits formed in lower energy areas of a braided river system	Fluvial
	F8	Sm to Ss	Featureless fining upward silty-sandstone	Featureless to very-faint trough cross stratified and parallel laminated, 0.3 to 3 m thick beds containing well-rounded, granular to pebble sized clasts occur along bedding planes within a yellowish-red or gray, very fine- to very coarse-grained, fining upward sandstone facies form beds which are.	Bedload and suspension deposits formed in shallow channels of a braided channel systems	Fluvial
	F9	Fl, Fsm, and Fr	Blocky clay-siltstone	Blocky to fissile, 0.5 to 9 m beds containing reddish-brown clay-siltstone. The unit contains vague bedding marked by jointing, occasional zones of grayish-green mottling (reduction spots), small (1 cm) nodules, and slickensides.	Overbank to abandoned channel floodplain deposits with indications for incipient soil formation	Fluvial
Eurydice	F10	Wave	Cross-stratified sandstone	Cross-stratified, 2 to 45 cm thick beds comprising very fine- to fine-grained, sub-angular to sub-rounded, yellowish-brown sandstone.	Wave-dominated – tidal flat deposits	Wave-tidal
	F11	Tidal	Heterolithic sandstone and siltstone	Alternating sandstone and siltstone, 5 to 50 cm thick beds containing reddish-brown, featureless siltstone and yellowish-brown, very fine- to fine-grained, well sorted sandstone.	Tidal dominated – mixed-energy tidal-bar (tidal-channel) deposits	Tidal-fluvial
	F12	Tidal	Poorly stratified to featureless sandy-siltstone	Poorly stratified to featureless, 1 m thick beds containing reddish-brown siltstone, very fine-grained sandstone, and small (1-3 mm) anhydrite nodules.	Tidal dominated – suspended sediment settling in low-energy mud flat deposits	Tidal

2.3.2 The Wolfville Formation

Five representative facies forming two facies associations are recognized in lowermost part of the Wolfville Formation. Facies codes for this section have been identified using a modified version of Miall's (1978) facies classification (Table 2.1). A summary of the facies and facies associations can be found in Table 2.3 and representative photographs of each facies can be found in Figure 2.2.

Facies 1: Matrix supported intrabasinal-clastic breccia

Description

Facies 1 comprises weakly stratified to completely chaotic, 0.75 m (average) thick beds containing poorly sorted, angular to sub-angular, 1 to 10 cm metasedimentary clasts in a red, silty fine- to coarse-grained sandstone matrix (Figure 2.2). An upward fining in clast size and clast abundance is evident, with larger clasts preferentially deposited near the base of the beds. Gray redox spotting, small (cm scale) reddish-white nodules, and sub-rounded pebbles are present in the upper portion of this facies. No biogenic structures are present. The average bed thickness is approximately 0.75 m.

Interpretation

Vaguely stratified to chaotic matrix supported breccia (facies code **Gmm**) are interpreted as low strength, viscous debris flows (Miall, 1978; Blair and McPherson, 1994; James and Dalrymple, 2010). Angular clasts, from the underlying Horton Group, suggest the debris flows were likely short-travelled. Sub-rounded pebbles, of an unknown source, suggest an influx of extrabasinal clasts, perhaps indicative of a more extensive alluvial sediment transport system within the region, or, erosion of an older similar facies (basal Horton Group?). The reddish-white

nodules are most likely reworked carbonate deposits (caliche), suggesting deposition under semi-arid climatic conditions (James and Dalrymple, 2010).

Facies 2: Clast- to matrix-supported, crudely stratified conglomerate

Description

Facies 2 comprises crudely visible trough and planar cross-stratified, 1 to 3 m thick beds containing poorly sorted, pebble to cobble, rounded to sub-angular clasts of variable lithology (dark metasediments, sandstones, quartzites, siltstones, and granites) hosted in a fine- to coarse-grained, red silty-sandstone matrix (Figure 2.2). Clast content typically decreases upward, changing from a clast-supported to matrix-supported conglomerate. The beds typically have erosive basal contacts recording some erosional relief.

Interpretation

The clast- to matrix-supported, crudely stratified conglomerate (facies code **Gt** to **Gmm**) represent traction current bedload deposits (channel infill or bar deposits) from a braided river system (Miall, 1978; James and Dalrymple, 2010). The maximum clast size and presence of trough cross-stratification together represent subaqueous, medium-scale dunes (bar deposits) formed during maximum discharge within a braided channel system (Ashley, 1990; James and Dalrymple, 2010). Planar cross-stratified units represent progradation (Steel and Thompson, 1983) or lateral accretion (Ramos and Sopeña, 1983) of the fluvial barforms and will usually have a decrease in pebble content downstream.

Facies 3: Matrix supported conglomerate

Description

Facies 3 comprises horizontal to trough cross stratified, 0.5 to 1 m thick beds containing poorly sorted, angular to rounded, pebble to cobble (up to 50 cm) sized clasts of variable lithology in a silty fine- to coarse-grained sandstone matrix (Figure 2.2). The beds typically show normal grading with clasts forming bedding-parallel fabric. The beds typically have an erosive basal contact with evident erosion.

Interpretation

The matrix supported conglomerate (facies code **Gmm**) represents a debris flow comprising sheet-flood, clast poor units with debris-flow clast-rich conglomeratic units (Miall, 1978; Blair and McPherson, 1994; James and Dalrymple, 2010). Larger clasts and coarser sands were transported and deposited as bedload and saltation material during higher transport velocities, while finer grained sands were deposited from suspension during periods of slower transport velocities and waning flood conditions (James and Dalrymple, 2010)

Facies 4: Pebbly to clean sandstone

Description

Facies 4 comprises near-horizontal planar cross-stratified, 0.5 to 5 m thick beds containing angular to round, mixed lithology (dark metasediments, sandstones, quartzites, siltstones, and granites) pebbles in a yellowish-red, medium- to very coarse-grained fining upward sandstone matrix (Figure 2.2). Pebbles may comprise up to 20% of the unit and are often preserved along the base of bedding planes. The basal contacts of the beds are either sharp or erosional in nature.

Interpretation

The pebbly to clean sandstone (facies code St, Sp, and Ss) represent bedload and suspension deposits formed in a braided channel system (Miall, 1978; James and Dalrymple, 2010). Beds containing preserved trough cross-stratification are organized into multistory stacked units which represent channel infill or parts of bar deposits (Ramos and Sopeña, 1983; Miall, 1996). Near-horizontal planar or parallel cross-stratification beds represent upper flow-regime plane bed, fluvial channel deposits (James and Dalrymple, 2010).

Facies 5: Carbonate-nodule-rich paleosol

Description

Facies 5 comprises featureless 0.5 m thick beds containing a series of calcareous nodules in a mottled, silty-sandstone matrix. The nodules increase in size and number upwards until passing into a thick (5 cm) carbonate crust of coalesced nodules (Figure 2.2). The bed developed gradationally at the top of a fining upward sandstone layer and is laterally extensive except in areas of erosion below overriding sandstone or conglomeratic beds.

Interpretation

The carbonate-nodule-rich paleosol (facies code P) represents mature calcic paleosol layers (James and Dalrymple, 2010).

Facies Associations

The alluvial fan facies association constitutes roughly 20% of the section, forms bedsets 4 to 6 m in thickness, and comprises breccias (facies 1) with carbonate nodules (facies 5). The coarse-grained, poorly sorted breccias, and some conglomerates, were deposited by alluvial debris flows in topographic lows that cut into the underlying Carboniferous Horton Group. The carbonate nodules indicate periods of incipient soil formation under semi-arid climatic

condition. Breccia deposits are limited to the basal 4 to 6 meters of the Rainy Cove measured sections (Figure 2.1).

The fluvial facies association constitutes the remaining 80% of the section, is 25 m thick, and comprises most conglomerates (facies 2 and 3), sandstones (facies 4), and carbonate nodule-rich paleosol (facies 5) successions. This facies association overlies the alluvial fan facies in the area (Figure 2.1). The conglomerates and sandstones are interpreted as traction current bedload deposits from a high-energy braided river system.

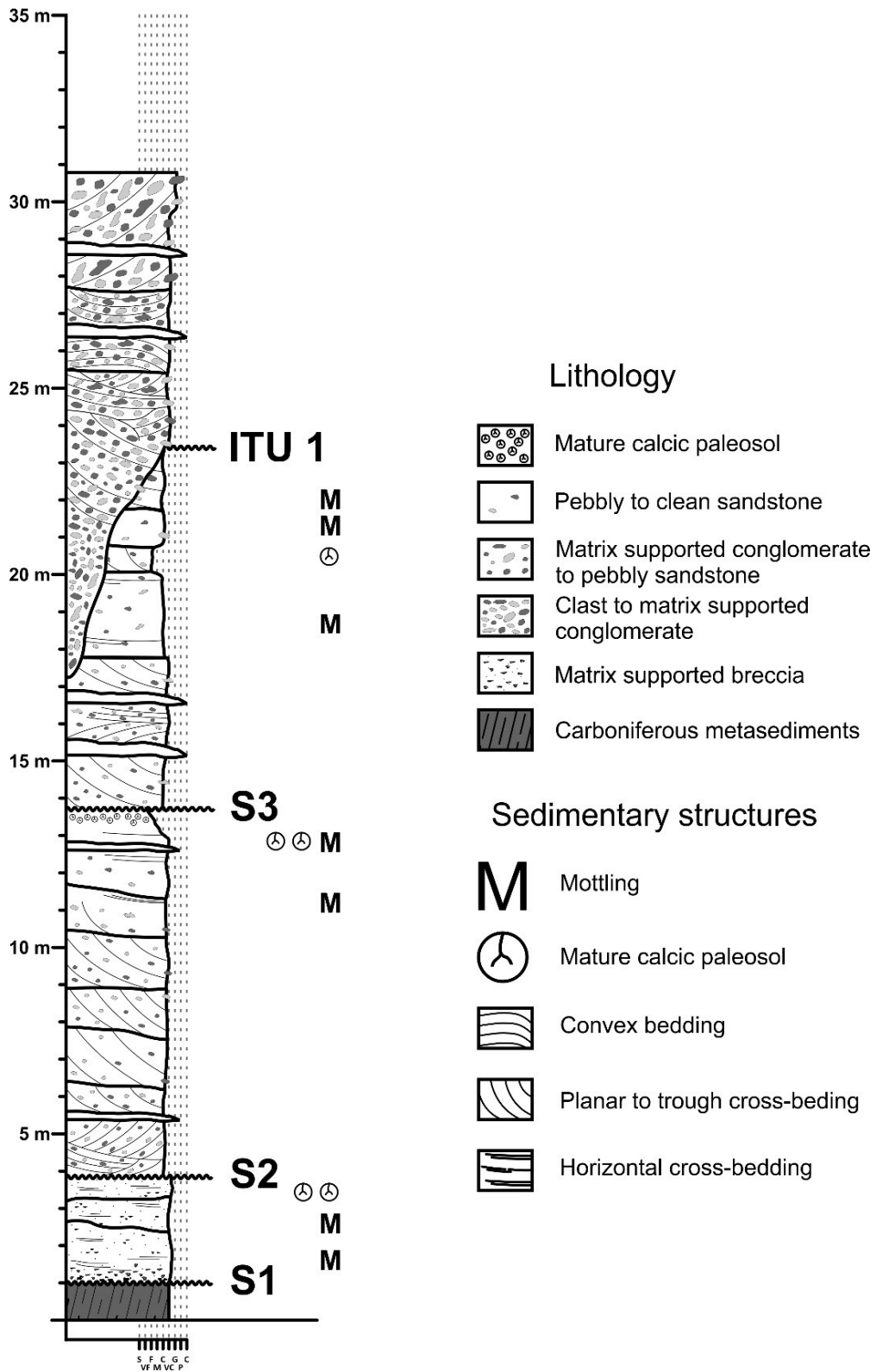


Figure 2.1: A detailed sedimentary composite-log of the Late Triassic Wolfville Formation section at Rainy Cove, Nova Scotia.. Nomenclature for bounding surfaces has been modified from Leleu et al. (2009). S surface (S1, S2, and S3) can be traced regionally and are major boundaries with evident erosion. Intra-Triassic Unconformity (ITU) are major unconformity surfaces with multi-meter (7 m) erosion relief that can be traced locally for ~100 m.

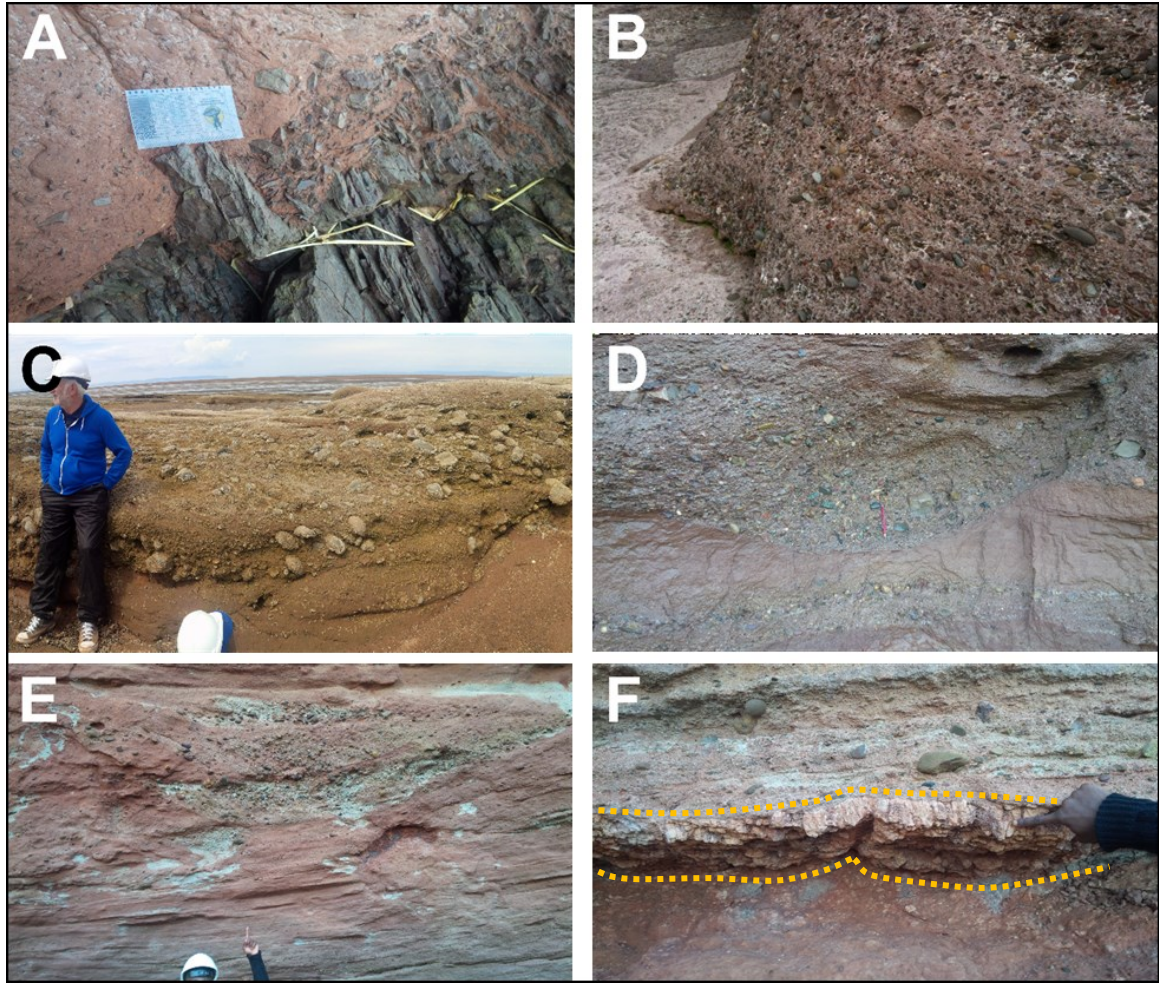


Figure 2.2: Representative facies from the Wolfville Formation near Rainy Cove, NS. A) Facies 1 – matrix supported intrabasinal-clastic breccia. The image shows the unconformable contact between the metasediments of the Carboniferous Horton Group and the overlying clastic synrift sediments of the Wolfville Formation. Angular clasts from the Horton Group are concentrated at the base of the unit and are sporadically found in the upper section. The clasts are angular and range in size from 1 cm to 15 cm. Grain size chart for scale. B) Facies 2 and 3 – clast to matrix supported conglomerate. The image shows a contact between lower, matrix supported and upper, clast supported conglomerate. Clasts from the upper section are rounded and of mixed lithologies which show imbrication and vague stratification. C) Facies 3 – matrix supported conglomerate. Rounded clasts in a coarse-grained, mildly cross-stratified sandstone matrix. D and E) Facies 3 and 4 – Matrix supported conglomeratic deposits scouring into pebbly to clean sandstone deposits. F) Facies 5 – carbonate-nodule-rich paleosol (outlined with yellow dotted line). The bottom half of the image shows a carbonate-rich, sandy zone capped by a 5 cm thick carbonate crust. Pebbly sandstone to matrix supported conglomeratic material deposits are above this layer.

2.3.3 The Chedabucto Formation

Four representative facies forming two facies associations are recognized in the Chedabucto Formation type section (Figure 2.4). Facies codes for this section have been identified using a modified version of Miall's (1977) facies classification (Table 2.1).

Facies 6: Matrix supported conglomerate

Description

Facies 6 comprises featureless to vaguely laminated, 0.05 to 1 m thick beds containing quartzitic to mafic, angular to subrounded, randomly oriented, 1 to 10 cm clasts hosted in a fine- to coarse-grained silty sandstone (Figure 2.4 F). Clasts typically comprise 10-20% of the beds, but may comprise up to 60% locally. The beds have both erosional and sharp basal contacts.

Interpretation

Matrix supported conglomerate (facies code **Gmm**) represent traction current bedload deposits (channel infill or bar deposits) related to a braided river system or debris flow deposits from local faulting (Miall, 1978; Ashley, 1990; James and Dalrymple, 2010). Random grading within the units are characteristic of debris flow deposits; however fluvially-derived bedforms are present above and beneath the successions, suggesting some fluvial reworking during deposition (Tanner and Brown, 1999)

Facies 7: Fine to coarse grained pebbly sandstone

Description

Facies 7 comprises planar to trough cross stratified, 0.2 to 1.2 m thick beds comprising rounded to sub-rounded, granular to pebbly clasts in a yellow-brown or greenish-gray, lower

fine- to upper coarse-grained sandstone with a single 10 cm clast present (Figure 2.4 D and E). Occasional parallel laminations and jointing along weathered surfaces are evident.

Interpretation

Fine- to coarse-grained pebbly sandstone (facies code **St** and **Sp**) represent bedload deposits formed in deeper parts of a braided channel system (Miall, 1978; James and Dalrymple, 2010). The cross-stratified bedforms represent subaqueous dune formation in a relatively high discharge current and, together with pebble lags and erosive basal contacts, represent deposition of sediment in multi-channel streams with significant discharge (Miall, 1978; Miall, 1996).

Facies 8: Featureless to fining upward silty-sandstone

Description

Facies 8 comprises featureless to very faint trough cross stratified and parallel laminated, 0.3 to 3 m thick sandstone beds (Figure 2.4 B, C, and D). Well-rounded, granular to pebble sized clasts occurring along bedding planes within a yellowish-red or gray, very fine- to very coarse-grained, fining upward sandstone facies. In areas of increased silt, a blocky texture is present (similar to facies 1). Upper contacts are gradational to sharp while basal contacts are sharp to erosional. Reduction halos and carbonate nodules are rare and usually occur on pinch-out sections. Small faults, possibly syn-sedimentary, are evident within some of the beds. Root traces are present but rare.

Interpretation

Featureless to fining-upward sandstone (facies code **Sm** to **Ss**) units represent bedload and suspension deposits formed in shallow channels of braided channel systems (Miall, 1978;

James and Dalrymple, 2010). Channel migration and abandonment resulted in the fining-upward sequences. Vaguely preserved sedimentary structures suggest depositional processes such as debris flows (Blair and McPherson, 1994), however the general featureless character of the beds may be due to outcrop weathering. Complete destruction of sedimentary structures due to bioturbation is unlikely due to the variable strength of discharge associated with the deposits and non-marine setting.

Facies 9: Blocky clay-siltstone

Description

Facies 9 is composed of blocky to fissile, 0.5 to 9 m beds containing reddish-brown clay-siltstone (Figure 2.4 A). The unit contains vague bedding marked by jointing, occasional zones of grayish-green mottling (reduction spots), small (1 cm) nodules, and slickensides.

Interpretation

The reddish-brown, blocky, muddy-siltstones (facies code **Fl** to **Fsm**) represent overbank to abandoned channel floodplain deposits with indications for incipient soil formation (Miall, 1978). Pedogenic slickensides and calcareous nodules indicate the onset of soil formation under sub-humid to semi-arid climatic conditions (Tanner and Brown, 1999).

Facies Associations

The alluvial fan facies association constitutes roughly 5 to 10 % of the sections and comprises matrix supported conglomerate (facies 6). The matrix supported conglomerate was deposited as alluvial debris flows in topographic lows, driven by syn-sedimentary faulting along the basin margin and climatic influences.

The fluvial facies association constitutes between 90 to 95 % of the sections and comprises matrix supported conglomerate (facies 6), pebbly sandstone (facies 7), silty-sandstone (facies 8), and clay-siltstone (facies 9). The conglomerate and sandstone facies were deposited as traction bedload deposits during high to low energy output in fluvial channels. The clay-siltstone facies (facies 9) was deposited as fines in a fluvial overbank or abandoned channel floodplain setting.

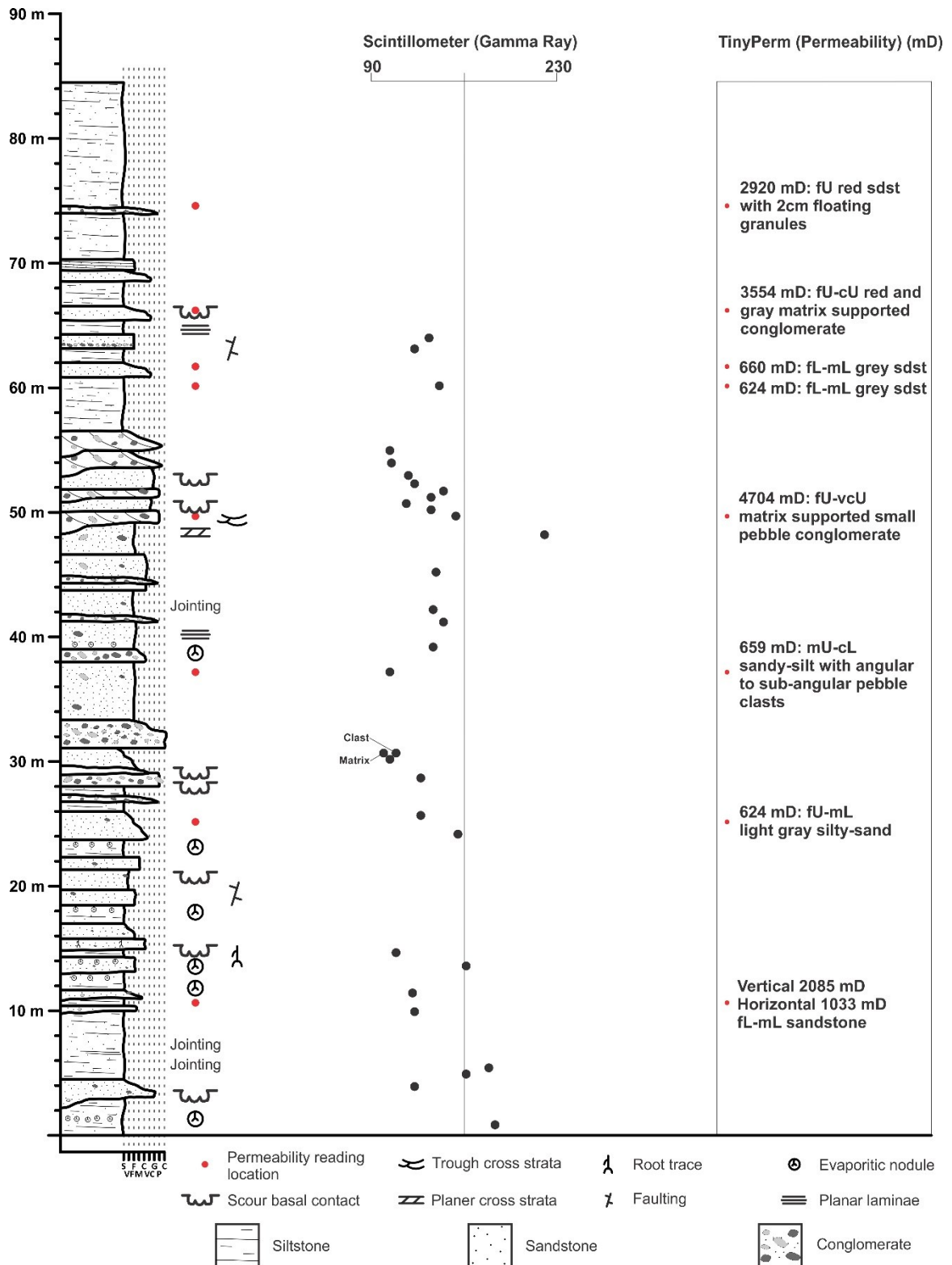


Figure 2.3: A detailed sedimentary log of the Late Triassic Chedabucto Formation section near McCaul Island, Nova Scotia; (left) a lithology log showing bed interval thickness, sedimentary structures, and faulting; (middle) a gamma ray log showing the gamma ray values of selected beds; (right) a chart showing field-recorded permeability values with a brief description of the bed lithology.

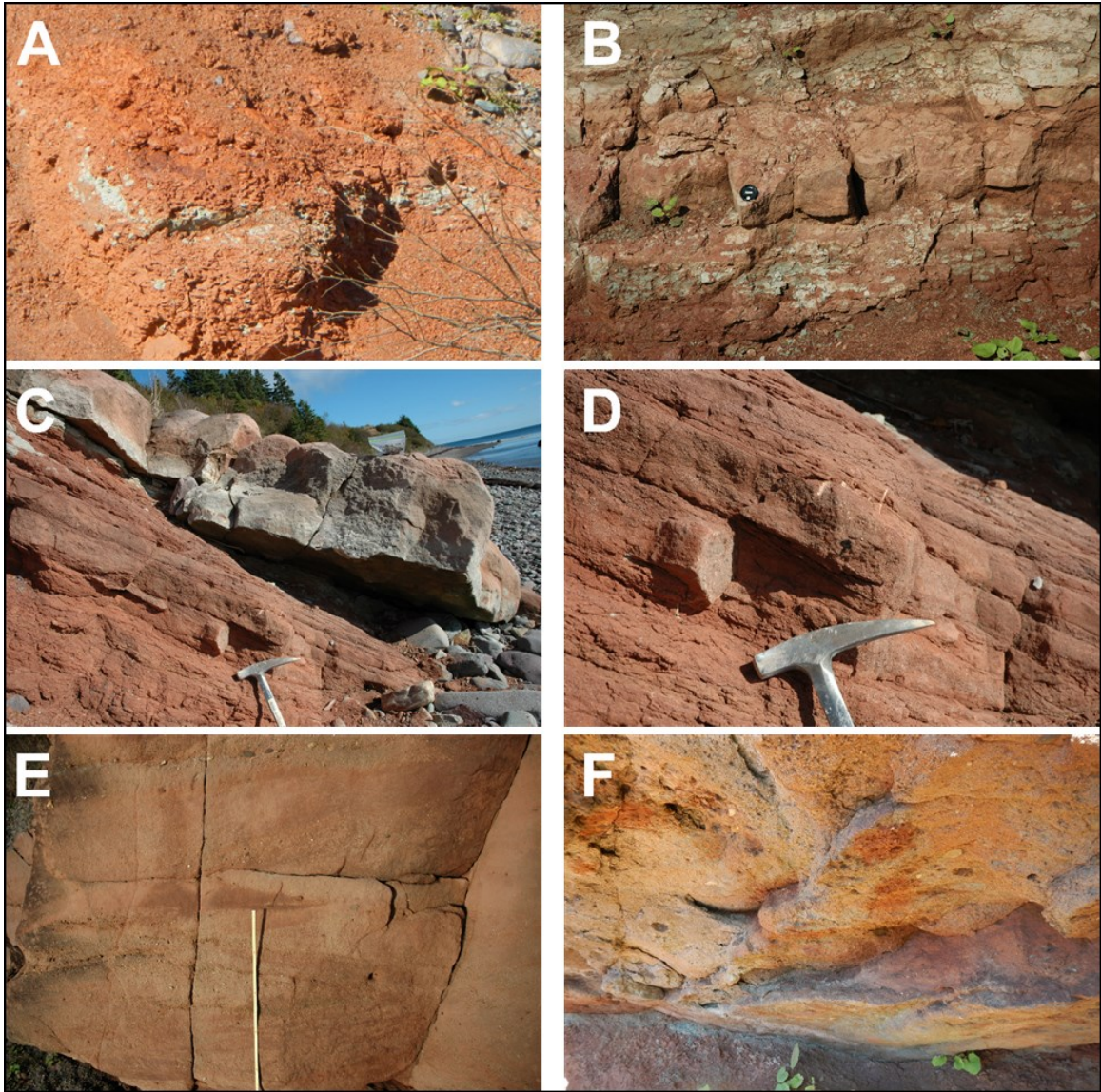


Figure 2.4: Representative facies from the Chedabucto Formation type section near McCaul Island, NS. A) Facies 9 – reddish-brown blocky muddy siltstone. The unit appears fissile to blocky and contains a thin layer of reduction spots. B) Facies 9 and 8 – The lower and upper portions of the image are of the blocky, muddy siltstone of facies 9. A 20 cm thick lens of featureless silty sandstone extends horizontally through the center which represents an isolated channel between two interfluvial events. C and D) Facies 7 and 8 – The lower section of the photo shows a red, fine to coarse-grained pebbly sandstone. This bed is mildly laminated and contains small clasts (see bottom left corner) and gray spots of reduction. Separated by a sharp contact, the bed above is a fining upward sandstone that is gray in colour (hammer for scale). D) Zoom of image C highlighting the coarser grain size of the sandstone beds. E) Facies 7 – cross-stratified pebbly sandstone containing pebbles marking cross-strata. Clasts are generally rounded and variable in nature (50 cm long scale bar in image) F) Facies 6 – The underside of a matrix supported conglomerate bed. Clasts are variable lithology, 1 to 10 cm in size, rounded, and are held in a medium to very coarse-grained sandstone matrix. A sharp contact with an underlying featureless silty sandstone marks the base of this unit.

2.3.4 The Eurydice Formation

Three representative facies forming two facies associations are recognized in the Eurydice Formation from core of the Eurydice P-36 well. The workflow for core description can be found in Appendix D. A summary of the facies and facies associations can be found in Table 2.3, a logged core section in Figure 2.5, and representative photographs of each facies in Figure 2.6, Figure 2.7, and Figure 2.8. Facies codes for this section have been identified using coastal process classification ternary plots (wave, tidal, or fluvial dominated) from Ainsworth (2011).

Facies 10: Cross-stratified sandstone

Description

Facies 10 comprises cross-stratified, 2 to 45 cm thick beds containing very fine- to fine-grained, sub-angular to sub-rounded, yellowish-brown sandstone (Figure 2.6). Beds showing preserved sedimentary structures including low- to high-angle, concave-up cross-stratification and bipolar-oriented planar cross-stratification, both of which may contain millimeter scale silt-rich laminae and silt rip-up clasts. The structures are, on average, 1 cm in height and 3 cm in length. The contacts between beds are typically sharp and can be marked by thin laminae of reddish-brown siltstone, but this is not always the case. This facies comprises up to 15% of the Eurydice Formation type section.

Interpretation

Cross-stratified sandstone facies represent a wave-dominated, lowermost tidal flat depositional system (Davis et al., 2011). The low- to high-angle trough cross-stratification features are current ripples which deposited by high-energy environments. The higher energy is also indicated by the presence of rip-up clasts from thin silt laminations between sand bodies,

when present. Tidal influence in the system is present as bipolar oriented sequential planar cross-stratified beds suggesting deposition from currents of ebb and flood tides.

Facies 11: Heterolithic sandstone and siltstone

Description

Facies 11 comprises alternating sandstone and siltstone, 5 to 50 cm thick beds containing reddish-brown, featureless siltstone and yellowish-brown, very fine- to fine-grained, cross-bedded sandstone (Figure 2.7). Flaser to lenticular bedding dominate this unit, but sections of planar laminated siltstone and sandstone are evident. The siltstone may contain occasional small (<1 mm) anhydrite nodules. Bedforms within the sands display low- and high-angle cross-stratification and wavy upper, sharp basal contacts. Biogenic sedimentary structures include a single shell fragment (3 cm in length) and a number of trace fossils including five identified ichnospecies. Horizontal and vertical burrows are evident. This facies comprises approximately 35% of the Eurydice Formation type section.

Interpretation

Alternating sandstones and siltstones represent heterolithic bedding (flaser and lenticular) which deposit in a mixed energy tidal-flat system and is characteristic of tidal rhythmites (Smith et al., 1991; Hovikoski et al., 2008). Periods of relatively higher energy (sand deposition during high tidal currents) alternate with periods of relative quiescence (silt deposition during slack water). The reddish colour of both the silts and sands suggests oxidation of the sediments through periodic exposure to the atmosphere. Anhydrite nodules indicate the system was under evaporitic stress, in an arid to semi-arid climate. Silt rip-up clasts within the sandstone units suggest increased energy in the system. Near-symmetrical ripples suggest bidirectional flow of water during deposition, suggesting opposing tidal currents such as ebb and

flood tides. Trace fossils were interpreted as *Anconichnus*, *Diplocraterion*, *Skolithos*, *Palaeophycus*, *Conichnus*.

Facies 12: Poorly stratified to featureless sandy-siltstone

Description

Facies 12 comprises poorly stratified to featureless, 1 m thick beds containing reddish-brown siltstone, very fine-grained sandstone, and small (1-3 mm) to large (5 cm) anhydrite nodules. The lithofacies may be vaguely stratified with sporadic occurrences of sandstone and sub-parallel aligned, elongate anhydrite nodules (Figure 2.8). In areas where featureless, very fine-grained sandstone and sporadic anhydrite nodules are present but have no preferred orientation. The facies comprises approximately 50% of the total type section.

Interpretation

The poorly stratified to featureless reddish-brown siltstones represent suspended sediment settling in a low-energy mud flat system marking the transition between the intertidal zone or the lower part of the supratidal zone (Smith et al., 1991; Fenies and Tastet, 1998; Davis et al., 2011). The reddish-brown colour suggests subaerial exposure. The sporadic occurrence of sand suggests higher energy transportation mechanisms and represents either a transition into a mixed flat environment or proximity of a tidal channel (James and Dalrymple, 2010). Anhydrite nodules represent deposition under climatic stress (arid to semi-arid conditions) in shallow marine to non-marine sabkha environments (James and Dalrymple, 2010).

Facies Associations

The wave facies association constitutes roughly 15% of the Eurydice P-36 core and comprises cross-stratified sandstone (facies 10). This facies association was deposited in a wave-dominated, tidally-influenced estuarine environment

The tidal facies association constitutes roughly 85% of the Eurydice P-36 core and includes heterolithic sandstone and siltstone (facies 11) and poorly stratified to featureless sandy-siltstone (facies 12). The heterolithic sandstone and featureless siltstone (mudstone) suggest that the sediments were deposited dominantly in a tidal flat / estuary with possible wave and fluvial influence.

2.3.5 Summary

A total of twelve lithofacies were identified and used in this outcrop and core study. In the Wolfville Formation at Rainy Cove, five lithofacies were identified and together can be used to identify two facies associations (alluvial fan and fluvial). In the Chedabucto Formation at McCaul Island, four lithofacies were identified and together are used to identify two facies associations (alluvial fan and fluvial). In the Eurydice Formation, three lithofacies were identified and used to show to presence of two facies associations (intertidal wave / estuarine and tidal flat).

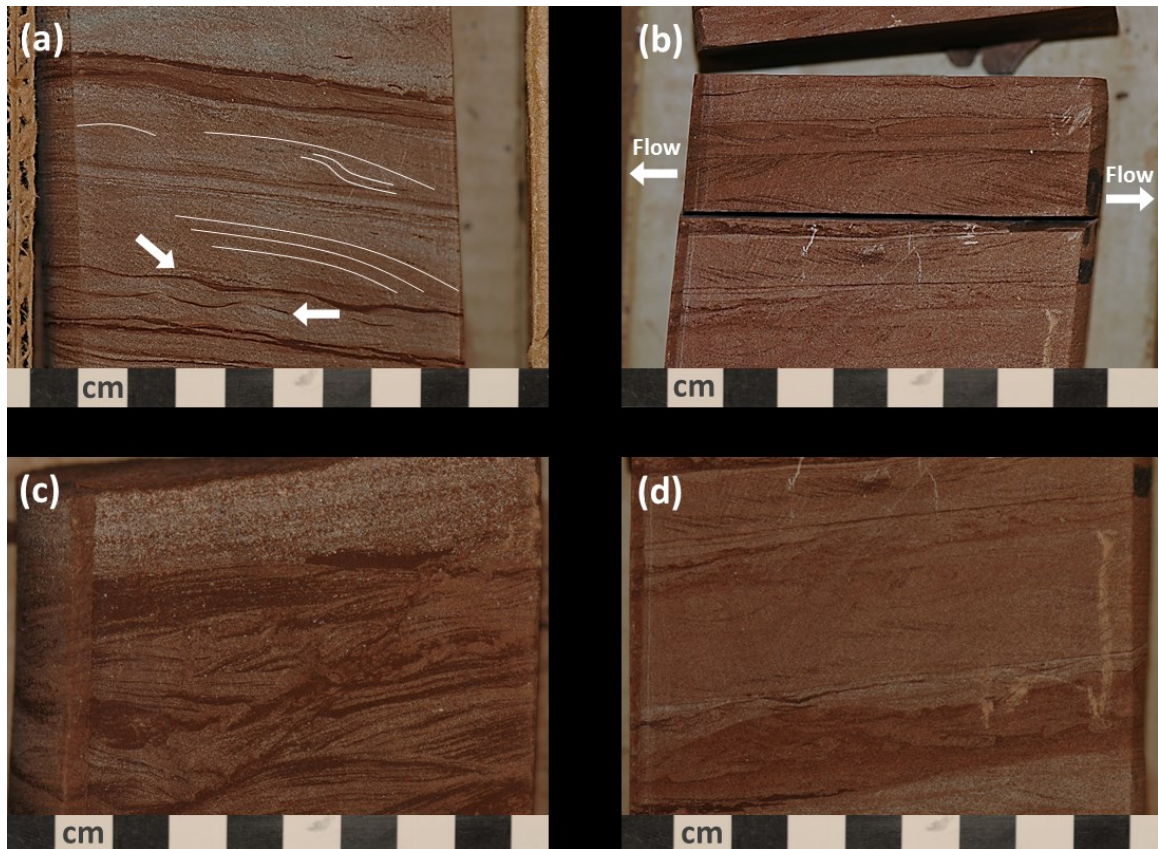


Figure 2.6: Representative photographs from facies 10 (cross stratified sandstone) from the Eurydice Formation type section from the Eurydice P-36 offshore well. (a) alternating layers of sand and silt. The sandstone contains preserved crossbedding and on occasion rippled top boundaries. The siltstone layers are approximately a mm thick and deposit along the tops of sandstone beds or within the troughs of ripples from the sandstone beds. (b) alternating trough cross laminations with interpreted flow direction. (c) climbing ripples composed of sand and silt. (d) a thick sandstone to silty sandstone unit. No clean siltstone layer is noted, suggesting continuous higher energy deposition.

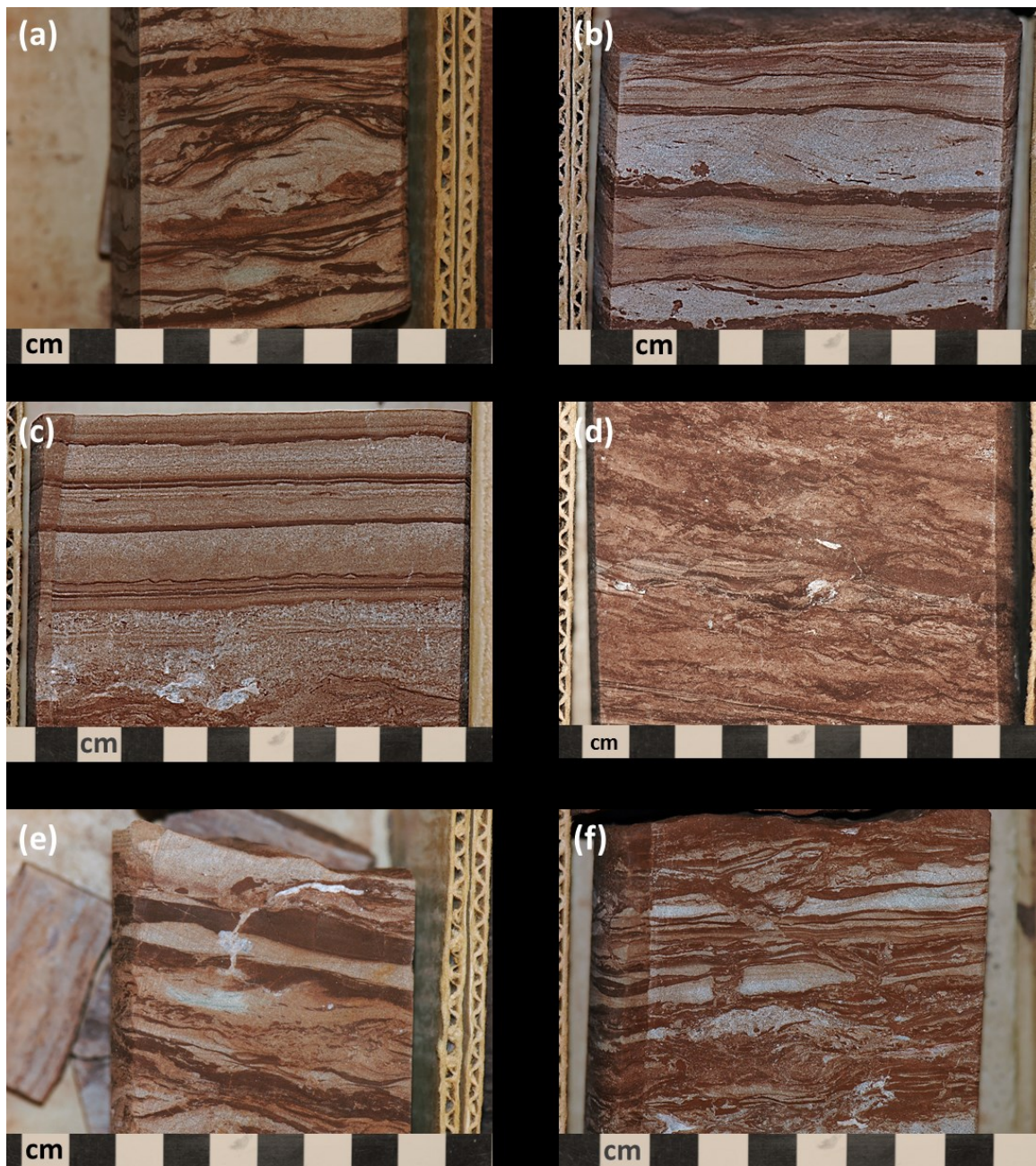


Figure 2.7: Representative photographs from facies 11 (Heterolithic sandstone and siltstone) from the Eurydice Formation type section from the Eurydice P-36 offshore well. (a & b) representative images of the heterolithic bedding which is persistent within this facies. Alternating sandstone and siltstone layers, of various thicknesses, with silt rip up clasts and crossbedding within the sand units. (c) horizontal alternating sandstone and siltstone tidal rhythmites. Sand-poor packages suggest neap-tides while sand-rich packages suggest spring-tides. Sandstone units commonly have rippled upper boundaries. (d) faulted perturbed heterolithic sandstone. (e) shell fragment within heterolithic bedding. (f) vertical trace burrow with highly perturbed upper and lower layers.

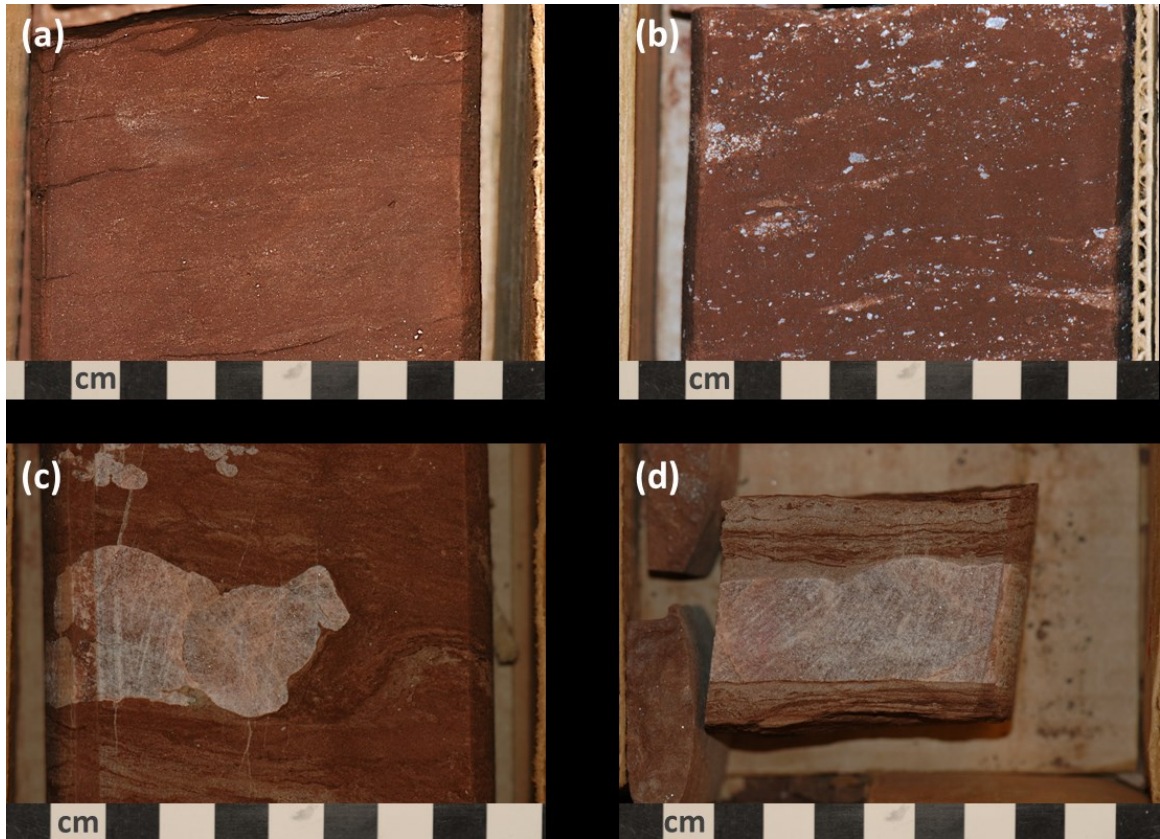


Figure 2.8: Representative photographs from facies 12 (Poorly stratified to featureless sandy siltstone) from the Eurydice Formation type section from the Eurydice P-36 offshore well. (a) featureless siltstone with vague, small anhydrite nodules. (b) siltstone with parallel to subparallel oriented sandstone layers and mm sized anhydrite nodules. (c) large anhydrite nodule in a siltstone dominated matrix. (d) A complete layer of evaporitic deposition.

2.4 Fluvial Architecture and Paleoflow of the Wolfville and Chedabucto Formations

2.4.1 Architectural elements – Definition and Use

Architectural elements were first introduced by Allen (1983) and summarized by Miall et al. (1985; 1996) as a method for facies analysis applied to fluvial successions. Allen (1983) believed the existing and widely accepted method (facies models), which relied principally on vertical profiles, did not adequately represent the three dimensional heterogeneities in facies and geometries which were present in fluvial systems. Miall (1985) defined architectural elements as “lithosomes characterized by geometry, facies composition, and scale which represent a particular process or suite of processes occurring within a depositional system” and suggested that a good application of the method requires “outcrops that are big enough to reveal their cross sectional geometry.” Architectural elements, as well as facies, lateral trends, and geometry, are commonly grouped together in distinct units, characteristic of a particular depositional setting, known as facies associations (Reading, 1996).

A total of seven architectural elements were defined in this study. Classification is based on, and modified from, schemes of Miall (1977; 1996) (Table 2.2). Channel fill and bar architectural elements consist of channels (CH), gravel bars and bedforms (GB), sandy bedforms (SB), downstream accretion macroforms (DA), sediment gravity flows (SG), and laminated sand sheets (LS). Architectural elements of overbank environments consist of floodplain fines of abandoned channels (FF). Due to the gravelly nature of the Wolfville Formation at Rainy Cove, and the dip of the beds obscuring the lateral continuity of the Chedabucto Formation, some beds could not readily be attributed to any element.

In this section, the Wolfville and Chedabucto formations are analyzed using the architecture element analysis technique from Miall (1985).

2.4.2 Wolfville Formation

2.4.2.1 Overview

The Wolfville Formation is the oldest synrift unit within the Minas Subbasin. At its maximum the unit is thought to be up to 3000 m in thickness and sits unconformably on Carboniferous and older metasediments and igneous rocks of the Meguma Terrane (Wade et al., 1996). The formation comprises synrift sediments consisting of alluvial fan, fluvial, lacustrine, and aeolian deposits which were deposited as early as the Anisian (Middle Triassic) (Wade et al., 1996; Sues and Olsen, 2015).

At Rainy Cove, the formation contains coarse-grained alluvial and fluvial sediments which lie unconformably on pre-rift metasediments of the Carboniferous Horton Group (Figure 2.9). Previous sedimentological work in the area (Leleu et al., 2009; 2010) examined the lithofacies and sedimentary architecture, highlighting the presence of local and regional bounding erosional surfaces and their relationship to lithofacies. The work defined the system as an erosion-dominated, large-scale, sheet-like series of stacked fluvial bodies of coarse lithic sandstone to clast supported conglomerate.

The bounding surfaces (Figure 2.10) in this study have been modified from work by Leleu et al. (2009). Bounding surface S1 marks the onset of rifting and the initial influx of sediment into the Minas Basin. Sediment deposited comprises matrix supported breccia. S2 and S3 mark major bounding surfaces indicating onset of fluvial rejuvenation within the system. The sediment deposited typically includes pebbly sandstone with some conglomeratic material. These bounding surfaces are correlateable across the study area. The last bounding surface at the

study location is the intra-Triassic unconformity (ITU 1). This boundary has up to 7 m of erosion into the previously deposited fluvial sediments and, rather than being laterally continuous across the study location, it is only 35 to 40 m in width. Infill within this channel comprises a series of cut and fill conglomerates and coarse grained, poorly sorted sandstones. The following provides an overview of the architectural elements and their relationships to the bounding surfaces at Rainy Cove (Figure 2.11 and Figure 2.12).

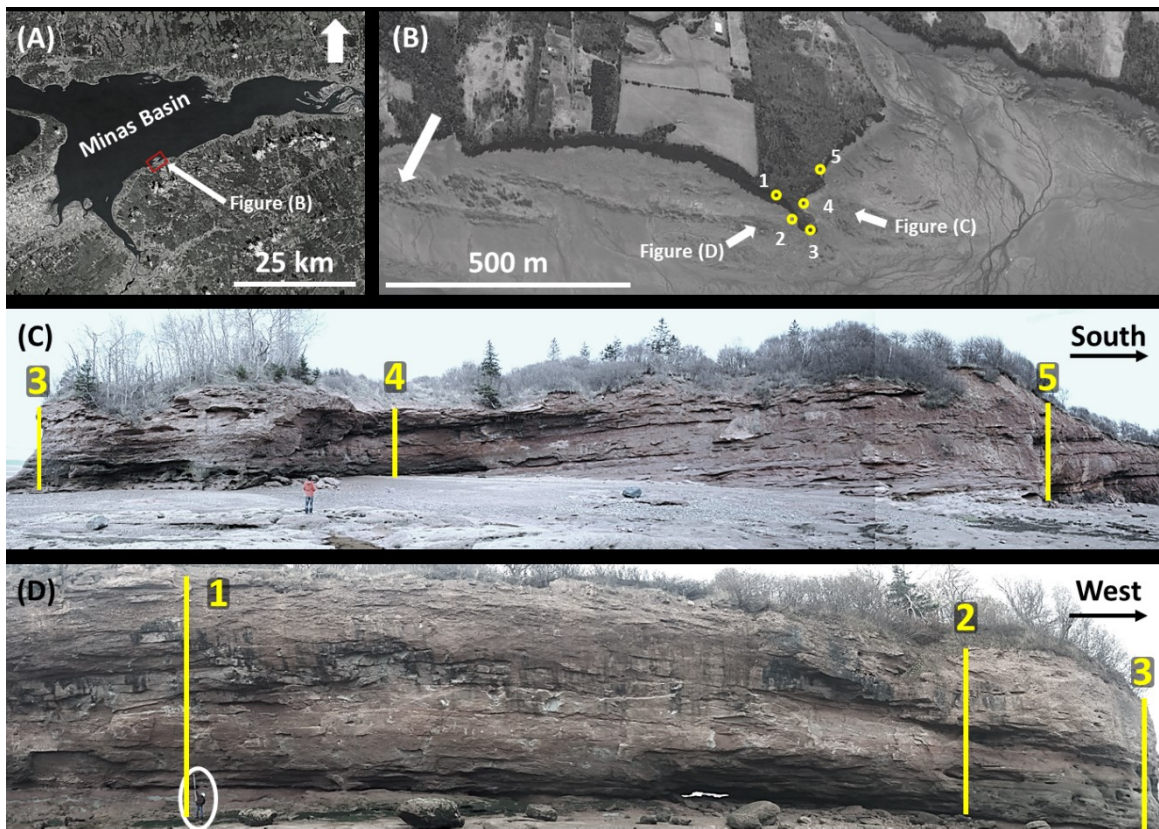


Figure 2.9: Map location and field view of the studied Wolfville Formation at Rainy Cove. (A) map view showing the general location of Rainy Cove within the Minas Basin, Nova Scotia. (B) Map view of the study area at Rainy Cove. The bottom of the image shows the intertidal zone which was traversed to gain access to the cliff face. The numbered circles identify the locations of five measured sections described for this study. Arrows represent the location and directions in which field view images were captured. (C & D) Field view of the studied Wolfville Formation at Rainy Cove. Image (C) captures the southwestern side of the promontory and shows the location for three of the measured sections. Image (D) captures the northeastern side of the promontory and shows the location for three of the measured sections. Measured section three was captured at the point of the promontory and appears in both field view images. Note the circled person for scale.

2.4.2.2 Architectural Elements

The lowermost section of the Wolfville Formation at Rainy Cove is composed of five architectural elements (Table 2.2, Figure 2.11, Figure 2.12, and Figure 2.13) which include: (1) gravel bars and bedforms (42 %), (2) sandy bedforms (22%), (3) downstream accretion macroforms (18%), (4) sediment gravity flows (13%), (5) and laminated sandsheets (5%). These elements for the Wolfville Formation are described below.

Gravel bars and bedforms (**GB**) elements compose 42% of the architectural elements in the Wolfville Formation observed at Rainy Cove. These elements are composed of clast and matrix supported conglomerate (facies F2 and F3) and represent large gravel dunes which are preserved in both the cliff face and in the intertidal zone. The dunes are laterally discontinuous, 1 to 3 m in height, and are highly variable in size 3 m to 10's of m wide. These elements can be traced for long distances in the intertidal zone and offer excellent exposures for paleoflow indications. These deposits form in channel and channel margin blanket barforms.

Sandy bedform (**SB**) elements compose 22% of the architectural elements in the Wolfville Formation at Rainy Cove. These elements are dominated by matrix-supported conglomerate and pebbly medium- to very coarse-grained sandstone (facies F3 and F2) and were deposited along with the GB elements parallel to flow. Planar and trough cross-beds are present within these elements. These represent in channel fill and contribute to in-channel bars, but occur in lower energy flows compared to element GB. Due to the gradation of this element with the gravel bar element, the size and distribution is difficult to discern. However, it can be assumed to be similar to that of the gravel bar element.

Downstream accretion macroforms (**DA**) comprise 18% of the architectural elements of the Wolfville Formation at Rainy Cove. These elements are dominated by matrix-supported

conglomerate and pebbly to clean sandstones (facies F3 and F4). They occur in the cliff outcrop as lenses with convex up erosional surfaces and are similar in size to the gravel bar elements. These elements deposits parallel to paleoflow.

Sediment gravity flow (**SG**) elements compose 13% of the architectural elements in the Wolfville Formation at Rainy Cove. These elements are composed of matrix supported intrabasinal clastic breccia (facies F1) and were deposited as gravity driven, high strength debris flows. These elements for 0.5 to 1.5 m thick beds and appear to be laterally continuous, however their lateral exposure is limited to approximately 50 m. These successions form thick sheet deposits marking the onset of rifting.

Laminated sandsheet (**LS**) elements comprise 5% of the architectural elements in the Wolfville Formation at Rainy Cove. These elements are composed of pebbly to clean sandstone (facies F4), were deposited parallel to paleoflow, and are dominated by horizontal laminations. Bedsets range in thickness from 0.5 to 1 m and are laterally confined to 1 to 2 meters. These elements appear as clearly defined beds within the gravel bar elements and only occur above the ITU 1 erosional surface at Rainy Cove.

2.4.2.3 Paleocurrents

Paleocurrent indicators abundant at this exposure and consist of trough cross bedded sandstones in cliff outcrop and in preserved 3D dunes exposed in the intertidal zone. Six paleocurrent measurements were made from the outcrop at Rainy Cove, with azimuths ranging from 340°-016° N, with a mean paleoflow direction of 354° N (Figure 2.23). This direction poses southward constraints on the source of infill during early synrift sediment deposition.

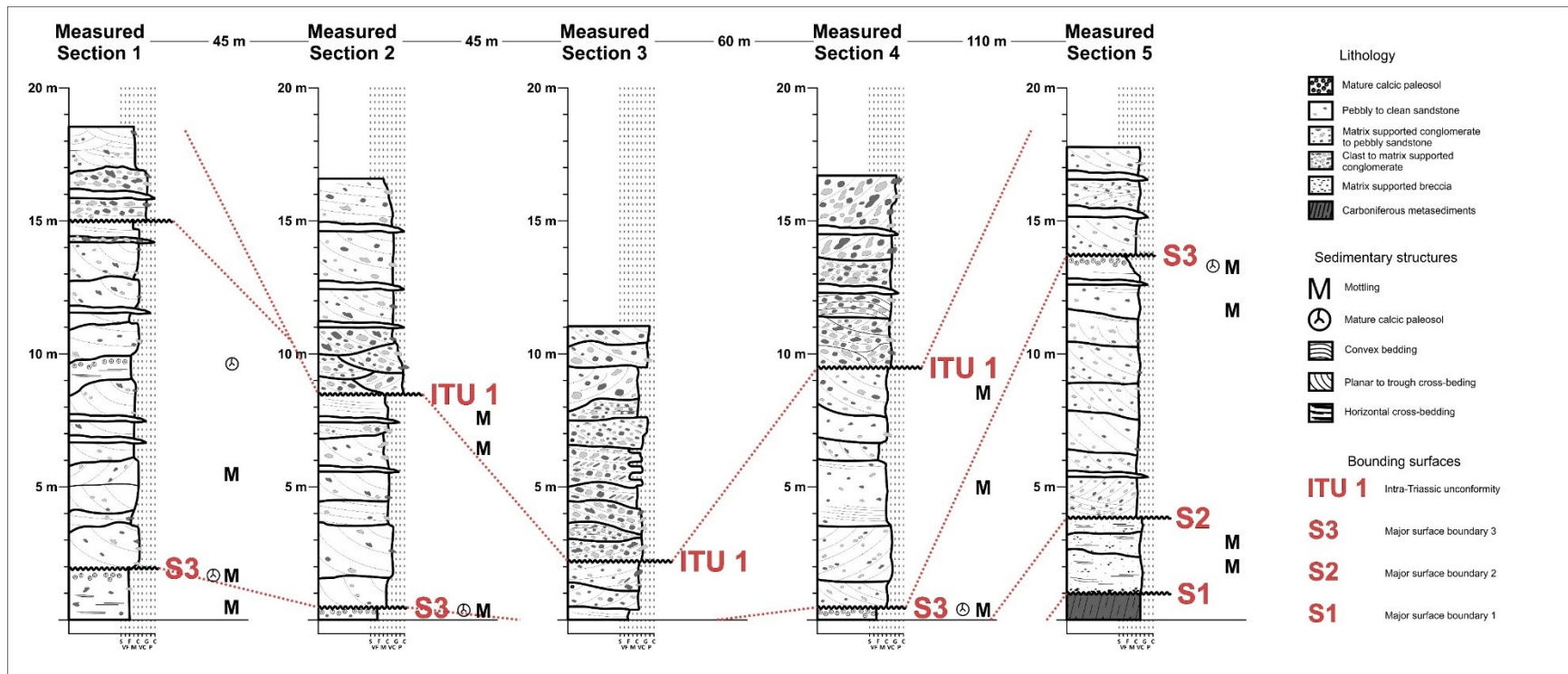
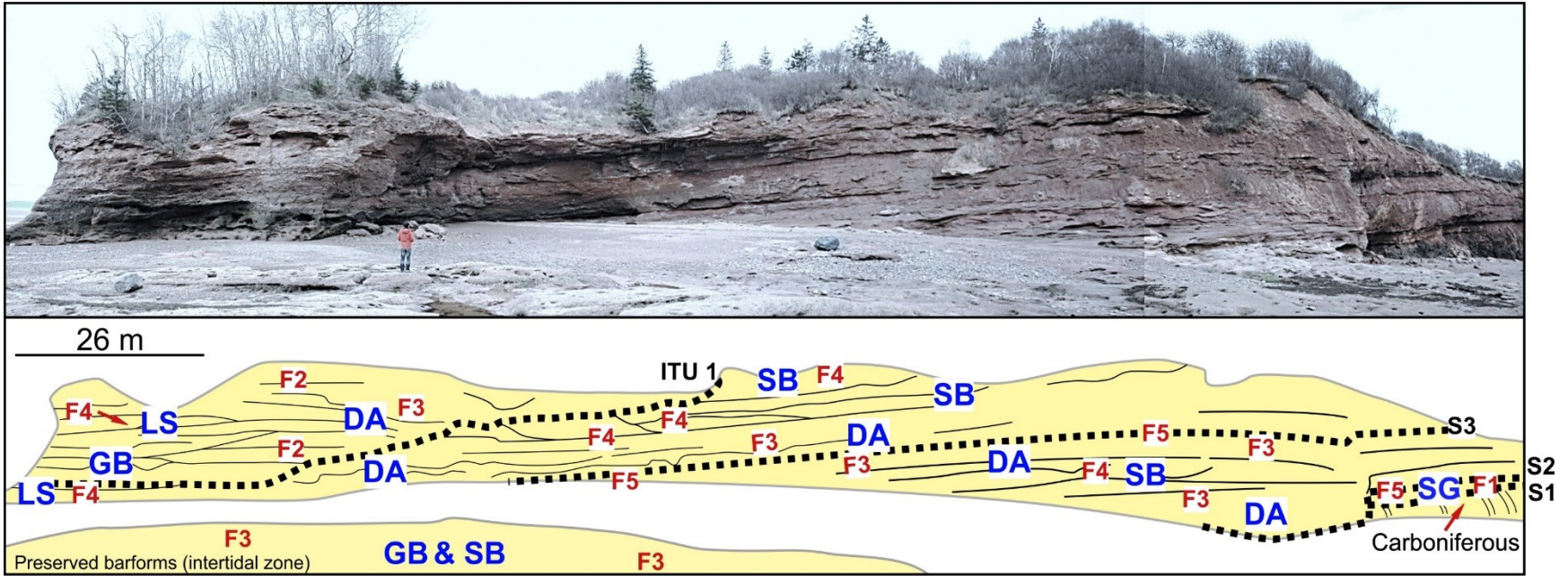


Figure 2.10: Five measured sections from the Wolfville Formation at Rainy Cove. The location of the measured sections is found in Figure 2.9. The sections display the lithology, sedimentary structures, and the major bounding surfaces found in the Wolfville Formation at Rainy Cove.



65

Figure 2.11: Field view of the Wolfville Formation at Rainy Cove with sketch showing the facies distribution and architectural elements present within the outcrop. Solid lines represent major bounding surfaces which can be traced through the outcrop (labelled S1, S2, S3, and ITU 1). Dotted lines represent evident but minor bedding surfaces, many of which are not continuous through the outcrop due to stratigraphic pinch out, erosion from overlying beds, or weathering of the outcrop. Symbols F1 through F5 are the facies which a description of these facies can be found in Table 2.3. Architectural elements present in the outcrop are listed in blue and are selected based on classification from Miall (1985)

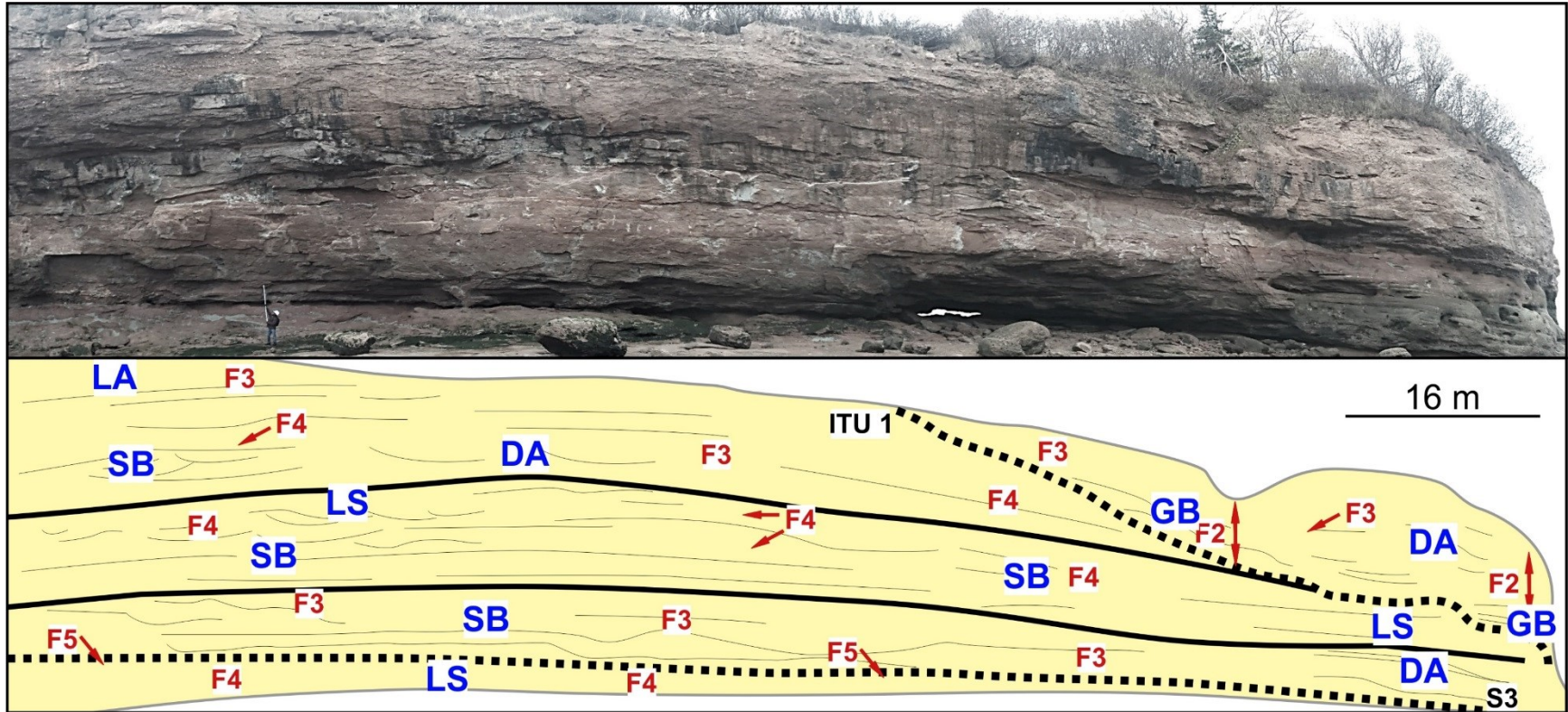


Figure 2.12: Field view of the Wolfville Formation at Rainy Cove sketch showing the facies distribution and architectural elements present within the outcrop. Solid lines represent major bounding surfaces which can be traced through the outcrop (labelled S1, S2, S3, and ITU 1). Dotted lines represent evident but minor bedding surfaces, many of which are not continuous through the outcrop due to stratigraphic pinch out, erosion from overlying beds, or weathering of the outcrop. Symbols F1 through F5 are the facies which a description of these facies can be found in Table 2.3. Architectural elements present in the outcrop are listed in blue and are selected based on classification from Miall (1985)

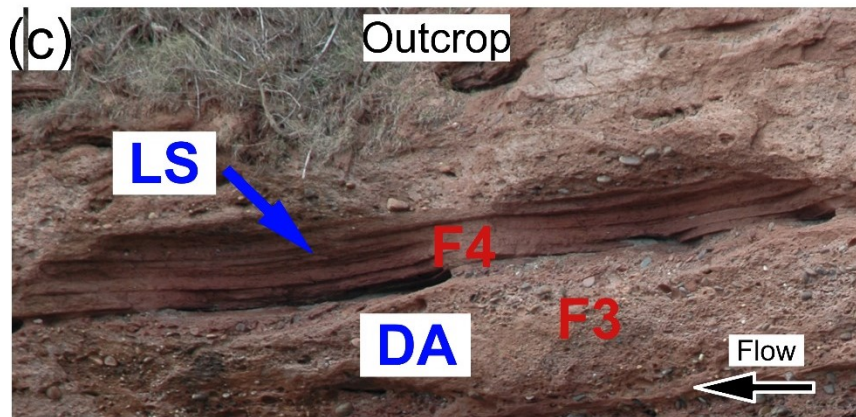
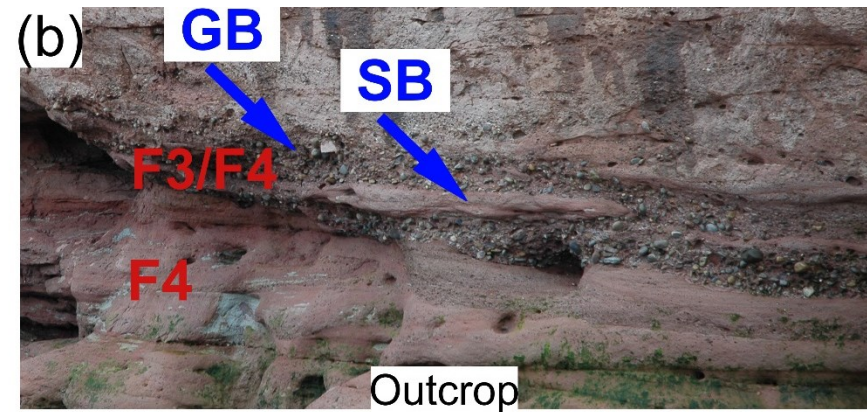
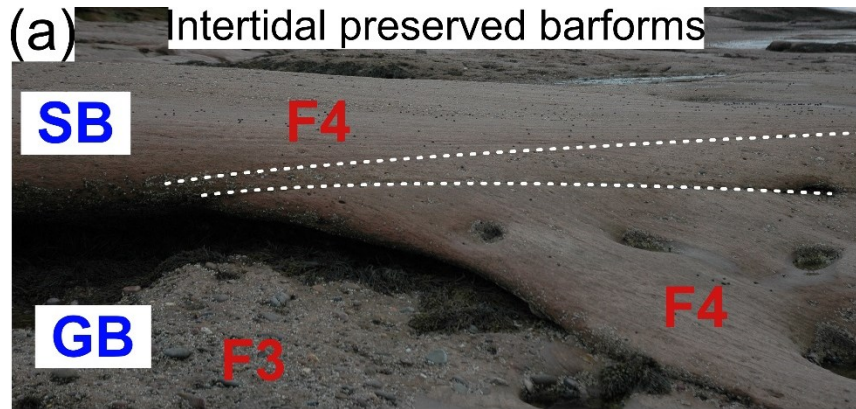


Figure 2.13: Examples of architectural elements and associated facies from the Wolfville Formation at Rainy Cove. (a) from the preserved barforms in the intertidal zone, two architectural elements are visible; (1) SB (sandy bedforms) and (2) GB (gravel bars and bedforms). (b) From outcrop the same two architectural elements as in image (a). (c) Architectural elements LA (laminated sand sheet) and DA (downstream-accretion macroform). (d) Architectural element SG (sediment gravity flow).

2.4.3 Chedabucto Formation

2.4.3.1 Overview

The Chedabucto Formation is presumed to be Late Triassic aged synrift succession comprising predominantly fluvial deposits. These deposits are believed to be updip equivalents to deep synrift successions in the Orpheus Graben and lateral equivalents of middle to upper Wolfville Formation successions of the Minas Basin (Tanner and Brown, 1999; 2003). At McCaul Island, the Chedabucto Formation comprises interbedded conglomerate, sandstone, and mudstone. The succession is believed to have been deposited in a sand-dominated braid-fluvial system with minor debris flow deposits derived from local talus faulting (Tanner and Brown, 1999). The following section provides an overview of the architectural elements of the Chedabucto Formation present at McCaul Island. This work confirms the conclusions from Tanner and Brown (1999), but is a more refined interpretation and adds further information on the distribution of architectural elements along the synrift margins of Nova Scotia.

2.4.3.2 Architectural Elements

The Chedabucto Formation near McCaul Island is composed of four architectural elements (Figure 2.15, Figure 2.16, and Figure 2.17) which include: (1) gravel bar and bedforms (4%), (2) sandy bedforms/channel elements (46%), and (3) abandoned channel or floodplain fines elements (50%). These elements are described below.

Gravel bars and bedform (**GB**) elements compose 4% of the architectural elements of the Chedabucto Formation at McCaul Island. These elements dominantly comprise matrix supported, conglomerate (facies F6). The lateral relationship of these elements are obscured due to the dip of the outcrop, however their bedset thickness ranges between 0.1 cm to 0.5 m

and appears constant over the observable lateral extent. These elements represent in-channel fill and minor in-channel or marginal bars.

Sandy bedform (**SB**) and channel (**CH**) elements compose 46% of the architectural elements of the Chedabucto Formation at McCaul Island (Figures 2.16 and 2.17). These elements are composed of fine- to coarse-grained pebbly sandstones which can be planar and trough cross stratified or featureless and fining upward. These elements are occasionally interbedded with gravel bar and bedform elements and range in thickness from 10 cm to 2.5 m. The lateral relationship of the element is largely obscured due to the dip of the outcrop but the bedsets are noted to have erosional basal contacts and deposited as lenses and sheets comprising channel infill. Two channels are present at the base of the section, shown in the strike orientation in outcrop. These channels are lens-shaped with an erosional base and convex-up upper boundaries. The first channel is 1.5 m thick and 15 m wide, whereas the second is 0.06 m thick and but extends over 60 m in width.

Floodplain fine (abandoned channel) (**FF**) elements compose 50% of the architectural elements of the Chedabucto Formation at McCaul Island (Figure 2.15 and 2.16). This architectural element is dominantly composed of siltstone (facies F9) but also contains some fine grained sandstone (facies F8). This element is either deposited parallel to paleoflow (abandoned channel) or in any direction relative to paleoflow (floodplain). Thickness of the element ranges from 10's of cm's to 10 m. This element is present at the base of the section, which shows the strike orientation in outcrop. The element can be traced laterally for over 100 m, with little variation in element thickness.

2.4.3.3 Paleocurrents

Paleocurrent indicators are scarce at this exposure and consist of planar cross bedded sandstones in cliff outcrop. Two paleocurrent measurements were made from the outcrop with azimuths ranging from 110°-112° N, with a mean paleoflow direction of 111° N. These measurements are representative of the entire section and show a drastic change in orientation from paleocurrent data collected at Rainy Cove within the Minas Basin.

2.4.3.4 Palynology

Palynological data from four samples from the Chedabucto Formation generated one positive result showing the presence of an *in situ* pollen grain in Sample GW 304. It was identified as the genus *Classopollis sp.* which has a range from Triassic (Norian) to middle Cretaceous (Fensome, 2013, pers. comm.; Appendix B). Although this range is broad, the source lithologies are very similar to Late Triassic rocks in the Minas Subbasin to the west, they rest on basement rocks, and dip to the east into the Orpheus Graben. It is therefore believed that these sediments, younger than the Carnian Wolfville Formation, equate to the overlying Norian Blomidon Formation in the Fundy Basin complex

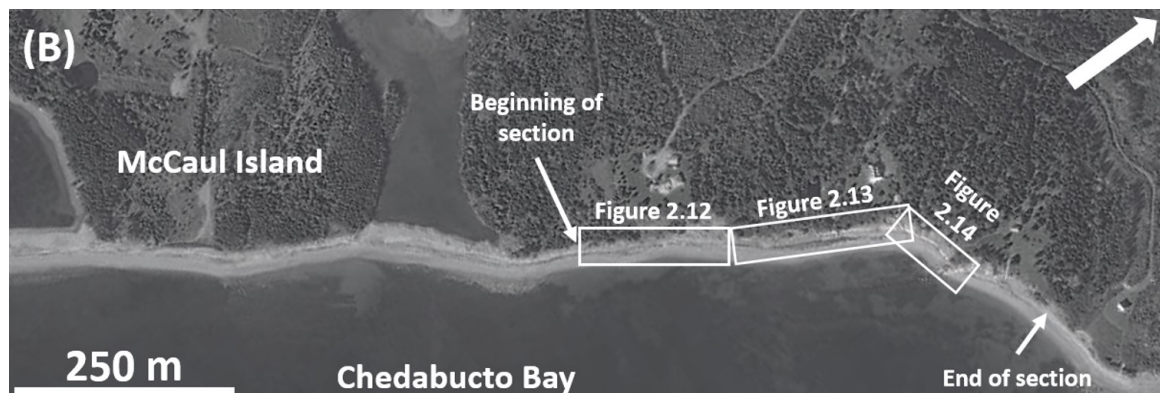


Figure 2.14: Map view of McCaul Island the location of the Chedabucto Formation type section. The beginning and end of the section are noted as well as the location of panoramic photo collages of the outcrop with facies and architectural element descriptions.

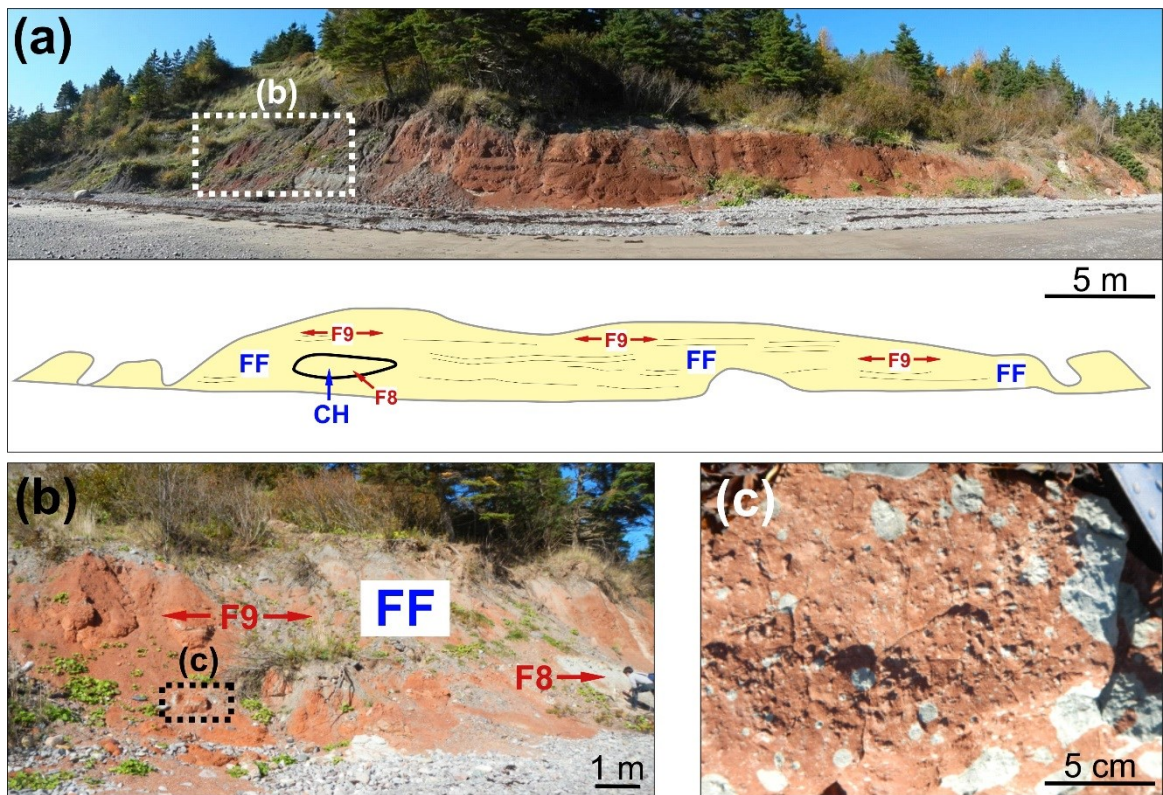


Figure 2.15: Field view, facies distribution, and architectural elements of the Chedabucto Formation at McCaul Island. (a) Base of the section with a sketch showing the distribution of facies and the presence of FF and CH architectural elements. (b) Examples of facies and architectural elements at the base of section. (c) Facies 9 (F9) showing gray redox spotting in clay-siltstone

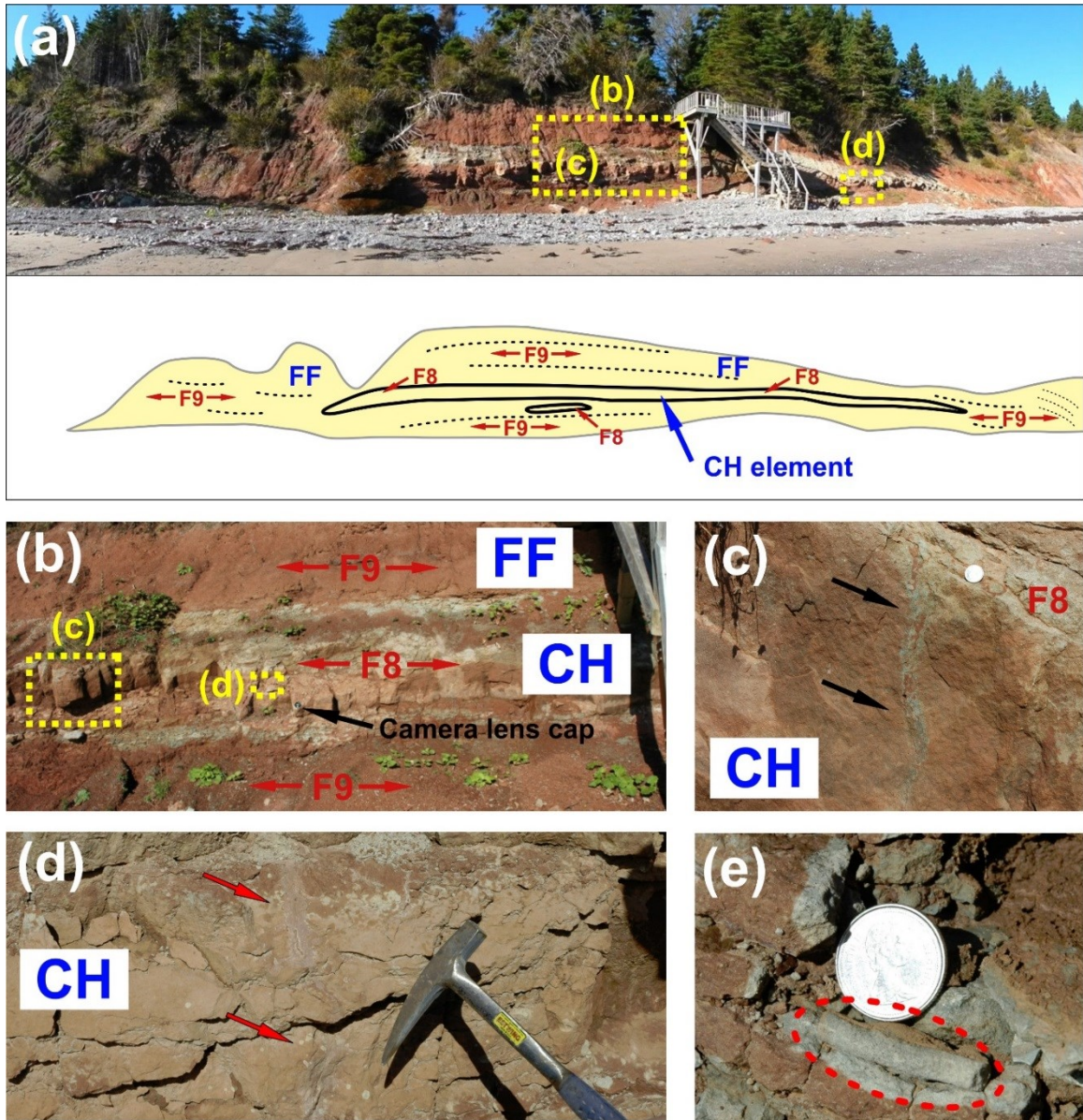


Figure 2.16: Field view, facies distribution, and architectural elements of the Chedabucto Formation at McCaul Island. (a) Field view of the lower section with a sketch showing the distribution of facies and the presence of FF and CH architectural elements. (b) Channel element (CH) between abandoned channel floodplain fines (FF) elements. (c) Root trace. (d) Root trace. (e) Scoyenia burrows.

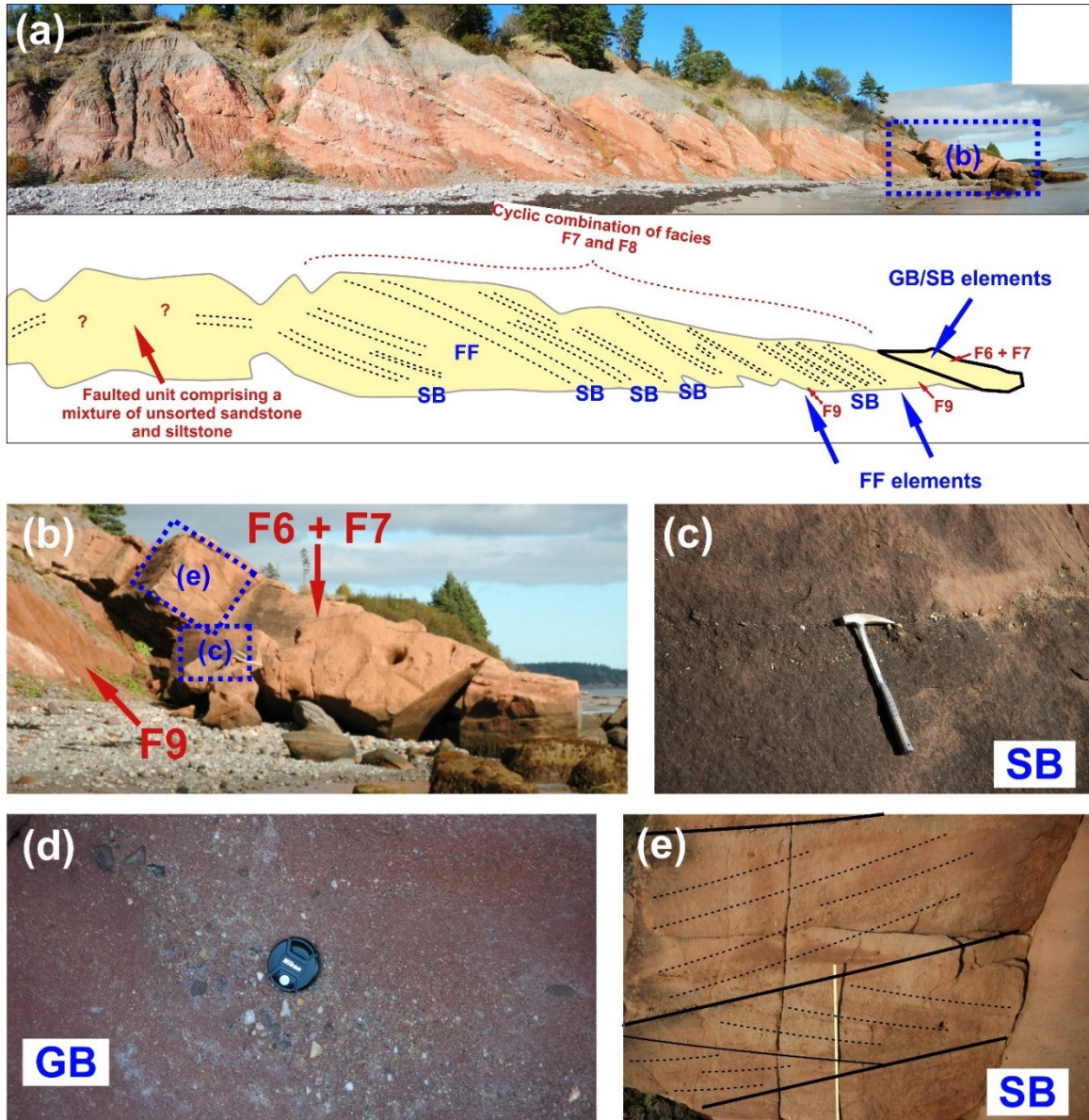


Figure 2.17: Field view, facies distribution, and architectural elements of the Chedabucto Formation at McCaul Island. (a) Field view of the middle to upper section with a sketch showing the distribution of facies and the presence of SB, CH, FF, and GB architectural elements. (b) Gravel bar and sandy bedform channel elements (F6 and F7) above abandoned channel floodplain fines elements (F9). (c) pebble lag deposit in a pebbly sandstone. Photo from fallen block next to outcrop (facies F7). (d) Matrix supported conglomerate (facies F6) located on the underside of the overhanging outcrop. (e) Planar crossbedding in sandy bedform architectural element.

2.4.4 Summary

The two study sections are composed of stacked channel bodies with associated abandoned channel and floodplain deposits. A total of seven architectural elements make up the stacked channel and overbank deposits at the Wolfville Formation at Rainy Cove (Minas Basin) and the Chedabucto Formation at McCaul Island (Chedabucto Bay) respectively. Within the Wolfville Formation, architectural elements (Miall, 1978) consist of GB, SB, DA, SG, and LS whereas within the Chedabucto Formation architectural elements consist of GB, SB/CH, and FF.

Channel bodies in the Wolfville Formation comprise poorly sorted coarse sandstones and conglomerates. The channels can be divided into laterally continuous packages, as identified in outcrop by continuous erosional boundary surfaces. The most significant of these is the ITU-1 boundary located within and marking the promontory at Rainy Cove. The boundary indicates erosion of up to 7 meters into the underlying stacked channels. Infill above the ITU-1 surface comprises a series of cut and fill, coarse-grained conglomerates and sandstones. Channel bodies in the Chedabucto Formation have thicknesses that range from a few cm's to 1.5 m. Due to the stratal dip in outcrop, the lateral extent of the channels is often obscured. However, two channels are present in the strike section of the outcrop show thicknesses of 1.5 and 0.6 m and widths of 15 and 60 m.

Paleoflow data are available at both study locations. Barforms from the Wolfville Formation indicate near northerly paleoflow while crossbeds from the Chedabucto Formation indicated easterly paleoflow during deposition. The geographic position of the two basins may lead one to believe that northerly flowing rivers from the south into the Minas Basin may have been rerouted to the east towards the Orpheus Graben.

Palynological analysis from a sample from the Chedabucto Formation reveals deposition of the successions sometime between Triassic (Norian) to middle Cretaceous. However, the similarity of this succession with those of the Fundy Basin would suggest deposition during the Late Triassic to earliest Jurassic period, though most likely in the Norian.

Results are summarized below:

- Facies of the Wolfville Formation are classified using a modified version of Miall's (1978) facies classification system. Five facies, forming two facies associations, were recognized and described in this study. They are located along the southeastern hingeline margin of the Fundy Basin's Minas Subbasin near Rainy Cove and comprises alluvial and fluvial strata. The strata are tilted at approximately 5° towards the basin axis, are laterally continuous over the studied section, and rest unconformably on metasedimentary strata of the early Carboniferous Horton Group.
- The Chedabucto Formation type section is located along the westernmost margin of the Orpheus Graben near McCaul Island, Chedabucto Bay. The formation comprises interbedded conglomerate, sandstone, and mudstone facies that strike northeast at 030° to 050° and dip at 20° to 40° to the east, obscuring some lateral facies relationships.
- The Eurydice Formation type section is found in the Eurydice P-36 well located about 100 km east of the McCaul Island outcrops offshore in the Orpheus Graben. The formation comprises fine-grained sandstone, siltstone, and shale with sporadic anhydrite nodules throughout. The formation comprises the youngest synrift sedimentary units which are interpreted to have deposited in a wave influenced, tide dominated estuarine environment.

2.5 Paleoenvironments

Wolfville Formation at Rainy Cove

To better understand the paleoenvironment of the Wolfville Formation exposed at Rainy Cove during synrift deposition, examination of the key facies present within the system is required.

The successions - debris flow breccias, trough cross bedded conglomerates and pebbly sandstones - represent an alluvial-fan and fluvial depositional system. These lie directly above the rift onset unconformity with the Early Mesozoic on Carboniferous, and expose the earliest synrift successions of the Minas Basin, with the Mesozoic on Carboniferous, and show the earliest synrift successions of the Minas Basin. Sediments deposited during the active alluvial fan system are limited to the basal 4 m of the outcrop. Due to the dip of the strata, this unit is only exposed laterally for approximately 50 m. The disorganized fabric of the breccias suggest that they were deposited by debris flows (Blair and McPherson, 1994), which agrees with interpretations from this study.

Conglomeratic and pebbly sandstone lithofacies of the fluvial system dominate the upper 27 m of the outcrop. Two fining-upward, laterally continuous sequences are bounded on their upper contacts by the S3 and ITU-1 interpreted surfaces (Figure 2.10). Each of the fining-upward sequences comprises pebbly sandstones and some matrix-supported conglomerate. Both sequences contain intermittent calcrete paleosols at their upper boundaries and generally tend to have fewer clasts compared to successions above the major ITU-1 unconformity. The ITU-1 boundary is an erosional surface with approximately 7 m of erosion into the lower stacked fluvial sequences. Above the ITU-1 boundary is a series of cut and fill, erosionally-dominated conglomerates, pebbly sandstones, and plane-bedded sandstones.

The calcareous paleosols (or caliche deposits) form in depositional settings in which breaks of short duration occur. Additionally, these units suggest deposition occurred in a climate transitional zone of either semiarid or humid climates, or that they mark the seasonality of wet and dry climates (e.g. Blodgett, 1988). The presence of these units also suggests that erosion of the upper boundaries was limited or non-existent and is not evident at the Rainy Cove section.

Sedimentation appears to have been restricted between the caliche deposits and the lower interpreted boundary (e.g. between the S2-S3 and S3-ITU-1 boundaries) which comprises downstream accretion macroforms and sand bedforms. These are dominated by conglomerates and pebbly sandstones at the base and clean to minor pebbly sandstones near the top. The change in pebble content has been attributed to fluctuations in fluvial energy (Leleu et al., 2009). Low energy or non-deposition would correspond with the subsequent formation of caliche deposits. The dry to wet transition, which could range from seasonal to a much longer time span, would see an increase in fluvial energy until a maximum energy was reached. During this point, the largest grain and clast fraction would be transported and deposited at the base of the succession as bedload through traction currents. As the climate transitioned back into less humid conditions, the energy of the fluvial system would have decreased causing a finer grained fraction and clast size to be transported. Leleu et al. (2009) suggested that these gradients in grain and clast size, as well as the presence of the caliche deposits, are due to changes in seasonality and climate, but provided no clear evidence for controlling the time frame.

The large ITU-1 unconformity presents a different pattern of sedimentation. Above the unconformity, sediments are coarser and comprise cut and fill sequences of cobble-size conglomerates, pebbly sandstones, and horizontally laminated sandstones. Each of these lithologies suggests a potential increase in energy of the flow regime transporting the material. As these sediments are unlike those of the laterally continuous succession below, the

mechanism for their deposition may be different. Leleu et al. (2009) suggests that the driver for this change in sedimentation could be due to a significant seasonal wet period, a change in the source of material in the catchment area, a base level change due to tectonic uplift in the basin ramp margin hinterland, or down-dropping of the basin along its northern fault-bounded margin. Without the presence of caliche deposits within these successions, it is difficult to determine the relative time over which they were deposited.

Overall, the fluvial system developed under fluctuating hydrological conditions, evident by the variation in vertical and horizontal sediment distribution. These fluctuations are probably driven by climatic changes due to seasonal wet and dry periods and also possibly by tectonic activity during rifting.

Chedabucto Formation at McCaul Island

The nature of the stratal successions at McCaul Island about 200 km to the east are dominated by intermittent channel and sandy bedforms with fine-grained overbank deposits. These channel deposits are comprised of featureless to trough and planar cross-bedded, very-fine to coarse-grained sandstones with caliche deposits at the top of these units.

The channels range from 0.1 to 2 m in thickness with a lateral extent of <60 m and were likely active during periods of seasonal precipitation. Within the channels, the fining-upward grain size may be attributable to the seasonal transition from wet to dry periods. As runoff energy was reduced in dry times, the ability to transport the same fraction of sands was reduced, resulting in a fining-upward sequence. Unlike the successions at Rainy Cove, episodes of dryness, or arid phases, appear more prevalent during deposition of the Chedabucto Formation successions. The occurrence of caliche deposits at the top of these channel

successions, as well as the presence of root traces within the channel bodies, suggests that extended periods of climatic dryness occurred.

Over this time, the channels were filled and subsequently abandoned, but moderate waning of flow still occurred as thick abandoned channel fines were deposited. These thick sandy siltstone packages located between intermittent sandy channels suggest the channels avulsed periodically. However, due to the nature and dip of the outcrop, the lateral relationships within the succession are obscured which in turn make it difficult to understand the relationship of the two channel and overbank successions.

Much like the successions at Rainy Cove, those at McCaul Island appear to be driven by changes in seasonal runoff. However, examining the measured section (Figure 2.3) from the formation shows that a thick package of coarser-grained sandy channels are deposited between thick fine-grained overbank successions. Channel avulsion may have resulted in a sustained period of channelization in the local area. However, an increase in sediment supply and exotic clasts in pebbly sandstones may suggest a change in the catchment area due to tectonic activity.

In summary, the Wolfville and Chedabucto formations represent alluvial fan and fluvial successions comprising mixed conglomerates and sandstones, and, fine-grained overbank and abandoned-channel deposits. The coarse-grained fraction was deposited in fluvial systems that are often associated with paleosol development. This suggests that the two successions were deposited in braided channel systems that underwent wet and dry episodes that may have been seasonal. The two formations were deposited in an overall arid to semi-arid climate reflecting the near equatorial paleolatitudes of the basins during the Late Triassic (Kent et al., 1995; Kent and Tauxe, 2005).

The siltstones and minor sandstones of the Eurydice Formation were deposited in a wave influenced tidally dominated marginal marine environment near the end of Mesozoic rifting (Tanner and Brown, 2003). Herring bone cross stratification suggests that a tidally-influenced system was well underway during deposition while the presence of anhydrite nodules in the thick siltstones of facies 12 indicate deposition in an arid to semi-arid climatic environment.

The Eurydice Formation from the Eurydice P-36 well

The Eurydice Formation was deposited in a wave influenced, tidally-dominated depositional system, most likely in a tidal flat estuarine environment under arid climatic conditions. Evidence for this has been presented in section 2.3, with the documentation of three facies:

1. high-energy, flood tide dominated sandstones in the lower intertidal zone
2. mixed energy ebb and flood tide heterolithic sandstone and siltstones
3. low-energy, upper intertidal to supratidal fines containing evaporitic nodules

The vertical facies succession formed during deposition (Figure 2.5) is a 9 m thick, coarsening-upward repetitive succession. Two sand units, showing cross bedded sandstone (facies 10), are separated from one another by heterolithic (facies 11) and generally featureless siltstones (facies 12) units. The repetitive change in depositional style found in this core suggests the possibility of two periods of local (regional?) transgression and regression or possibly a lateral change in coastline morphology. In either instance, we can see that the system is highly dynamic.

Ainsworth et al. (2011) use a process-based classification scheme, which relates the importance of identified sedimentary structures to wave, tide, and fluvial processes to predict the depositional environment and sedimentary architecture, including the basin shape, coastal

morphology, accommodation space, sediment supply, shoreline trajectory, and shelf width of clastic coastline depositional systems. The classification system is a ternary plot which uses wave (W), tide (T), and fluvial (F) process classifiers.

Using this classification scheme on identified processes from the Eurydice Formation (Figure 2.18) suggests that the depositional system was tide-dominated (85%), wave-influenced (15%), and non-fluviatile (Tw) (Figure 2.18). Using these results, and observations derived from modern coastlines (Ainsworth et al., 2011), an idealized schematic plan view geometry of the system is shown in Figure 2.19. Using the ratio of sand to shale (silt), and the total thickness of the measured section, the ratio of accommodation to sediment supply (A/S_s) can be calculated:

$$\frac{A}{S_s} = \frac{Th}{\frac{S}{Sh}},$$

where A is accommodation, S_s is sediment supply, Th is thickness of measured section (meters), S is total sand, and Sh is total shale (silt). Results from the measured core reveal an S/Sh ratio of 0.51 and a total thickness of 9.1 m. Using these values, the ratio of A/S_s is calculated as 17.84. This value suggests a high ratio of A/S_s (Figure 2.20). However, Ainsworth et al. (2011) are careful to note that these values are only indicative and further work is required to generate ranges of values that can be equated to relatively high and relatively low A/S regimes.

Using these classifications from Ainsworth et al. (2011), a predicted coastal process dominance decision tree can be constructed (Figure 2.21). From this it can be determined that the dominant coastal process acting on the system was tidal, the shoreline morphology was moderately embayed, there was a high accommodation to sediment supply ratio, and wave effectiveness dominated over fluvial effectiveness in this system.

In the subsurface, a full suite of data is not commonly available so any method of prediction will have aspects of uncertainty (Smalley et al., 2008). In this classification only a single core from a regionally widespread (Scotian margin) and thick (3000 +) formation was used. As Ainsworth et al. (2011) illustrate, interpretations from single offshore core only offer restricted windows to view the depositional system and, without further information, these interpretations may only hold true to the local environment.

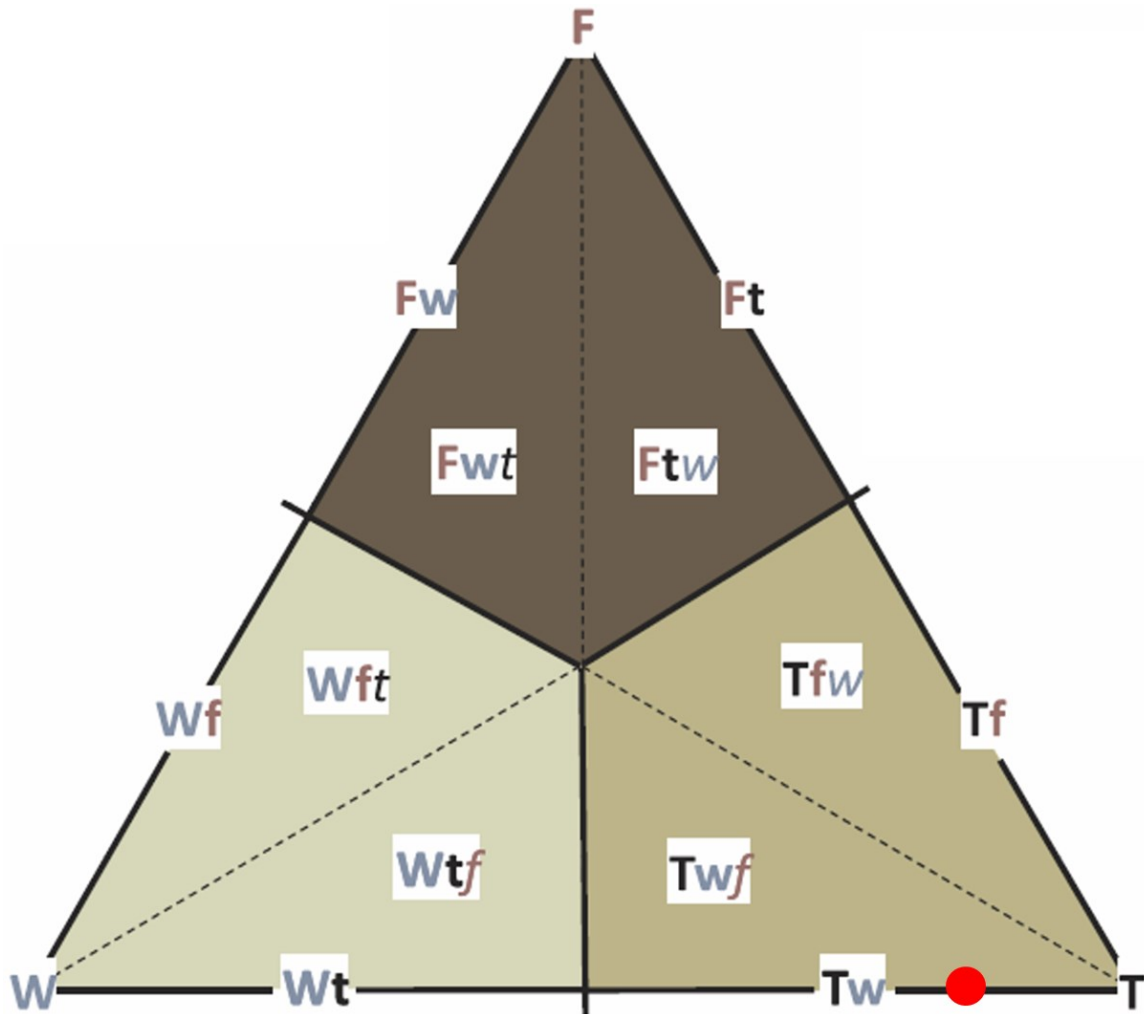


Figure 2.18: Coastal process classification ternary plot (modified from Ainsworth et al., (2011)) The red dot signifies the tide-dominated wave-influenced facies as preserved in the Eurydice Formation core. There is no fluvial influence on this system. Abbreviations: F = Fluvial dominated; W = Wave dominated; T = Tide dominated; Fw = Fluvial dominated, wave influenced; Ft = Fluvial dominated tide influenced; Tf = Tide dominated fluvial influenced; Tw = Tide dominated wave influenced; Wt = Wave dominated tide influenced; Wf = Wave dominated fluvial influenced; Fwt = Fluvial dominated, wave influenced, tide affected; Ftw = Fluvial dominated, tide influenced, wave affected; Tfw = Tide dominated, fluvial influenced, wave affected; Twf = Tide dominated, wave influenced, fluvial affected; Wtf = Wave dominated, tide influenced, fluvial affected; Wft = Wave dominated, fluvial influenced, tide affected; fw = fluvial and wave influenced; tf = tide and fluvial influenced; wt = wave and tide influenced; fwt = fluvial, wave and tide influenced; Fwt = Fluvial dominated, wave and tide influenced; Twf = Tide dominated, wave and fluvial influenced; Wtf = Wave dominated, tide and fluvial influenced.

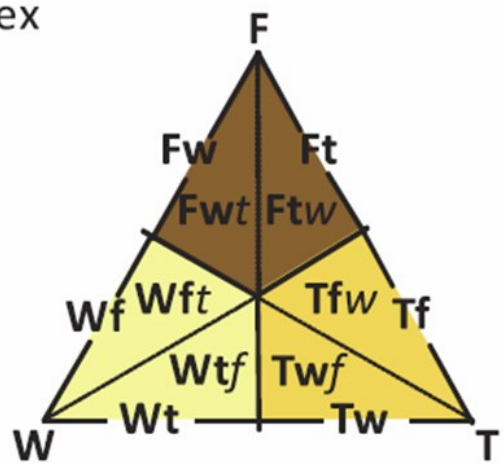
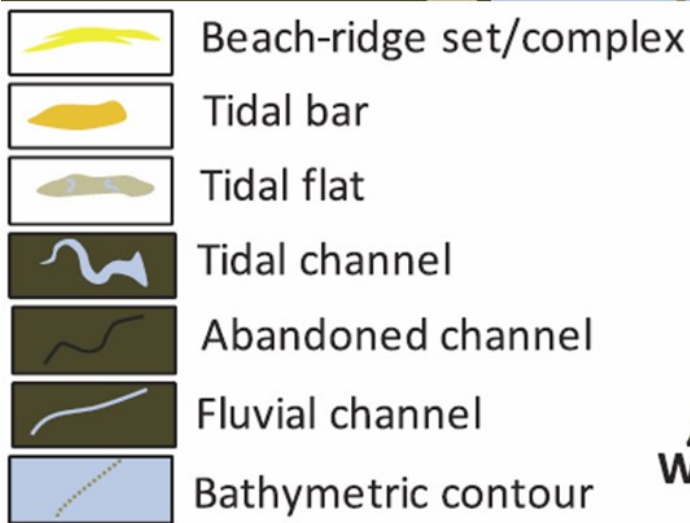
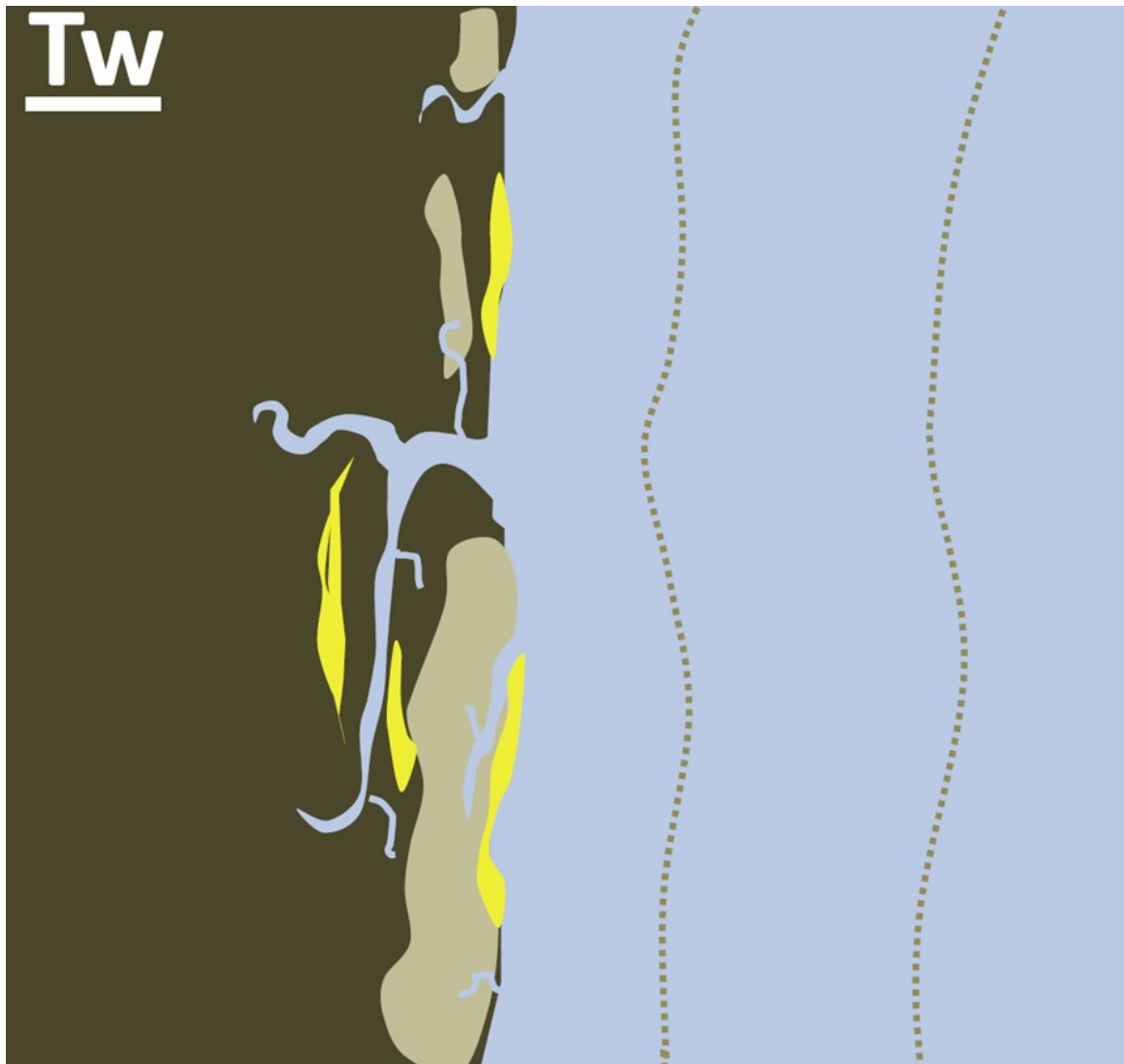


Figure 2.19: Representative schematic depositional model of the Eurydice Formation (from Ainsworth et al., 2011).

2.6 Basin Configuration and the Broad Terrane Hypothesis

Fundy and Minas basins and the Orpheus Graben

The Fundy Basin is a tripartite basin, containing three structurally similar rifts known as the Fundy, Chignecto, and Minas subbasins (Wade et al., 1996). Border faults of the subbasins occur along the north or northwestern edges of the depocenters. The border faults of the Fundy and Minas subbasins belong to a larger fault complex known as the Minas Fault Zone (MFZ). All basins exhibit a complex history containing sustained periods of extension, followed by short-lived quiescence, a later period of compression, and finally a sustained period of passive margin quiescence and erosion.

The Orpheus Graben is a rift basin which shares structural and stratigraphic relationships with the Fundy and Minas basins but is separated by about 200 km of elevated topography. Synrift successions along the western margin of the graben suggest that axial river systems deposited in the early parts of the basin formation, while fine grained sabkha and deeper marine successions in the offshore subsurface regions deposited later in the rifting history of the graben. Structurally, the basin shares a common border fault with the Minas Basin. The Minas Fault Zone, which borders the northern side of the Minas Basin, extends east into the Orpheus Graben and further into the offshore margin.

Olsen et al. (2000) have shown that within the Fundy and Minas basins, fluvial sedimentation occurred from the Carnian (or possibly in the Permian) until the Norian. At this point deposition largely switched into mostly lacustrine sediments from the Norian until the Hettangian or early Sinemurian (end of rifting). This change from fluvial to lacustrine is marked by a transition from coarser grained to finer grained successions. Wade et al. (1996) believe that seismic reflection architectures in the Fundy Basin depocenter indicate that the lacustrine

successions are present and laterally equivalent to the Wolfville fluvial facies indicating a closed basin since inception.

Tanner and Brown (1999) further speculated a similar transition of coarse- to fine-grained sedimentation (Chedabucto Formation) along the western margin of the Orpheus Graben at McCaul Island and attempted to link these successions to those of the Minas Basin, based on the similarity in facies and architecture. In this work, the Chedabucto Formation is constrained as Norian (Fensome, 2013, pers. comm.) using palynological evidence, suggesting that the constraints proposed by Tanner and Brown (1999) are correct.

Tanner and Brown (2003) postulated that the Chedabucto Formation may be an updip equivalent to deeper, undrilled successions in the offshore subsurface Orpheus Graben. They show evidence for coarser grained synrift successions drilled in the Mohican Graben Complex along the central/southern parts of the Scotian margin, and use this to infer similar deposits in the Orpheus Graben. Although the present work was unable to discern successions which were deeper or older than those of the Chedabucto Formation, the upper parts of the offshore successions are defined as fine-grained intertidal deposits. Using the Chedabucto Formation as an updip equivalent to deeper offshore succession, an overall transition from coarse fluvial dominated deposition to finer intertidal dominated deposition is observed. This coincides in time with the transition from fluvial to lacustrine in the Minas Basin and, as occurs in the deeper parts of the Minas Basin, suggests that coarse fluvial and alluvial (reservoir?) successions may be present in undrilled synrift sediments in the deepest parts of the Orpheus Graben.

Broad Terrane Hypothesis

The broad-terrane hypothesis (Russell, 1880) suggests that once-connected basins have since been separated through uplift and erosion of their connecting sedimentary successions.

Evidence from this project (similarities in lithology and architectural elements and the presence of paleo-flow indicators inferring eastward flow from the Minas Basin to the Orpheus Graben) suggests that the Minas Basin and Orpheus Graben were possibly once part of a larger, connected basin during active Mesozoic rifting but now exist as separate basins. This connection would have been along the Minas Fault Zone (MFZ) and within the adjacent Carboniferous age, St. Marys Graben. Evidence is limited due to significant erosion, though outliers may exist, buried under glacial deposits in the graben. Paleoecurrent studies (Figure 2.23) by Klein (1962), Hubert and Forlenza (1988), and work from Tanner and Brown (1999; 2003) suggested this connection. This study reveals the style of deposition of the lowermost Wolfville Formation and the Chedabucto Formation are similar in genesis with both comprising a series of alluvial and fluvial successions deposited during Early Mesozoic rifting.

It is assumed that the Chedabucto Formation was deposited in the Norian (Fensome, 2013, pers. comm.; Appendix B). In relation to the Minas Subbasin, these units would be equivalent in time to the upper parts of the Wolfville Formation (fluvial and aeolian) or the base of the Blomidon Formation (lacustrine). By Norian time, synrift sedimentation in the Minas Subbasin indicates a less fluvial-dominated system. It may be difficult to argue that large fluvial systems connecting the Minas Basin to the Orpheus Graben were active at this time, though the connection could be hydrologic / erosional and not depositional. However, the rift onset unconformity is not observed at McCaul Island suggesting that older sediments (possibly equivalent in time to the lower or middle Wolfville Formation) may have existed but do not crop out or have been eroded entirely. Knowing that the Fundy Basin experienced post-rift uplift and erosion (Withjack et al., 1995), the same probably occurred along the transpressional Minas Fault Zone resulting in uplift and erosion of synrift strata in the region connecting the two basins.

Therefore, the available evidence permits only speculation that fluvial systems existed along the Minas Fault Zone connecting the Minas Subbasin and Orpheus Graben during Mesozoic rifting.



Figure 2.22: Field view image from Rainy Cove highlighting the rift onset unconformity. The right side of the photo shows the lower Carboniferous Horton Group near vertical meta-sediments. These are truncated by the angular Rift Onset Unconformity with deposition of alluvial and fluvial sediments of the Triassic Wolfville Formation above.

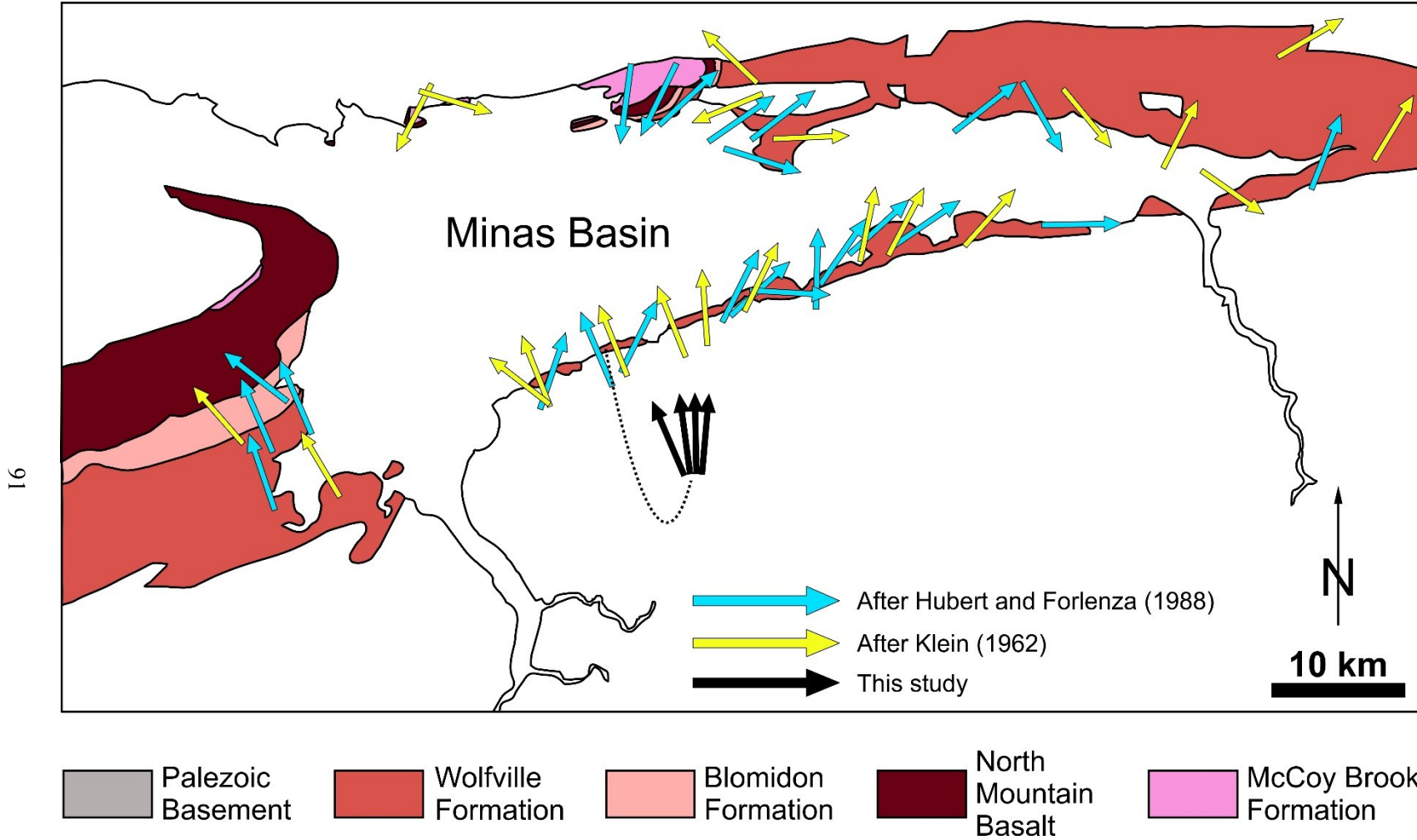


Figure 2.23: Geologic map of the Minas Basin showing paleocurrent indicator data gathered from the Minas Basin (left). Paleocurrent data from the Minas Basin are from Hubert and Forlenza (1988) (light blue), Klein (1962) (yellow) and from this work (black). Most of the paleocurrent measurements show north or south oriented flow into the central parts of the basin. However, paleocurrent indicators in the northeastern part of the basin show eastward flow, near parallel to the Minas Fault Zone. Paleocurrents for this study are from trough axes.

2.7 Conclusions

The facies and architectural elements from Triassic synrift successions were characterized with facies from the Wolfville and Chedabucto formations classified using a modified version of Miall's (1978) facies classification system. Facies from the Eurydice Formation were described and classified using the clastic coastal ternary diagram from Ainsworth et al. (2011).

Five facies are recognised in the lowermost part of the Wolfville Formation which form two facies associations (alluvial fan and fluvial). Four facies are recognized in the Chedabucto Formation which form two facies associations (alluvial fan and fluvial). The Eurydice Formation from the Eurydice P-36 well in the Orpheus Graben comprises three facies (cross-stratified sandstone, heterolithic sandstone and siltstone, poorly stratified to featureless sandy-siltstone) forming two facies associations (tide and wave influenced).

The lowermost section of the Wolfville Formation at Rainy Cove demonstrates five architectural elements (Figure 2.10 and Figure 2.11), which are: GB, SB, DA, SG, and LS. The Chedabucto Formation near McCaul Island shows four architectural elements (Figure 2.14, Figure 2.15, and Figure 2.16) which are: GB, SB/CH, and FF.

Sedimentology of the Wolfville Formation at Rainy Cove reveals an inhospitable ecosystem dominated by high energy, seasonally-derived flash floods mixed with periods of intense aridity. The paucity of fossil / trace fossils in this dynamic system demonstrates the stresses (aridity, salinity) of this environment. At Rainy Cove, fluvial systems were sourced from the south and deposited northward into the distal parts of the Minas Basin.

The Chedabucto Formation at McCaul Island reveals a similar environment, although of much weaker energy. Seasonally-derived flash floods mixed with periods of intense aridity did

occur, as evident by the stacked channel and floodplain architectural elements. However, rare root traces suggests that this environment was more benign and hence biologically active. Fluvial systems were sourced from the west and deposited eastward into the distal parts of the Orpheus Graben.

The Eurydice Formation from the Eurydice P-36 offshore well was deposited in a tidal-dominated, wave-influence tidal flat system under arid to semi-arid climatic conditions, possibly approaching sabkha-type environment. Evidence from the core suggests deposition of these successions occurred under repetitive (cyclic?) sequences, transitioning between middle intertidal to upper intertidal or supratidal environments.

Paleoflow data from the Wolfville and Chedabucto formations suggests possible stratigraphic linkages between the Minas Basin and Orpheus Graben, but this remains speculative.

Chapter 3: Provenance, diagenesis, and reservoir quality from early Mesozoic synrift infill – examples from the Fundy Basin and Orpheus Graben, Nova Scotia

3.1 Introduction

Recent discoveries of giant working petroleum systems in synrift (and pre-salt) rocks from the Santos and Campos basins of Brazil and Kwanza Basin of Angola have sparked a global pursuit of similar systems along other regions of the Atlantic margins. Most recently, the Scotian margin has seen a resurgence in exploration activity with deep water seismic and drilling activity and record bids for offshore drilling leases. With recent discoveries offshore Brazil and Angola, drilling programs on the Scotian margin may be targeting undrilled and previously unexplored synrift or pre-salt rocks in the deep subsurface. This study aims to build on the few studies (Bell, 1958; Kettanah, 2013; Brown, 2014) which have previously examined these successions in terms of petroleum systems.

This study examines the reservoir characteristics of Late Triassic synrift successions from outcrops in the Minas Basin and Chedabucto Bay areas, and conventional drill core from the offshore Scotian Shelf using thin section petrography, X-ray fluorescence, and handheld permeability and gamma ray (radioactivity) tools. The objective is to provide new insight into the petroleum system elements of synrift successions of the Scotian margin. Specific objectives include:

- Determining and comparing the provenance of early and late synrift successions from the Minas Subbasin and Orpheus Graben.
- A complete paragenesis of their early and late synrift successions.
- Determining their porosity and permeability and hence reservoir potential

3.1.1 Study Area and Location

The study areas for this paper are located within and along the margins of the Minas Basin (Bay of Fundy), along the margins of Chedabucto Bay, and within offshore subsurface regions of the Orpheus Graben (Figure 1.2). The following describes the location and access to each of these areas:

- 1) The Minas Basin is located along the western margin of offshore Nova Scotia, approximately 100 km northwest of Halifax. The study area here is divided into two locations; (1) the northern margin at Red Head in Five Islands Provincial Park and (2) the southwestern margin near Rainy Cove (Figure 3.1 and Figure 3.2). At both study areas, laterally continuous Triassic synrift successions of the Minas Subbasin are exposed in 20+ m high coastline cliff faces which are accessed along coastal intertidal zones.
- 2) Chedabucto Bay is located along the eastern margin of Nova Scotia, approximately 200 km northeast of Halifax. The study area is located along the western margin of Chedabucto Bay, just north of McCaul Island, and is accessed through a privately owned, seasonal property located on the south side of Parker Hart Road. At the study area, outcrop is exposed along 5+ m high cliff faces for approximately 500 m along a coastal beach (Figure 3.3).
- 3) Data from the Orpheus Graben comes from the offshore Eurydice P-36 well (Figure 1.2). The Eurydice P-36 well is located offshore Nova Scotia in the Orpheus Graben (45.42981, -60.07972). The exploratory well was drilled by Shell Canada in September of 1971 to test a salt- and basement-related structural closure defined by seismic. Core collected during drilling was accessed through the Canadian Nova Scotia Offshore Petroleum Board's (CNSOPB) Dartmouth Geoscience Research Centre (GRC), and online Data Management Center (DMC) (Figure 3.4).

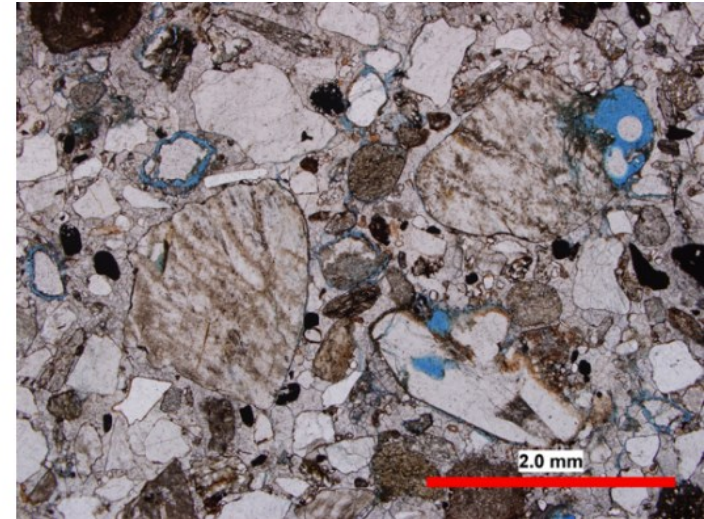


Figure 3.1: Field view of the studied Triassic Wolfville Formation at Rainy Cove showing the angular unconformity (rift onset unconformity) with the truncated Carboniferous Horton Bluff Formation (left). A representative photomicrograph of the grain distribution from the fluvial Wolfville Formation successions (right).

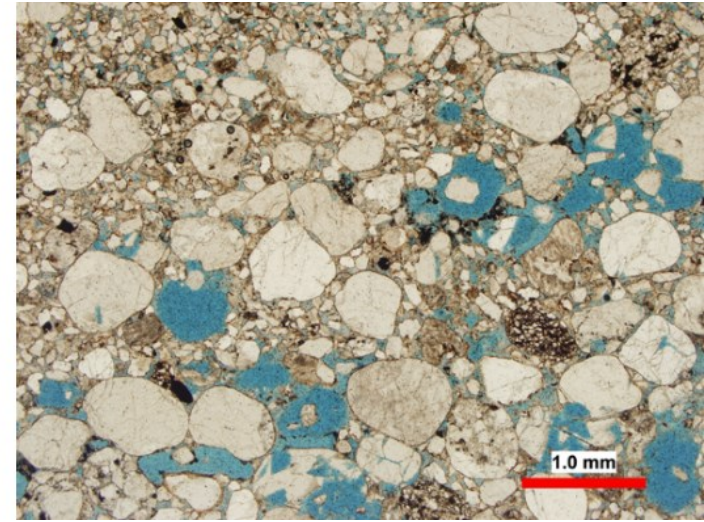


Figure 3.2: Field view of the studied Wolfville Formation aeolian successions at Red Head in Five Islands Provincial Park (left). A photomicrograph showing the representative grain distribution of the aeolian successions (right).

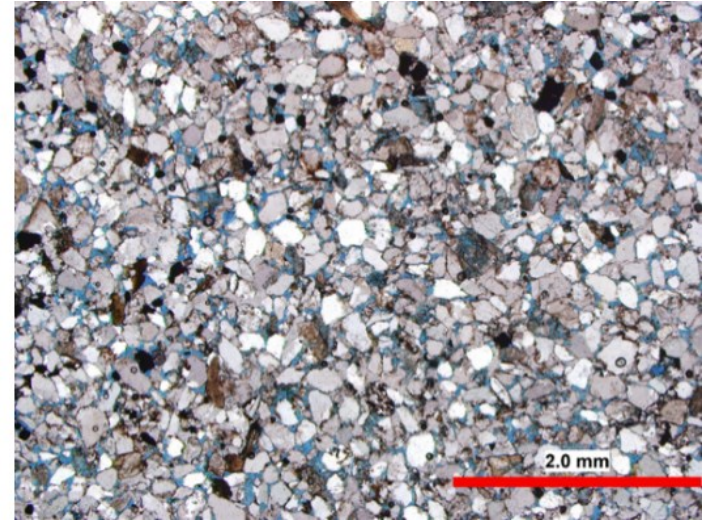


Figure 3.3: Field view of the Chedabucto Formation at McCaul Island showing cyclic stacked channels (left). A photomicrograph for a sample taken from the McCaul Island outcrop showing the representative distribution of grains in the Chedabucto Formation (right).

Box 1 & 2

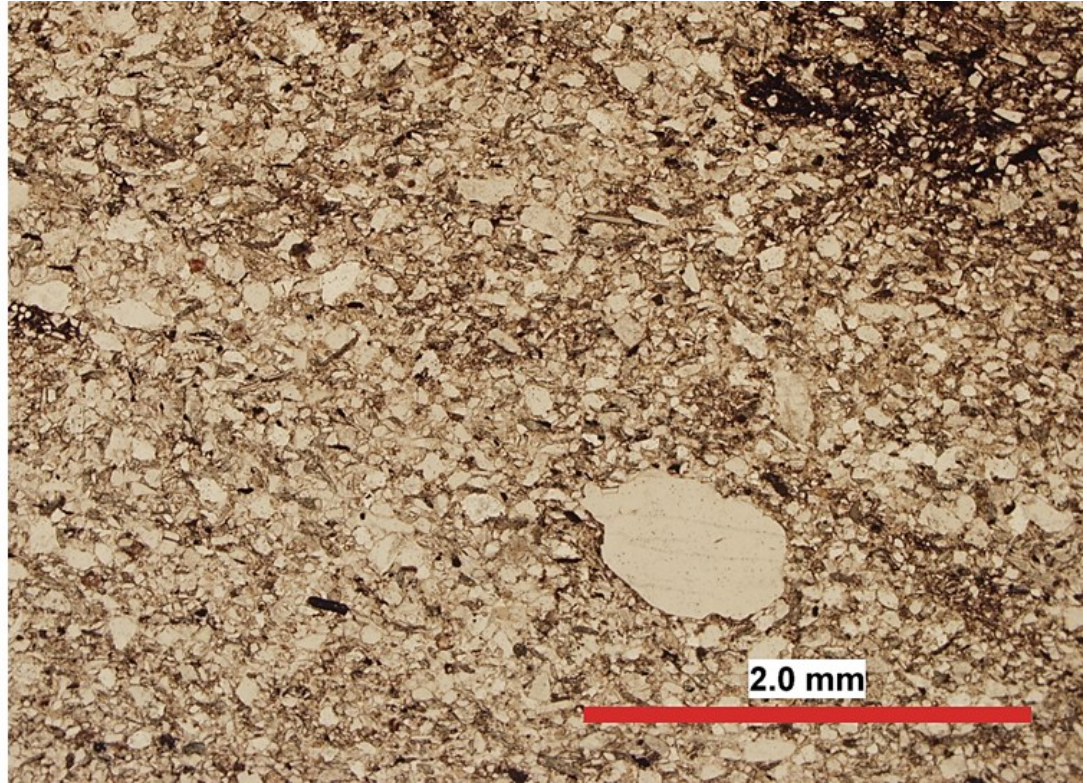


Figure 3.4: View of Eurydice Formation core from the Eurydice P-36 well (left). A photomicrograph for a sample taken from the core showing the representative distribution of grains (right).

3.2 Methods and Data

3.2.1 Sample Collection

A total of thirty-three rock samples from the three field study areas were collected as a representative basis for the entire formation in each area:

- Chedabucto Formation (McCaul Island) – 9 samples
- Wolfville Formation (Red Head / Five Islands Provincial Park) – 8 samples
- Wolfville Formation (Rainy Cove) – 16 samples

Samples were collected from the outcrop face using a rock hammer, put into sample bags, and labeled. The location of the sample was recorded on a photopan of the area and later digitized onto the photopan using CorelDraw®. In addition, five previously prepared thin sections from core of the Eurydice P-36 were collected from the Canada Nova Scotia Offshore Petroleum Board. Samples were brought back to Dalhousie University for thin section and X-ray fluorescence preparation.

3.2.2 X-Ray Fluorescence

Samples from the three field locations were analyzed using a handheld Niton™ XL3t 950 X-Ray Fluorescence (XRF) Analyzer made by Thermo Scientific™ (Figure 3.5). Outcrop samples were brought back to Dalhousie University and cut with a rock saw to make a smooth flat surface. The flat surface of each sample was placed facing downward inside the XRF base-station (Figure 3.6); the lid of the base station was closed; and the XRF was attached to the underside of the base station and was used to analyze each sample. All measurements were completed using the standard Mining Cu/Zn mode, unless otherwise stated.

X-Ray Fluorescence spectroscopy works through the transfer of energy from the XRF unit to the sample being analyzed. A gamma ray (light wave or photon) is emitted from the XRF unit and is shot at the sample (atom). If this photon is of sufficient strength, an electron from the inner orbital (lower energy) will be ejected from the atom. The space left from the ejected electron will be filled by an electron from a higher energy orbital. During this transition, the difference in energy between the higher and lower energy orbitals will be released as a photon. Photons released during this process are characteristic of a particular element and each element will always display the same energy release. Therefore, by determining the energy of the X-ray emitted by a specific element, it is possible to identify and determine that element.

There are limitations to the use of XRF in determining the elemental concentrations within samples. One of these limitations, pertinent to this study, is the identification and recognition of “light” elements (hydrogen through sodium). The light elements are smaller in atomic size than their heavier counter parts. The small size causes the electrons to be loosely bounded to the nucleus, and, due to this loose bounding, a scatter of many electrons are released during excitement from an XRF photon. This scatter does not produce a characteristic release of energy from the atom, making the identification of the element type impossible (Brouwer, 2006).

Representative sampling of the Eurydice P-36 core was completed at CNSOPB’s GRC in the same manner. Due to the size of the enclosure on the benchtop XRF unit, only loose pieces of core which fit under the lid of the base station could be analyzed. A total of 33 samples were taken.

To take measurements with the XRF, the following steps were completed:

1. The XRF, base station, and computer were connected and the XRF gun was powered on. The XRF software (NDTr) was opened on the attached computer and this software allowed for the XRF unit to be run.

2. The sample was placed with its flattest side down on the central part of the base station platform. The lid was closed and then locked using the lock switch.

3. On the virtual XRF screen, the analyze button was selected. All of the analyses were completed using the Mining Cu/Zn mode. Each analysis took approximately three minutes. Due to the coarse grained nature of some of the rocks, multiple readings were taken on each sample to ensure accurate representation was collected.

4. After completion of an analysis, the sample was removed from under the lid and the same process was followed for the next sample. For every tenth sample analyzed, a standard of known chemical constituents was ran.

Using the chemical concentrations from the known standard (Till-4 from the CCRMP), a 'correction factor' was calculated and applied to each of the sample analyses. The precision, accuracy, and 'correction factor' were calculated for each element. The elemental concentration average for each element of the known standard was calculated by taking the sum of each element and dividing it by the total number of analyses. A correction factor for each element was then calculated by dividing the known element concentration by the average element concentration from above. The correction factor for each element was then applied to the sample analyses.

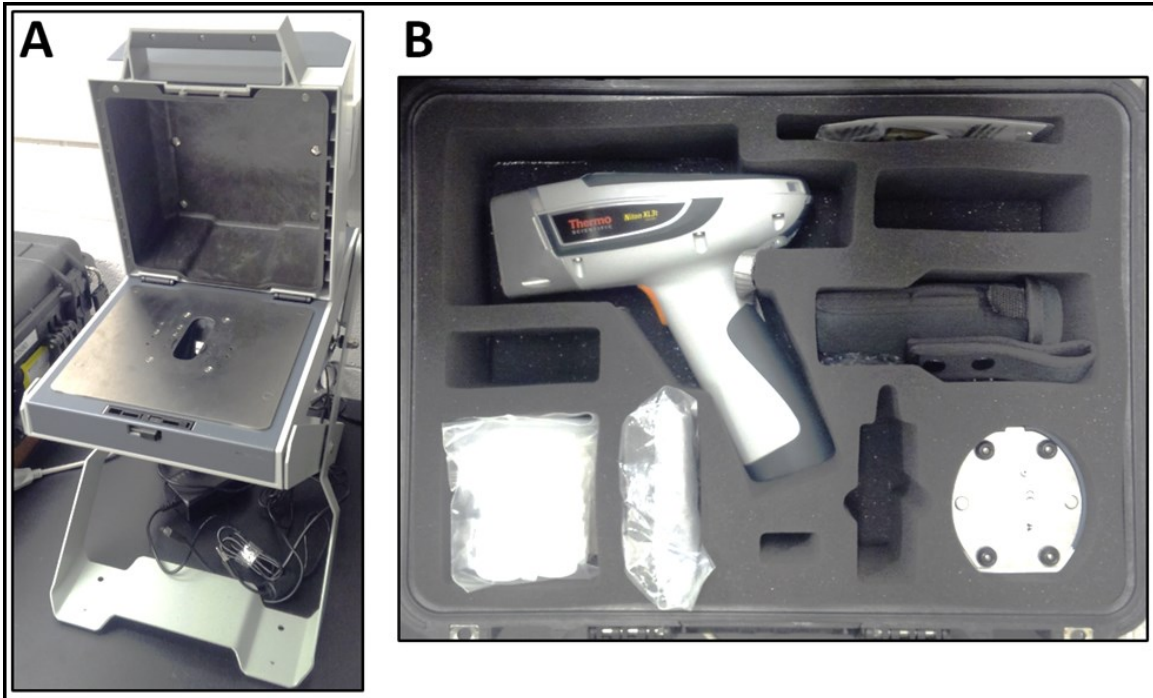


Figure 3.5: Niton™ XL3t 950 X-Ray Fluorescence (XRF) Analyzer. (A) Photograph of the XRF base station with the lid opened and the XRF not attached. The samples would be placed on the opening, seen on the metallic base plate, and the lid would be shut during analysis. (B) The XRF (top left) stored in the carrying case. Additional parts, including batteries, battery charger, and extra cords, can be seen in the other slots of the carrying case.

3.2.3 Microscopy

From the 30 samples collected, 21 thin sections were prepared at Dalhousie University. In addition to these sections, 5 thin sections from the Eurydice Formation were burrowed from the CNSOPB GRC. The thin sections from each formation include:

- Chedabucto Formation (McCaul Island) – eight (8) thin sections
- Wolfville Formation (Red Head / Five Islands Provincial Park) – five (5) thin sections
- Wolfville Formation (Rainy Cove) – eight (8) thin sections
- Eurydice Formation (Eurydice P-36 well) – five (5) thin sections.

These thin sections were analyzed using an Olympus BX51 polarising microscope (Figure 3.6) with an attached digital camera (Olympus DP71) located in the Basin and Reservoir

Laboratory of the Earth Sciences Department at Dalhousie University. The sections were examined for their overall mineral assemblages, their detrital mineral quantities, and their porosity.

Point count analyses were done using both Gazzi–Dickinson (Gazzi 1966; Dickinson 1970) methods. An automated stepping stage was used to count 400 points in the thin sections from Rainy Cove and McCaul Island and 300 points in the thin sections from Red Head. Thin sections from the Eurydice P-36 well were not point counted.

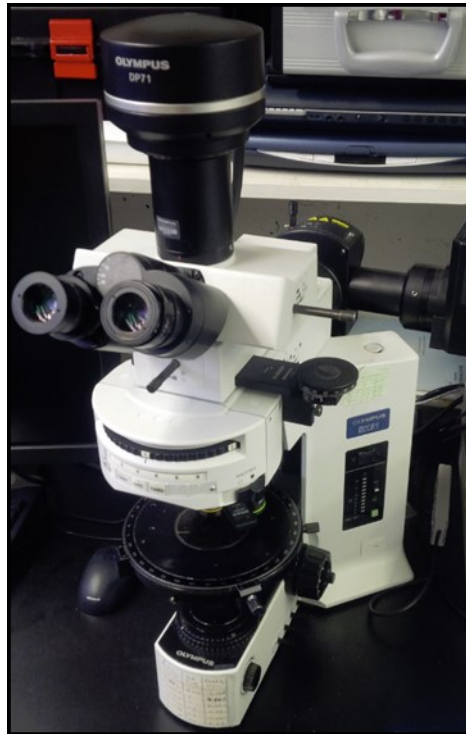


Figure 3.6: Photograph of the Olympus BX51 microscope, Basin and Reservoir Laboratory at Dalhousie University.

3.2.4 Handheld Permeameter Measurements

The TinyPerm II (Figure 3.7), developed by New England Research (NER) Incorporated, is a handheld air permeameter which allows for the instantaneous collection of permeability readings or effective aperture on rock (outcrop, core, and loose samples) or other material. The

unit works by creating a vacuum within itself and drawing air from the item it is pressed up against. As air moves through the item and into the vacuum, a microcontroller unit simultaneously monitors the syringe volume and the transient vacuum pulse created at the sample surface. To take measurements with the TinyPerm II, the following steps were completed:

1. TinyPerm II was turned on.
2. The plunger was pulled all the way out, and the computer screen reading was “Push + Hold”. The number displayed on the right side of the screen is the current vacuum status. This value should be centered on 0 (no vacuum) before a measurement begins.
3. The rubber nozzle was firmly pressed against the rock surface that was to be measured. If you are measuring a fracture aperture, make sure the nozzle is centered on the fracture.
4. The plunger depressed completely. The current vacuum and a measurement status bar will be displayed on the screen. The plunger was held in until the vacuum is 0 and the status bar indicates that the measurement is completed.
5. The results were displayed and recorded from the computer screen. TinyPerm II measurements can be cross-referenced to the included calibration curves in order to obtain absolute permeability or fracture aperture.
6. The TinyPerm II measured value was compared to a permeability calibration chart to find the measured permeability value for each sample (Figure 3.8).
7. The plunger was pulled out and the process was completed on the next sample.

Samples from the Wolfville (Rainy Cove and Red Head / Five Islands) and Chedabucto formations, and the Eurydice P-36 well core were analyzed using the TinyPerm II handheld permeameter to record measurements of rock matrix permeability. Samples were taken from the field, brought back to Dalhousie University, cut using a rock saw to give a smooth surface,

and permeability measurements were completed on these flat surfaces. Two to three readings were measured on each rock sample. The average reading for each sample was then calculated and used to determine the sample permeability. During core analysis, three permeability values were collected from each sample.

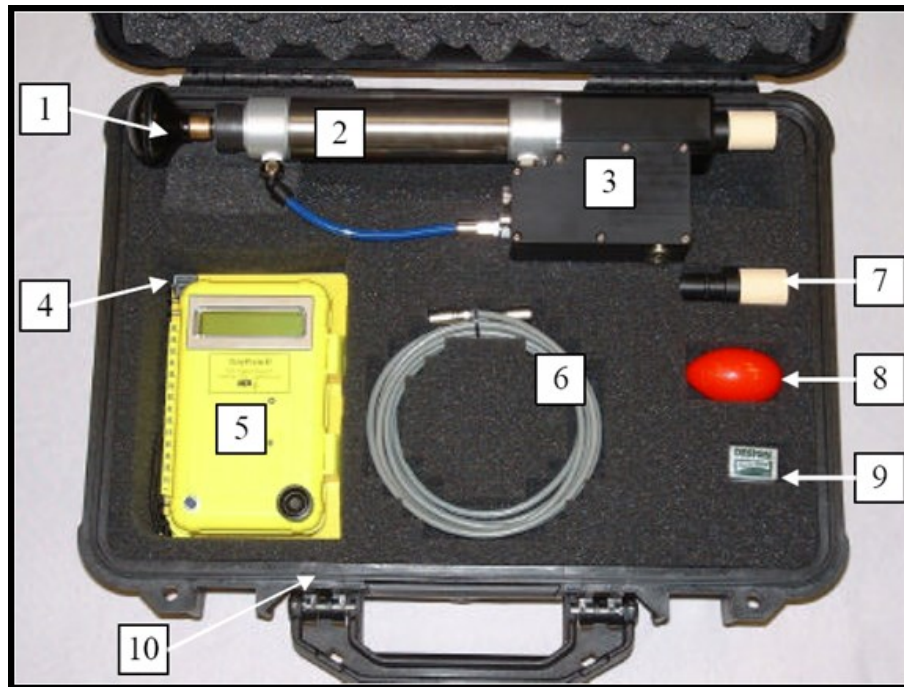


Figure 3.7: Photograph of the TinyPerm II and its associated parts (1. Handle and plunger, 2. Vacuum cylinder, 3. Pressure transducer enclosure, 4. Documentation with field notebook and calibrations, 5. Microprocessor and control unit, 6. Electrical cable, 7. Spare nozzle, 8. Silly putty (for sealing irregular surfaces), 9. Eraser, 10. Carrying case).

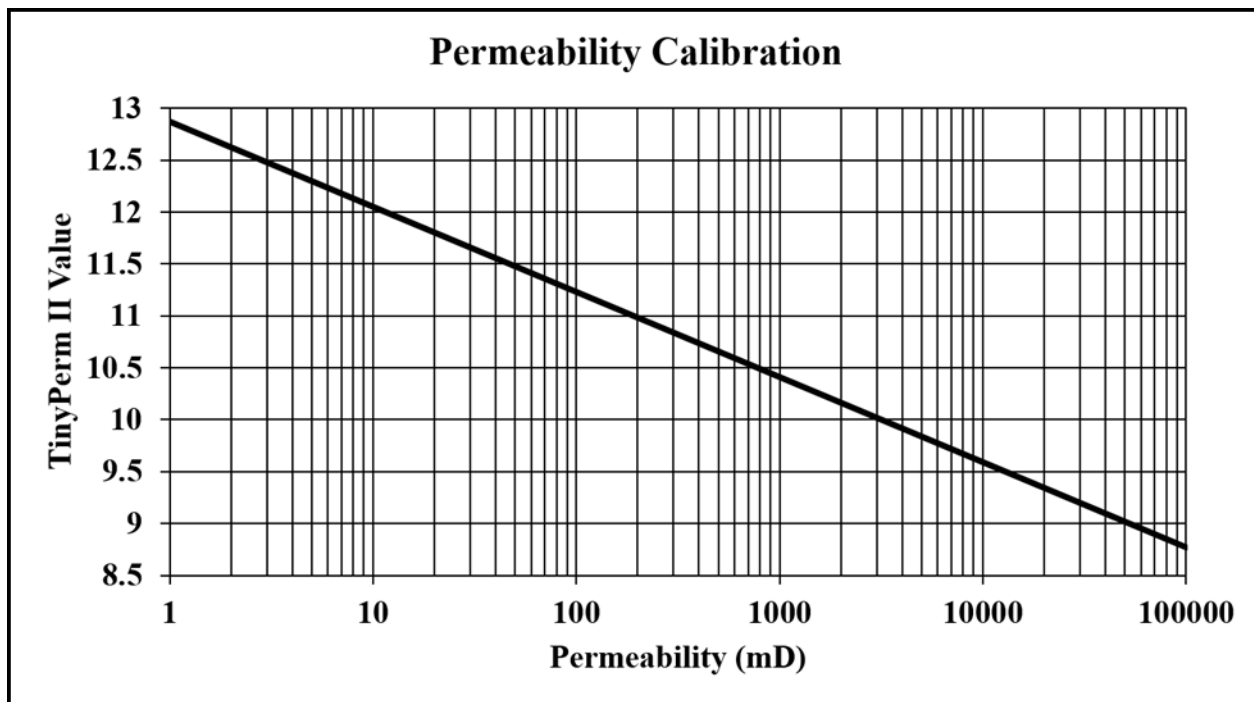


Figure 3.8: Permeability calibration chart, from NER, used to correlate TinyPerm II values to permeability values.

3.2.5 Handheld Gamma-Ray Spectrometer Measurements

The Exploranium GR-130 miniSPEC (Figure 3.9), developed by Science Applications International Corporation, and the GEORADiS GT-40 Multipurpose Gamma Center (Figure 3.10) are handheld radiation survey instruments (scintillometers) used to measure radioactive content through quantification of uranium, thorium, and potassium content within a sample.

To take measurements with the scintillometer, the following steps were completed:

1. The scintillometer was turned on and selected the survey mode.
2. The scintillometer was pushed up against the surface of the sample intended for measurement.
3. Readings from the LCD screen gave five second averages of gamma-ray radioactivity in counts per second. These values were copied down as they appeared on the LCD screen.

4. After six to twelve readings, the scintillometer was removed from the sample and placed on the next sample to be measured.

These two gamma ray scintillometers were used on collected rock samples and core to measure the gamma-ray radioactive content of variable stratal lithologies present in each formation. The scintillometer was turned on and the survey mode was selected from the main menu, which records radioactivity as a count rate in the format of counts per second (cps). For this study, the scintillometer was set up to record an average count rate over five seconds. The device was then held against outcrop or fallen blocks during field traverses, or against grab samples and core in the lab. Each measurement completed took approximately 30 to 60 seconds which in turn gave six to twelve averaged cps radioactivity readings. The individual sample measurements were averaged and the resulting value was used as the representative cps radioactivity value for that sample.



Figure 3.9: Photograph of the Exploranium GR-130 miniSPEC scintillometer. The device is a single unit with a LCD screen, a handle with a controlling nub, and a signal-to-noise apparatus (silver circle beneath the handle).



Figure 3.10: Photograph of the GEORADiS GT-40 Multipurpose Gamma Center and associated parts (1. The scintillometer, 2. The usb connective cord, 3. The power adaptor, 4. The carrying strap, 5. The user's guide, and 6. The protective carrying case)

3.3 Results: X-Ray Fluorescence, Petrography, and Permeability-Porosity Characteristics

3.3.1 X-Ray Fluorescence

Major-element concentrations of all samples from the Wolfville, Chedabucto, and Eurydice formations have been compiled and tabulated (Table 3.1, Table 3.2, and Table 3.3). An average elemental composition for the fluvial and alluvial Wolfville Formation and the Chedabucto Formation is presented in Table 3.4. Major elemental compositions are listed for the following oxides: SiO₂, TiO₂, Al₂O₃, Fe₂O₃, FeO, MnO, MgO, CaO, K₂O, and P₂O₅. The standard deviation, percent error, and correction factor for each element can be found in Table 3.5. The elemental correction factors were applied to each of the elements from the analysis (Table 3.1, Table 3.2, Table 3.3, and Table 3.4) of samples of the Wolfville and Chedabucto formations by multiplying the XRF analysis by the calculated correction factor (e.g. all analyses of SiO₂ were multiplied by 1.24).

Major elemental compositions for the Eurydice Formation were not used in this study since the classification system required that the rock unit under investigation be a sandstone. The Eurydice Formation is dominated by silts with a minor sand fraction. The summarized data table and discrimination plots for this formation can be found in Appendix C.

Table 3.1: Major elemental composition of aeolian sands and sandstones of the Chedabucto Formation at McCaul Island, Chedabucto Bay.

Sample:	Samples from the Chedabucto Formation near McCaul Island							
	GW_302	GW_303	GW_304	GW_305	GW_306	GW_307	GW_308	GW_309
SiO ₂	71.42	72.58	72.44	80.24	65.31	72.83	56.08	58.81
TiO ₂	1.01	0.81	0.39	0.39	0.34	0.23	0.29	0.80
Al ₂ O ₃	6.41	9.12	6.24	5.13	4.23	2.85	5.85	14.44
Fe ₂ O ₃ *	2.87	2.10	0.92	0.66	0.65	0.26	1.77	5.47
MnO	0.08	0.11	0.19	0.28	0.14	0.30	0.21	0.19
MgO	-	1.22	0.91	0.75	1.14	0.77	1.43	1.91
CaO	0.25	1.13	4.20	0.29	16.62	11.92	20.63	5.01
K ₂ O	1.59	2.21	1.61	1.27	0.82	0.80	1.53	3.28
P ₂ O ₅	0.29	0.08	0.07	0.11	0.00	0.07	0.06	0.14
Fe ₂ O ₃ */K ₂ O	1.81	0.95	0.57	0.52	0.80	0.33	1.15	1.67
SiO ₂ /Al ₂ O ₃	11.13	7.96	11.61	15.65	15.45	25.51	9.59	4.07
Fe ₂ O ₃ * + MgO	2.87	3.31	1.83	1.42	1.79	1.04	3.20	7.39
Al ₂ O ₃ /SiO ₂	0.09	0.13	0.09	0.06	0.06	0.04	0.10	0.25

Fe₂O₃* = Total Fe expressed as Fe₂O₃

Table 3.2: Major elemental composition of aeolian sands and sandstones of the Wolfville Formation at Five Islands Provincial Park, Nova Scotia.

Sample:	Samples from the Wolfville Formation at Five Islands Provincial Park							
	RHP base	RHP 1	RHP 2	RHP 3	RHP 4	RHP 5	RHP 7	RHP 8a
SiO ₂	50.64	46.32	47.17	52.95	50.03	49.45	56.89	50.28
TiO ₂	0.23	0.23	0.22	0.22	0.66	0.24	0.19	0.16
Al ₂ O ₃	3.71	3.15	3.19	3.92	9.22	3.16	3.84	3.24
Fe ₂ O ₃ *	1.12	0.97	1.09	1.23	4.25	1.10	0.91	0.89
MnO	-	0.01	0.01	0.01	0.08	-	-	-
MgO	-	-	-	-	0.77	0.38	-	-
CaO	1.42	1.79	3.11	1.69	0.56	0.38	1.42	5.01
K ₂ O	1.30	1.19	1.16	1.46	3.72	1.60	1.37	1.17
P ₂ O ₅	0.06	0.08	0.03	0.06	0.09	0.07	0.05	0.05
Fe ₂ O ₃ */K ₂ O	0.86	0.81	0.94	0.85	1.14	0.69	0.66	0.76
SiO ₂ /Al ₂ O ₃	13.64	14.72	14.80	13.50	5.43	15.64	14.80	15.54
Fe ₂ O ₃ * + MgO	1.12	0.97	1.09	1.23	5.03	1.48	0.91	0.89
Al ₂ O ₃ /SiO ₂	0.07	0.07	0.07	0.07	0.18	0.06	0.07	0.06

Fe₂O₃* = Total Fe expressed as Fe₂O₃

Table 3.3: Major elemental composition of alluvial and fluvial sands and sandstones of the Wolfville Formation at Rainy Cove, Nova Scotia.

Samples from the Wolfville Formation at Rainy Cove									
Sample:	GW_02_RC	GW_03_RC	GW_04_RC	GW_05_RC	GW_06_RC	GW_07_RC	GW_08_RC	GW_09_RC	GW_10_RC
SiO ₂	27.28	39.41	36.91	46.33	50.39	31.75	53.07	26.59	33.25
TiO ₂	0.18	0.62	0.22	0.43	0.57	0.09	0.15	0.38	0.47
Al ₂ O ₃	4.61	7.81	7.94	6.51	11.45	6.95	3.47	5.13	7.89
Fe ₂ O ₃ *	1.28	3.23	1.55	1.78	2.71	0.84	0.55	2.78	1.70
MnO	0.15	0.19	0.19	0.14	0.21	0.09	0.04	0.08	0.09
MgO	-	1.43	-	-	-	-	-	-	-
CaO	29.21	21.66	24.26	24.99	12.30	25.99	24.51	15.07	15.63
K ₂ O	0.88	1.49	1.34	1.22	1.94	0.98	1.17	1.30	1.35
P ₂ O ₅	-	-	-	-	0.05	-	-	-	-
Fe ₂ O ₃ */K ₂ O	1.46	2.16	1.16	1.46	1.40	0.86	0.46	2.13	1.26
SiO ₂ /Al ₂ O ₃	5.92	5.05	4.65	7.11	4.40	4.57	15.28	5.18	4.21
Fe ₂ O ₃ * + MgO	1.28	4.66	1.55	1.78	2.71	0.84	0.55	2.78	1.70
Al ₂ O ₃ /SiO ₂	0.17	0.20	0.22	0.14	0.23	0.22	0.07	0.19	0.24

Fe₂O₃* = Total Fe expressed as Fe₂O₃

Table 3.4: Average major element composition of Mesozoic synrift sandstones of the Wolfville and Chedabucto formations from the Fundy Basin and Orpheus Graben, Nova Scotia.

Sample:	Major element compositions of Mesozoic synrift sandstones of Nova Scotia		
	Chedabucto Formation	Wolfville Fm. (Rainy Cove)	Wolfville Fm. (Red Head)
SiO ₂	68.39	38.33	50.47
TiO ₂	0.52	0.35	0.27
Al ₂ O ₃	6.83	6.86	4.18
Fe ₂ O ₃ *	1.80	1.82	1.45
MnO	0.19	0.13	0.03
MgO	1.05	1.43	0.58
CaO	7.45	21.51	1.92
K ₂ O	1.64	1.30	1.62
P ₂ O ₅	0.10	0.05	0.06
Fe ₂ O ₃ */K ₂ O	0.97	1.37	0.84
SiO ₂ /Al ₂ O ₃	12.24	6.26	13.51
Fe ₂ O ₃ * + MgO	2.86	1.98	1.59
Al ₂ O ₃ /SiO ₂	0.10	0.18	0.08

Fe₂O₃* = Total Fe expressed as Fe₂O₃

Table 3.5: Known values and XRF analyses of known standard Till-4. The mean, standard deviation, % error, and correction factor for each major oxide examined is shown in the right four columns.

	Till-4 (known standard)	Till-4 (Reading 1)	Till-4 (Reading 2)	Till-4 (Reading 3)	Till-4 (Reading 4)	Mean Till-4 reading	Standard deviation	% Error	Correction Factor
SiO ₂	65	52.58	52.97	52.21	52.73	52.62	0.32	19.04	1.24
TiO ₂	0.81	0.67	0.70	0.69	0.68	0.69	0.01	15.27	1.18
Al ₂ O ₃	14.4	8.67	8.72	8.42	8.79	8.65	0.16	39.93	1.66
Fe ₂ O _{2(total)}	5.63	5.40	5.43	5.37	5.42	5.41	0.03	3.99	1.04
MnO	0.06	0.05	0.04	0.05	0.05	0.05	0.00	24.10	1.32
MgO	1.26	0.55	0.75	0.61	0.75	0.66	0.10	47.33	1.90
CaO	1.25	1.26	1.29	1.26	1.25	1.27	0.02	1.43	0.99
K ₂ O	3.25	2.72	2.70	2.70	2.73	2.71	0.01	16.63	1.20
P ₂ O ₅	0.2	0.41	0.40	0.35	0.37	0.38	0.03	91.14	0.52

3.3.2 Petrography

Textural study analyses were completed on all available thin sections from the Wolfville, Chedabucto, and Eurydice formations (Figure 3.11). In addition, point count analyses were completed on thin sections from the Wolfville and Chedabucto formations. These are summarized in Table 3.6, Table 3.7, and Table 3.8, and a compilation of the major point count grains used in later classification is summarized in Table 3.9.

Detailed petrographic descriptions for each sample is not presented here. Instead, a summary of the overall thin section characteristics and prominent features will be described as a representative sample of the formations, unless otherwise stated.

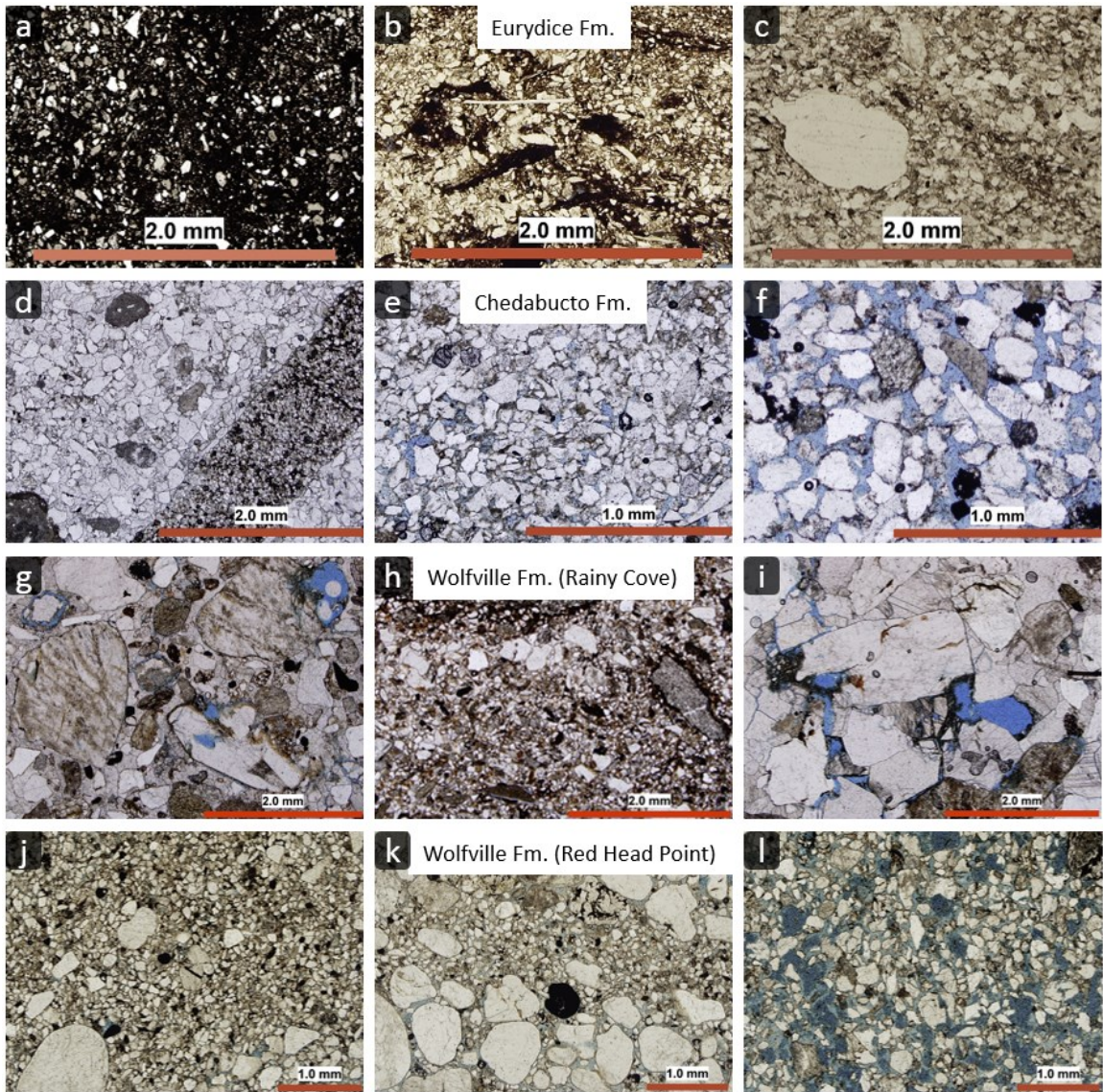


Figure 3.11: Photomicrographs showing the composition, textures, and porosity of studied successions from the Eurydice Formation (a – c), the Chedabucto Formation (d – f), and the Wolfville Formation (Rainy Cove: g – i; Red Head, Five Islands: j – l).

Eurydice Formation

Five thin sections were examined from the Eurydice Formation which typically showed a fine ground mass of clay minerals (with common muscovite, chlorite, and biotite), silts, and very fine-grained sands. Much of the detrital sand comprised elongate quartz grains, although infrequent feldspars were identified. The quartz grains are angular to subangular in shape and show moderate to no preferred orientation along their long axis.

A number of relatively large (1 mm) sized clasts are present. The clasts are often quartz or quartzite and are sub-round to round in shape. Opaque, lithic, and rip up clasts are also evident in thin section.

Cements are evident in all of the sections and include iron oxide cements that form rims around detrital grains. In other sections, quartz cementation dominates. Overgrowths of high birefringent minerals (possibly pyroxene) also appear. No porosity is found within the Eurydice with most grains being in contact (grain packed) or having void space filled by finer grained material and cement.

Chedabucto Formation

Nine thin sections from the Chedabucto Formation were examined. These show the typical composition of the formation is quartz with fewer lithic fragments and again fewer feldspars and heavy (opaque and transparent) minerals. Cementation is evident in all samples, but only comprises a high fraction in two samples. Cements are typically found as patches of calcite/silica and iron oxide around grain boundary rims.

Framework grains are moderately sorted and ranged in size from fine- to coarse-grained. Grains are typically sub-angular to sub-rounded and are moderately to tightly packed. Primary

porosity is abundant while secondary porosity is present in microfractured quartz grains, altered feldspar, and in the interior of sedimentary lithic grains.

The quartzose grain fractions dominate and consist mainly of simple microcrystalline quartz with undulatory and non-undulatory extinction. The quartz grains are mostly equant to prolate shaped. The sedimentary lithic fragments are the most abundant rock fragments in the sandstones comprising sandstones, siltstones. Of the feldspar, alkali feldspars are most abundant. Accessory minerals common in this formation are garnet, tourmaline, and zircon.

Wolfville Formation (fluvial successions at Rainy Cove)

Five thin sections from the fluvial Wolfville Formation successions were examined and showed that the typical composition of the formation was dominantly comprised of quartz with fewer lithic fragments and again fewer alkali feldspar, plagioclase, opaque, and muscovite grains. Cementation was evident in all thin sections and completely dominated by calcite. Accessory minerals were also evident in each section composed of garnet and tourmaline.

Detrital grains within the sections are poorly sorted and typically range in size from lower very fine-grained to upper coarse-grained. Grain shape varied from section to section, but overall is found as angular to subrounded. Grain packing varied from section to section, with three thin sections showing loose packing (framework grains rarely in contact), one thin section showing moderate packing, and one tightly packed grains.

Primary porosity is essentially negligible but is present along few grain boundaries. Secondary porosity could be considered micro porosity as it is present within smashed quartz grains and highly altered feldspars.

The quartzose grain fractions are the dominant grains consisting mainly of simple microcrystalline quartz with undulatory extinction, and mostly equant to prolate shaped. The

sedimentary lithic fragments are the most abundant rock fragments in the sandstones comprising sandstones, siltstones. Of the feldspars, potassium feldspars are most abundant.

Wolfville Formation (aeolian successions at Red Head, Five Islands)

Each thin section is composed of typical framework grains; quartz, feldspars and rock fragments, with a few cementing materials (iron oxide and calcite), micas (including muscovite and biotite) and heavy minerals (opaque and transparent). The sandstones contain minor amounts of cements that appear to coat grains (iron oxide) and occlude pore spaces (patchy calcite) in the sandstones.

The quartzose grain fractions are the dominant grains consisting mainly of simple microcrystalline quartz with undulatory extinction. The quartz grains are mostly equant to prolate shaped. They are matrix supported in the coarser sandstone fraction with many of the larger quartz grains showing heavy microfractures, whereas the fine to very fine quartz sandstone grains appear to be tangentially in contact with one another.

The sedimentary lithic fragments are the most abundant rock fragments in the sandstones composed of sandstones, siltstones and some shells. Igneous lithic fragments (granites) are next abundant, followed by quartzite and schist/slate metamorphic fragments.

The feldspars in the Red Head sandstones are chiefly potassium feldspar (including orthoclase and microcline), which can also be seen as part of a granophyric intergrowth with the quartz and mica grains observed in the granitic rock fragments. The feldspars are highly altered, attaining a dark brown color which can easily be differentiated from the other grains by their characteristic bladed shape.

Small amounts of detrital micas (mainly muscovite and some biotite) as well as some sericite (white mica) that is an alteration product of muscovite are observed in the Red Head sandstones. Also, the micas occur as inclusions in some detrital quartz grains.

Table 3.6: Statistics of point-counting results of the Chedabucto Formation redbeds near McCaul Island, Nova Scotia.

Grain Groups		Sample Type & No. Grain Type	Samples Chedabucto Formation near McCaul Island							All Samples			
			GW-301-2012	GW-302-2012	GW-303-2012	GW-304-2012	GW-305-2012	GW-306-2012	GW-307-2012	GW-308-2012	Av	Min	Max
Qt	Qm	Quartz	219	188	140	193	203	178	240	165	191	140	240
		Quartzite	0	0	0	0	0	0	0	0	0	0	0
	Qp	Chert	0	0	0	0	0	0	0	0	0	0	0
F		K-feldspar	9	15	6	11	13	6	15	6	10	6	15
		Plagioclase	9	5	2	7	3	2	3	2	4	2	9
Lt=L+Qp	L	Slate	0	0	0	0	0	0	0	0	0	0	0
		Siltstone	14	47	88	66	36	65	53	108	60	14	108
Volcanics		Volcanics	0	0	0	0	0	0	0	0	0	0	0
Carbonates		Limestone	0	0	0	0	0	0	0	0	0	0	0
Cement		Calcite	9	0	48	5	0	116	10	57	31	0	116
		Iron stain	42	4	56	1	8	15	0	18	18	0	56
		Clay+sericite	0	0	0	0	0	0	0	0	0	0	0
		Silica	15	0	0	3	12	0	1	0	4	0	15
Mica & Chlorite		Mica	4	3	0	1	0	0	0	1	1	0	4
		Chlorite	1	0	0	0	0	0	0	0	0	0	1
Heavy Minerals		Opaque	3	17	12	9	30	5	9	1	11	1	30
		Transparent	9	4	0	6	3	2	2	0	3	0	9
Others (highly altered grains)			27	34	24	54	33	3	21	0	25	0	54
Pore Spaces			39	83	24	44	59	8	46	42	43	8	83
TOTAL COUNTS			400	400	400	400	400	400	400	400	400	400	400
Porosity (%)			9.75%	20.75%	6.00%	11.00%	14.75%	2.00%	11.50%	10.50%	10.78%	2.00%	20.75%
Cement Counts			66	4	104	9	20	131	11	75	52.5	0	187
Total counts - Pores			334	396	296	391	380	269	389	325	347.5	269	396
Cement/Total Counts (%)			16.50%	1.00%	26.00%	2.25%	5.00%	32.75%	2.75%	18.75%	13.13%	1.00%	32.75%
Cement/ Grain Counts (%)			19.76%	1.01%	35.14%	2.30%	5.26%	48.70%	2.83%	23.08%	17.26%	1.01%	48.70%
(Quartz/Total Counts)%			54.75%	47.00%	35.00%	48.25%	50.75%	44.50%	60.00%	41.25%	47.69%	35.00%	60.00%
(Lithics/Total Count)%			3.50%	11.75%	22.00%	16.50%	9.00%	16.25%	13.25%	27.00%	14.91%	3.50%	27.00%
(Feldspars/Total Counts)%			4.50%	5.00%	2.00%	4.50%	4.00%	2.00%	4.50%	2.00%	3.56%	2.00%	5.00%
(Plagioclase/K-Feldspars)%			100.00%	33.33%	33.33%	63.64%	23.08%	33.33%	20.00%	33.33%	42.51%	20.00%	100.00%
(Calcite/Total Counts)%			2.25%	0.00%	12.00%	1.25%	0.00%	29.00%	2.50%	14.25%	7.66%	0.00%	29.00%
[(Mica+Chlorite)/Total Counts]%			1.25%	0.75%	0.00%	0.25%	0.00%	0.00%	0.00%	0.25%	0.31%	0.00%	1.25%
(Heavy Minerals/Total Counts)%			3.00%	5.25%	3.00%	3.75%	8.25%	1.75%	2.75%	0.25%	3.50%	0.25%	8.25%

Table 3.7 Statistics of point-counting results of the aeolian Wolfville Formation from Red Head, Five Islands Provincial Park, Nova Scotia.

Grain Groups		Sample Type & No. Grain Type	Samples						All Samples			
			Aeolian Successions at Red Head Point						Av	Min	Max	
			RHP Base	RHP 1	RHP 2	RHP 3	RHP 5	RHP 7	RHP 8			
Qt	Qm	Quartz	134	133	140	126	126	150	158	138	126	158
		Quartzite	9	15	6	7	5	14	6	9	5	15
	Qp	Chert	2	1	2	2	1	1	0	1	0	2
F		K-feldspar	10	15	13	13	18	17	11	14	10	18
		Plagioclase	5	2	2	1	4	1	2	2	1	5
Lt=L+Qp	L	Slate	0	0	0	0	0	0	0	0	0	0
		Siltstone	11	22	20	26	6	17	15	17	6	26
Volcanics		Volcanics	3	1	3	5	20	5	12	7	1	20
Carbonates		Limestone	0	0	0	0	0	0	0	0	0	0
Cement		Calcite	21	9	12	9	13	5	6	11	5	21
		Iron stain	30	32	21	30	36	18	12	26	12	36
		Clay+sericite	0	0	0	0	0	0	0	0	0	0
		Silica	4	3	3	2	6	2	1	3	1	6
Mica & Chlorite		Mica	5	5	9	7	6	7	5	6	5	9
		Chlorite	0	0	0	0	0	0	0	0	0	0
		Heavy Minerals	9	12	7	6	10	2	2	7	2	12
		Others (highly altered grains)	0	0	0	0	0	0	0	0	0	0
		Pore Spaces	57	50	62	66	49	61	70	59	49	70
TOTAL COUNTS			300	300	300	300	300	300	300	300	300	300
Porosity (%)			19.00%	16.67%	20.67%	22.00%	16.33%	20.33%	23.33%	20%	16.33%	23.33%
Cement Counts			55	44	36	41	55	25	19	39	19	55
Total counts -Pores			243	250	238	234	251	239	230	241	230	251
Cement/Total Counts (%)			18.33%	14.67%	12.00%	13.67%	18.33%	8.33%	6.33%	13%	6.33%	18.33%
Cement/ Grain Counts (%)			22.63%	17.60%	15.13%	17.52%	21.91%	10.46%	8.26%	16%	8.26%	22.63%
(Quartz/Total Counts)%			44.67%	44.33%	46.67%	42.00%	42.00%	50.00%	52.67%	46%	42.00%	52.67%
(Lithics/Total Count)%			4.67%	7.67%	7.67%	10.33%	8.67%	7.33%	9.00%	8%	4.67%	10.33%
(Feldspars/Total Counts)%			5.00%	5.67%	5.00%	4.67%	7.33%	6.00%	4.33%	5%	4.33%	7.33%
(Plagioclase/K-Feldspars)%			50.00%	13.33%	15.38%	7.69%	22.22%	5.88%	18.18%	19%	5.88%	50.00%
(Calcite/Total Counts)%			7.00%	3.00%	4.00%	3.00%	4.33%	1.67%	2.00%	4%	1.67%	7.00%
[(Mica+Chlorite)/Total Counts]%			1.67%	1.67%	3.00%	2.33%	2.00%	2.33%	1.67%	2%	1.67%	3.00%
(Heavy Minerals/Total Counts)%			3.00%	4.00%	2.33%	2.00%	3.33%	0.67%	0.67%	2%	0.67%	4.00%

Table 3.8: Statistics of point-counting results of the fluvial Wolfville Formation from Rainy Cove, Nova Scotia.

Grain Groups		Sample Type & No.	Samples				All Samples		
			Wolfville Formaiton at Rainy Cove				Av	Min	Max
		Grain Type	GW-02-RC-2013	GW-03-RC-2013	GW-05-RC-2013	GW-08-RC-2013			
Qt	Qm	Quartz	142	122	144	147	139	122	147
		Quartzite	0	0	0	0	0	0	0
	Qp	Chert	0	0	0	0	0	0	0
F		K-feldspar	43	21	24	46	34	21	46
		Plagioclase	2	8	3	2	4	2	8
Lt=L+Qp	L	Slate	0	0	0	0	0	0	0
		Siltstone	64	113	84	55	79	55	113
Volcanics		Volcanics	8	0	0	0	2	0	8
Carbonates		Limestone	0	0	0	0	0	0	0
Cement		Calcite	112	48	107	131	100	48	131
		Iron stain	0	0	0	0	0	0	0
		Clay+sericite	0	0	0	0	0	0	0
		Silica	0	0	0	0	0	0	0
Mica & Chlorite		Mica	2	16	8	3	7	2	16
		Chlorite	0	2	0	0	1	0	2
Heavy Minerals		Opaque	5	14	3	2	6	2	14
		Transparent	0	0	6	0	2	0	6
Others (highly altered grains)			0	0	0	0	0	0	0
Pore Spaces			22	56	21	14	28	14	56
TOTAL COUNTS			400	400	400	400	400	400	400
Porosity (%)			5.50%	14.00%	5.25%	3.50%	7.06%	3.50%	14.00%
Cement Counts			112	48	107	131	99.5	48	131
Total counts - Pores			288	352	293	269	300.5	269	352
Cement/Total Counts (%)			28.00%	12.00%	26.75%	32.75%	24.88%	12.00%	32.75%
Cement/ Grain Counts (%)			38.89%	13.64%	36.52%	48.70%	34.44%	13.64%	48.70%
(Quartz/Total Counts)%			35.50%	30.50%	36.00%	36.75%	34.69%	30.50%	36.75%
(Lithics/Total Counts)%			18.00%	28.25%	21.00%	13.75%	20.25%	13.75%	28.25%
(Feldspars/Total Counts)%			11.25%	7.25%	6.75%	12.00%	9.31%	6.75%	12.00%
(Plagioclase/K-Feldspars)%			4.65%	38.10%	12.50%	4.35%	14.90%	4.35%	38.10%
(Calcite/Total Counts)%			28.00%	12.00%	26.75%	32.75%	24.88%	12.00%	32.75%
[(Mica+Chlorite)/Total Counts]%			0.50%	4.50%	2.00%	0.75%	1.94%	0.50%	4.50%
(Heavy Minerals/Total Counts)%			1.25%	3.50%	2.25%	0.50%	1.88%	0.50%	3.50%

Table 3.9: Summary statistics of point-counting for the Chedabucto and Wolfville formations

Sample Type & No.	Samples								All Samples		
	Chedabucto Formation near McCaul Island								Av	Min	Max
Grain Type	GW-301-2012	GW-302-2012	GW-303-2012	GW-304-2012	GW-305-2012	GW-306-2012	GW-307-2012	GW-308-2012			
Qm	219	188	140	193	203	178	240	165	191	140	240
Qp	0	0	0	0	0	0	0	0	0	0	0
Qt=Qm+Qp	219	188	140	193	203	178	240	165	191	140	240
K	9	15	6	11	13	6	15	6	10	6	15
P	9	5	2	7	3	2	3	2	4	2	9
F=K+P	18	20	8	18	16	8	18	8	14	8	20
Lms	14	47	88	66	36	65	53	108	60	14	108
Lmv	0	0	0	0	0	0	0	0	0	0	0
L=Lms+Lmv	14	47	88	66	36	65	53	108	60	14	108
Lt=L+Qp	14	47	88	66	36	65	53	108	60	14	108

Sample Type & No.	Samples								All Samples		
	Aeolian Successions at Red Head Point								Av	Min	Max
Grain Type	RHP Base	RHP 1	RHP 2	RHP 3	RHP 5	RHP 7	RHP 8				
Qm	143	148	146	133	131	164	164	147	131	164	
Qp	2	1	2	2	1	1	0	1	0	2	
Qt=Qm+Qp	145	149	148	135	132	165	164	148	132	165	
K	10	15	13	13	18	17	11	14	10	18	
P	5	2	2	1	4	1	2	2	1	4	
F=K+P	15	17	15	14	22	18	13	16	13	22	
Lms	11	22	20	26	6	17	15	17	6	26	
Lmv	3	1	3	5	20	5	12	7	1	20	
L=Lms+Lmv	14	23	23	31	26	22	27	24	14	31	
Lt=L+Qp	16	24	25	33	27	23	27	25	16	33	

Sample Type & No.	Samples				All Samples		
	Wolfville Formaiton at Rainy Cove				Av	Min	Max
Grain Type	GW-02-RC-2013	GW-03-RC-2013	GW-05-RC-2013	GW-08-RC-2013			
Qm	142	122	144	147	139	122	147
Qp	0	0	0	0	0	0	0
Qt=Qm+Qp	142	122	144	147	139	122	147
K	43	21	24	46	34	21	46
P	2	8	3	2	4	2	8
F=K+P	45	29	27	48	37	27	48
Lms	64	113	84	55	79	55	113
Lmv	8	0	0	0	2	0	8
L=Lms+Lmv	72	113	84	55	81	55	113
Lt=L+Qp	72	113	84	55	81	55	113

3.3.3 Permeability, Porosity, and Gamma Ray Signature

Results from data collection of permeability and gamma ray signature value for the Eurydice, Chedabucto, and Wolfville formations are summarized in Table 3.10. The table presents the TinyPerm readings, the associated permeability value (using the chart from Figure 3.8), and the average scintillometer gamma ray reading.

In the Eurydice Formation, an average value for the TinyPerm and permeability is 12.48 and 10.18 mD respectively. Eight values from the scintillometer are listed and range between 100 and 121.7. In the Chedabucto Formation values for the TinyPerm range between 10.17 and 12.18, permeability 7.11 and 1971.44 mD, and scintillometer 199.2 and 126.6. The aeolian Wolfville Formation successions TinyPerm values range between 9.18 and 10.47. Permeability values range between 849.57 and 31711.63 mD, and the scintillometer values between 182.1 and 192.5. The fluvial Wolfville Formation successions have TinyPerm values ranging between 10.67 and 11.83, permeability between 17.19 and 497.415 mD, and scintillometer between 116 and 121.

Table 3.10: Summary of TinyPerm, permeability values, and gamma ray scintillometer values from the Eurydice, Chedabucto, and Wolfville formations. The Eurydice Formation has 8 gamma ray values, one from each box of core from Eurydice P-36 well. All other formations have samples with one value for all three data gathering methods

Summary of permeability and radioactivity values from the Eurydice, Chedabucto, and Wolfville formations					
Formation	Sample Name	TinyPerm reading	Permeability (mD)	Gamma Ray Scintillometer Count	
Eurydice	Multiple locations along Eurydice P-36 core (see Appendix C)	12.48	10.18	110	113.5
				112.7	114.3
				113.3	121.7
				116.3	113.7
Chedabucto (McCaul Island)	GW-301-2012	11.35	78.23	121.2	
	GW-302-2012	10.17	1971.44	121.2	
	GW-303-2012	11.91	14.94	122	
	GW-304-2012	10.93	233.69	120.2	
	GW-305-2012	10.53	717.93	126.6	
	GW-306-2012	11.91	14.94	120.8	
	GW-307-2012	10.17	1971.44	119.2	
	GW-308-2012	12.18	7.11	119.4	
	GW-309-2012	11.42	59.09	124.2	
Wolfville Formation (Red Head)	RHP-Base	10.47	849.57	190	
	RHP-1	10.38	1093.64	182.1	
	RHP-2	9.55	11228.69	192.1	
	RHP-3	9.86	4704.97	189.8	
	RHP-4	-	-	188.2	
	RHP-5	9.89	4325.12	189.9	
	RHP-7	9.18	31711.63	192.5	
	RHP-8	10.06	2684.31	192.2	
Wolfville Formation (Rainy Cove)	GW-02-RC	-	-	117	
	GW-03-RC	11.83	18.7	116	
	GW-06-RC	10.67	497.415	121	
	GW-08-RC	10.76	376.53	119.3	
	GW-04-RC	-	-	121	
	GW-07-RC	-	-	119.1	
	GW-05-RC	11.86	17.19	117.5	
	GW-09-RC	10.85	306.54	116	

3.4 Discussion: Petrography, X-Ray Fluorescence, and Permeability-Porosity Characteristics

The provenance, diagenesis, and reservoir quality of the early Mesozoic synrift infill successions were examined from the Wolfville, Chedabucto, and Eurydice formations using thin section petrography, X-ray fluorescence, and handheld permeability (TinyPerm) and gamma ray (scintillometer) tools. Samples were taken from outcrop along the western margin of Chedabucto Bay (McCaul Island), along the northern (Red Head, Five Islands) and the southern (Rainy Cove) margins of the Minas Basin, and from core of the Eurydice P-36 well (offshore Orpheus Graben).

3.4.1 Sandstone Classification, Tectonic Setting, and Sandstone Provenance

Classification of sandstone types was completed using both point count analysis (after Folk, 1968) and major elemental composition (after Herron, 1988). The following discusses the results from each classification systems.

From the point count results, Folk's (1968) classification QtFL ternary plot (Figure 3.12) shows that the Chedabucto Formation sandstones dominantly plot in the sublithic arenite and litharenite fields. The aeolian Wolfville Formation successions plot dominantly in the sublithic arenite field and the fluvial Wolfville Formation successions plot between the feldspathic litharenite and litharenite fields. All three groups show that the relative importance of grains type are (from most to least) quartz, lithic fragments, and feldspar.

From our major elemental concentration results, Herron's (1988) SandClass classification chart (Figure 3.14) shows that the Chedabucto Formation sandstones dominantly plot in the litharenite and sublitharenite fields, with outliers in the wacke and subarkose fields. The aeolian

Wolfville Formation successions plot in the sublitharenite field, and the fluvial Wolfville Formation in the wacke and litharenite fields, with outliers in the sublitharenite and Fe-sand fields.

The results from both point count analysis and the geochemical analysis show similar classification for the Chedabucto Formation (litharenite and sublitharenite) and the aeolian Wolfville Formation successions (sublitharenite). According to Dott (1964), lithic arenites are typical of fluvial conglomerates and other fluvial deposits while sublitharenites are affiliated with rocks that deposited in aeolian or shelf environments on stable cratons. There is variability in the classification of the fluvial Wolfville Formation successions when using both analyses.

Point count analyses uses the relative percent of detrital quartz, lithics, and feldspar in sandstones, while the geochemical analyses use whole rock geochemistry of any rock type. According to the SandClass classification, the fluvial Wolfville Formation should be classified as a wacke. Work by Dott (1964) describes the petrographic classification of sandstones, and in order to be classified as a wacke the rock must contain 15-75% matrix material. Work presented here shows the Wolfville Formation fluvial successions comprise less than 15% matrix material. However, both plots may infer a transitional stage of increasing mineralogical maturity that is characterized by an abundance of microcrystalline quartz and few feldspars. A QtFL plot with recalculated parameters after Ingersoll and Suczek (1979) and Dickinson (1985) (Figure 3.15) shows the fluvial sandstones are derived from a recycled orogenic source.

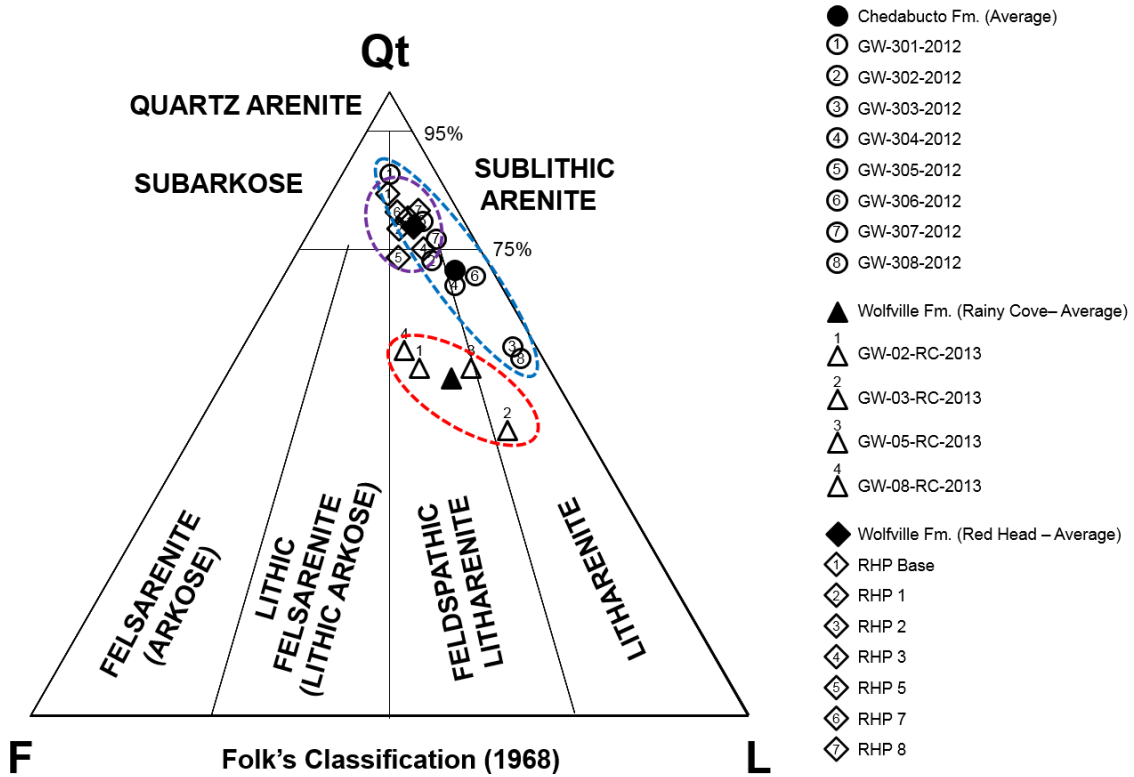


Figure 3.12: QtFL classification of Folk (1968) for the Wolfville and Chedabucto formations. The Chedabucto Formation (blue-outlined field) plots in the 'sublithic arenite' and 'litharenite' areas. The fluvial Wolfville Formation samples (red-outlined field) plot in the 'feldspathic litharenite' and 'litharenite' areas. The aeolian Wolfville Formation samples (violet-outlined field) predominantly plot in the 'sublithic arenite' area. Circle – Chedabucto Fm.; triangle – fluvial Wolfville Fm., diamond – aeolian Wolfville Fm. Dotted lines show the rough coverage area for each group of sample

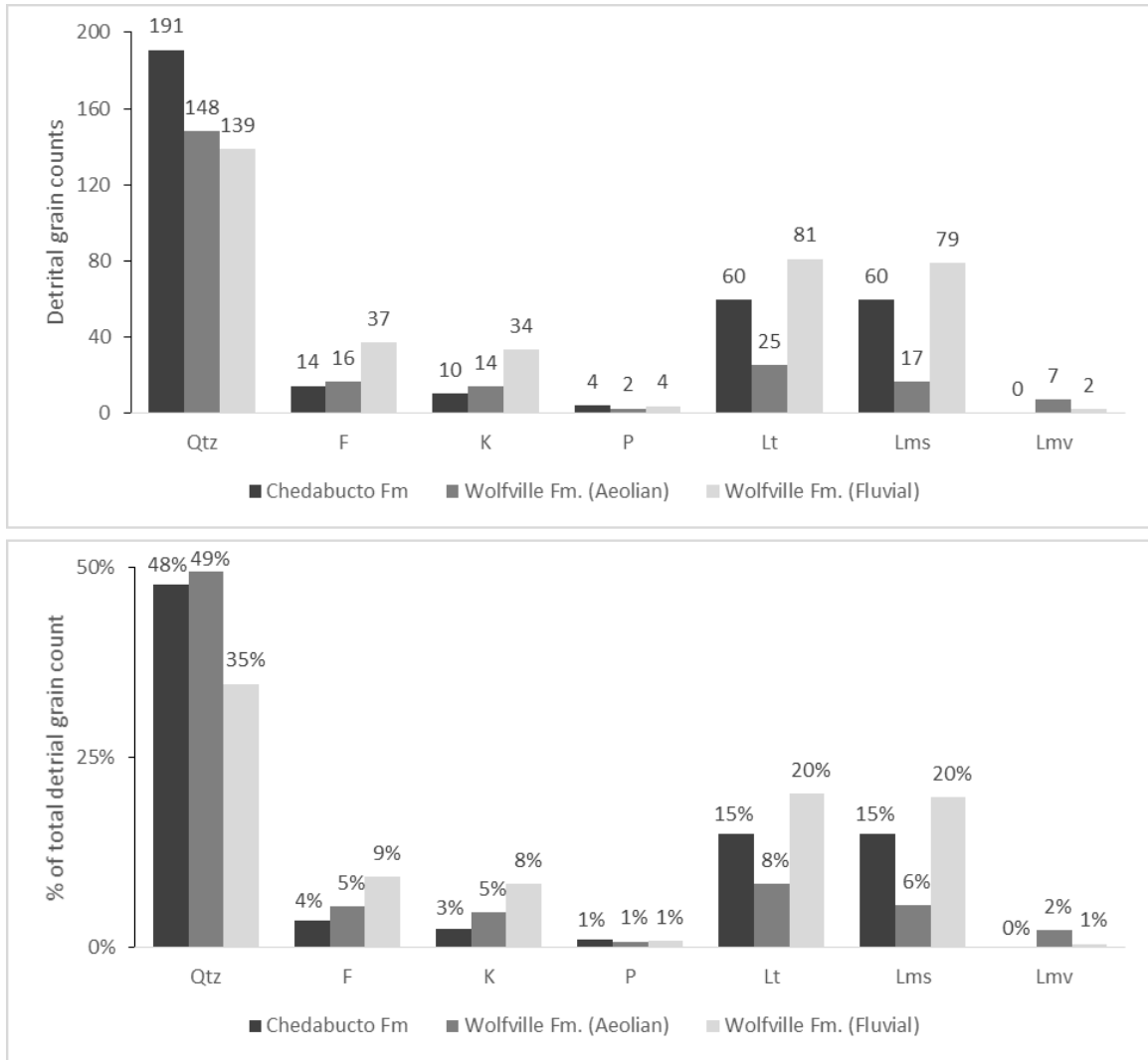


Figure 3.13: Distribution (relative) of detrital grains in the Wolfville and Chedabucto formations. Distribution as counts (upper graph). Distribution as percentage of total count (lower graph). Abbreviations along x-axis: Qtz – quartz, F – feldspar, K – alkali feldspar, P – plagioclase, Lt – total lithics, Lms – sedimentary lithics, Lmv – volcanic lithics.

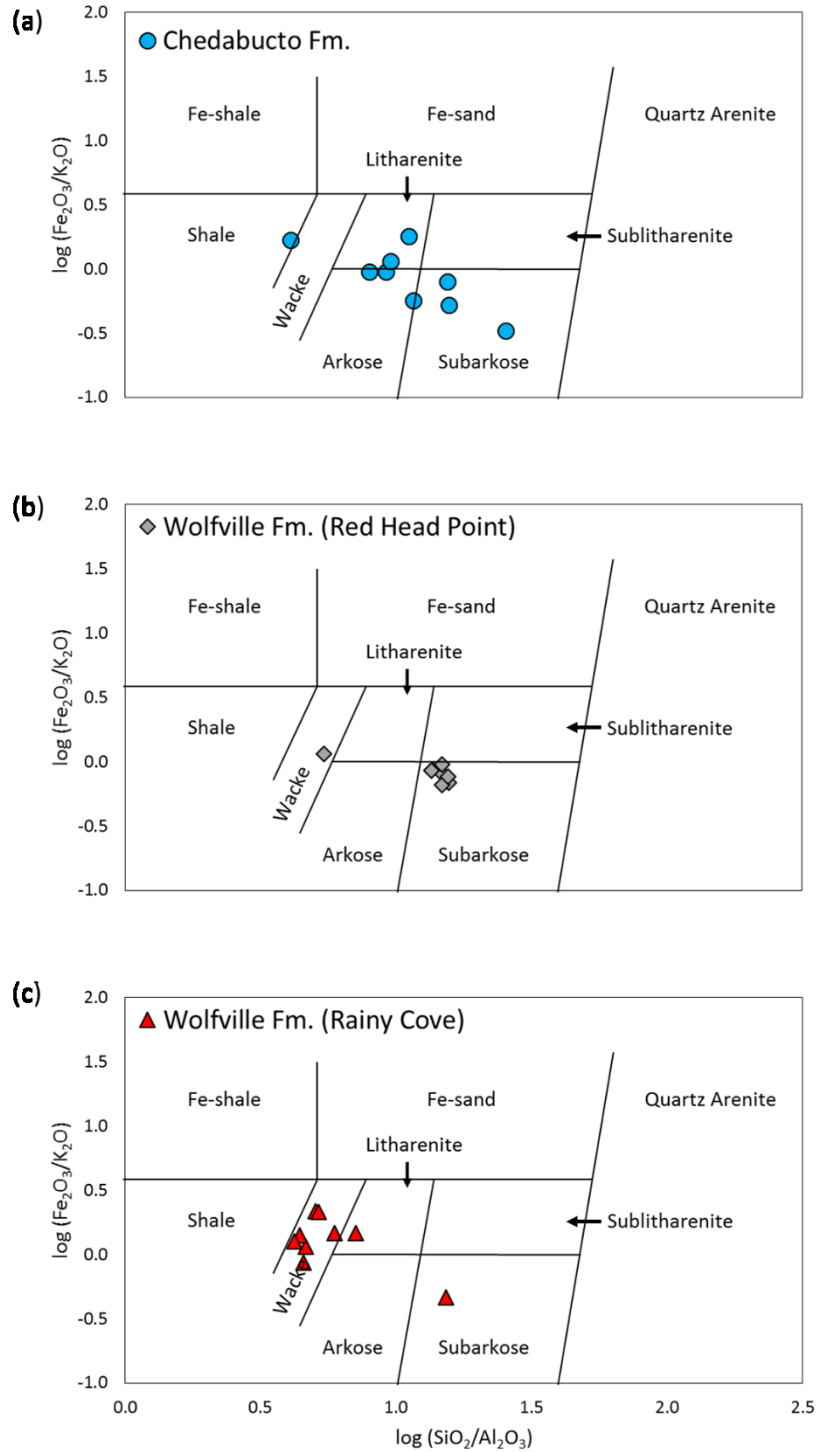


Figure 3.14: Sandstone chemical classification for the Wolfville and Chedabucto formations plotted on the SandClass scheme of Herron (1988). (a) Classification of the Chedabucto Formation with most points plotting in the litharenite and sublitharenite fields. Average value for all samples plots in the sublitharenite field. (c) Classification of the Wolfville Formation (Red Head, Five Islands) successions with most points plotting in the sublitharenite field, including the average for all samples. (d) Classification of the Wolfville Formation (Rainy Cove) with most points plotting in the wacke and Fe-sand fields. The average value for these points plots in the litharenite field.

Results for detrital grains counts (minerals and lithics) were plotted using the triangular diagrams of Dickinson and Suczek (1979), Dickinson et al. (1982, 1983) and Dickinson (1985) (Figure 3.15). As shown above, the QtFL Folk (1968) and SandClass Herron (1988) classifications indicate that the sandstones at all three locations have differences in their mineral and geochemical constituents, suggesting that there may be a difference in their provenance. The QtFL and QmFLt plots of Dickinson show that all three study locations fall into the field of 'recycled orogenic provenance (quartzose recycled and mixed)' with some samples from the Chedabucto Formation and aeolian successions from Red Head falling into the 'cratonic interior' segment. The QmPK triangle indicates all sandstones fall in the field of 'increasing maturity or stability from continental block provenances'. The Lvm-Qp-Lsm triangle shows that samples from the Chedabucto and Wolfville formations all plot in the field of 'collision orogen sources' and samples from the aeolian successions at Red Head are mixed and are concentrated in the field of 'collision orogen sources' and 'arc orogen sources' fields.

These results indicate that all three groups of samples have similar tectonic settings, and their accumulation and formation post-dated the collision orogen sources that can be interpreted as the Middle Devonian collision between the Meguma and Avalon terranes. The differences in abundance and composition of volcanic clasts at aeolian succession at Red Head (seen in the Lvm-Qp-Lsm plot) compared with other outcrops suggests a source from the Avalon Composite Terrane to the north (Cobequid and Antigonish highlands) which is dominated by metamorphic complexes and volcanic units (Lackey et al. 2007).

Lithological differences exist between the sandstones at the three locations, such as the higher abundance of lithic fragments in the fluvial Wolfville Formation successions and some of the Chedabucto Formation sands. The Wolfville Formation fluvial successions represent the oldest successions in this study and were deposited along the hanging wall / ramp margin of the

Minas Subbasin. The Chedabucto Formation successions are younger than the Wolfville and their location relative to the Minas Fault Zone (MFZ) border fault is uncertain. As Kettanah et al. (2013) suggested, the Bay of Fundy area was probably a 'transitional continental' environment during early rifting, but with time the tectonic conditions were changing towards a 'recycled orogenic environment'. This may explain why the fluvial Wolfville Formation successions in this study show a tendency to be clumped near the transition between the two fields, being deposited during the tectonic change from 'transition continental environment' to 'recycled orogenic environment'. The increase in lithic fragments in some Chedabucto Formation sands may be due to a variation in the sediment source. As suggested by Tanner and Brown (1999, 2003) the MFZ may have been a lowland during Mesozoic rifting and would have acted as a conduit for easterly-flowing fluvial systems between the Minas Subbasin and the Orpheus Graben. Because the relationship of the MFZ relative to the Chedabucto Formation is uncertain, it is speculated the sands at this location were possibly sourced from both the Avalon Terrane to the north of the MFZ, the Meguma Terrane to the south, or from fluvial successions from the Minas Basin which were derived 200 km to the west from the Meguma Terrane (Kettanah et al., 2013).

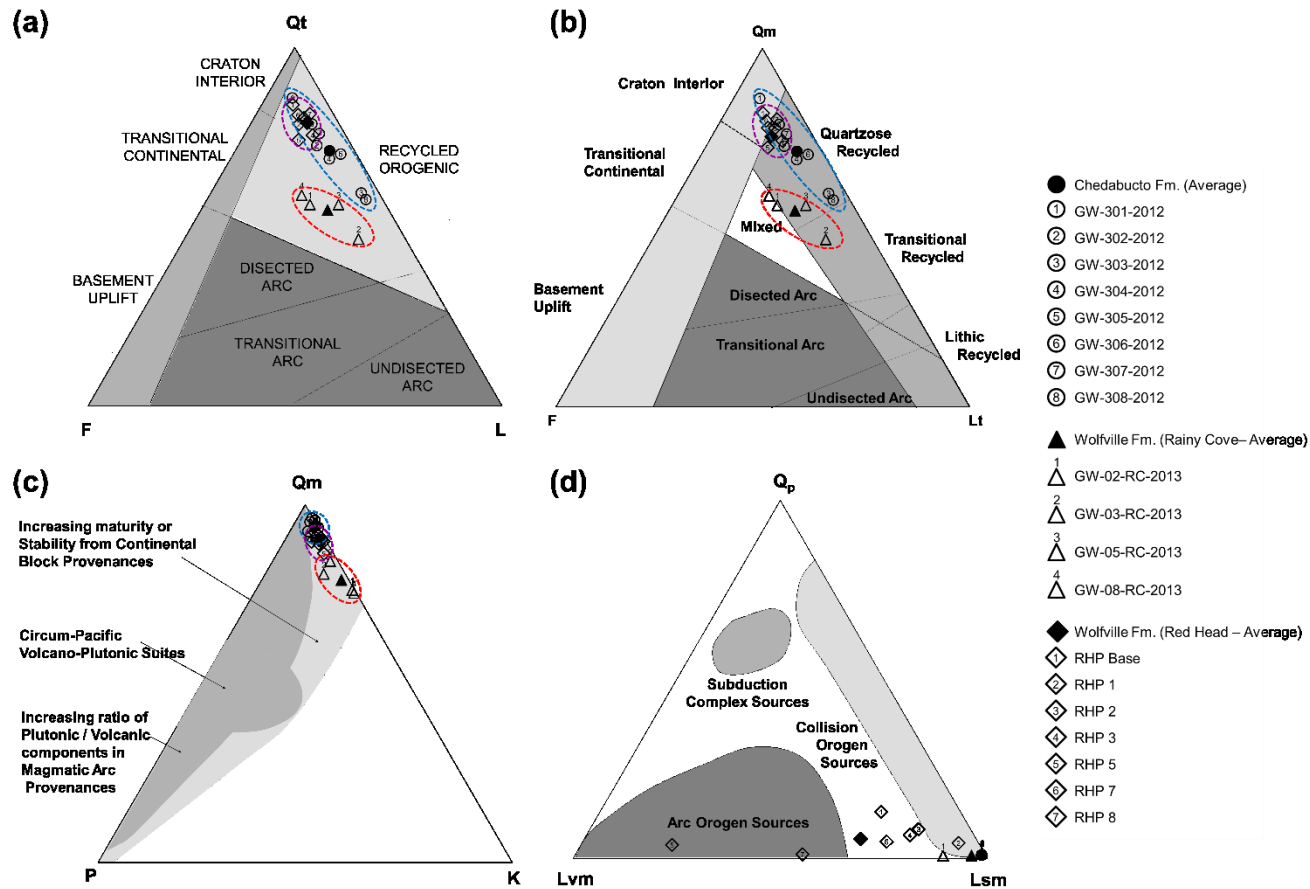


Figure 3.15: Distribution of major framework groups for the Wolfville and Chedabucto formations plotted on provenance indicator ternary diagrams of Dickinson & Suczek (1979), Dickinson et al. (1982, 1983), Dickinson (1985), and Folk (1968). Coloured dashed lines define the area covered by each of the study locations: red = Rainy Cove (Wolfville); blue = McCaul Island (Chedabucto); violet = Red Head (Wolfville). (a, b) FQtL & FQmLt: sandstones from all three study locations predominantly fall into the field of 'recycled orogenic provenance (quartzose recycled and mixed)'. Some of the samples from the younger Chedabucto Formation and aeolian successions from Red Head fall into the 'cratonic interior' (c) PmK: all sandstones fall in the field of 'increasing maturity or stability from continental block provenances'. (d) LvmQpLsm: fluvial samples from the Chedabucto and Wolfville formation (Rainy Cove) all fall into the field of 'collision orogen sources'. Samples from the aeolian successions at Red Head are mixed and fall into the field of 'collision orogen sources' and 'arc orogen sources'

Bhatia (1983) established a discrimination diagram using % (Fe₂O₃ + MgO) versus % TiO₂ or % (Al₂O₃/SiO₂) to determine the tectonic setting of terrigenous sedimentary rocks. All values for these variable are lowest for passive margin settings, and increase in the active continental margin, continental arc, and oceanic arc settings. Results from the average major element concentrations were plotted in the Bhatia (1983) discrimination diagrams (Figure 3.16).

From the % (Fe₂O₃ + MgO) versus % TiO₂ discrimination plot, the points for the aeolian Wolfville Formation successions are tightly clustered below the passive margin field. Points from the fluvial Wolfville Formation successions are scattered below the passive margin field and within the active continental margin field. Points from the Chedabucto Formation generally plot within and below the passive margin field, although three outliers plot around the continental arc field. Knowing that the fluvial successions were deposited in the early and mid-stages of rifting, it is expected that these points would plot in the active continental margin field, and for the aeolian successions the passive margin field. Although many of the points are located outside of the discrimination fields, either clustered or scattered, it is seen that they are generally slightly below the passive margin and active continental margin fields. Other works (Armstrong-Altrin, 2004) record similar results of point scatter, and even Bhatia (1983) had points which did not fit the discrimination fields. Therefore, those points which have <0.5% TiO₂ and <6% (Fe₂O₃ + MgO) can be grouped into either passive margin or active continental margin discrimination fields.

For the % (Fe₂O₃ + MgO) versus % (Al₂O₃/SiO₂) discrimination plot, a similar occurrence of point scatter and clusters outside and along discrimination fields occurs (Figure 3.16 b). Points for the aeolian Wolfville Formation successions are tightly clustered below the passive margin field. Those from the fluvial Wolfville Formation successions are scattered within and beside the active continental margin field and below the passive margin field. Chedabucto Formation points

generally plot below and to the side of the passive margin field. Using the same technique as for the previous plot, the minimum and maximum boundaries of the discrimination fields to include the points which plot outside of the fields can be assessed. Values of 0 - 1.2% ($\text{Al}_2\text{O}_3/\text{SiO}_2$) and 0 - 4% ($\text{Fe}_2\text{O}_3 + \text{MgO}$) can be included into the passive margin field. Values of 1.1 - 2.2% ($\text{Al}_2\text{O}_3/\text{SiO}_2$) and 2.0 - 6.5% ($\text{Fe}_2\text{O}_3 + \text{MgO}$) can be included into the active continental margin field. Points outside of these values would plot in the remaining two discrimination fields.

Therefore, the % ($\text{Fe}_2\text{O}_3 + \text{MgO}$) verses % TiO_2 reveals most of the points of all three successions plotting in either the passive margin or active continental margin fields. The % ($\text{Fe}_2\text{O}_3 + \text{MgO}$) verses % ($\text{Al}_2\text{O}_3/\text{SiO}_2$) discrimination plot see most of the points from the Chedabucto and aeolian Wolfville Formation plotting in the passive margin field, and most of the points from the fluvial Wolfville Formation plotting in the active continental margin field.

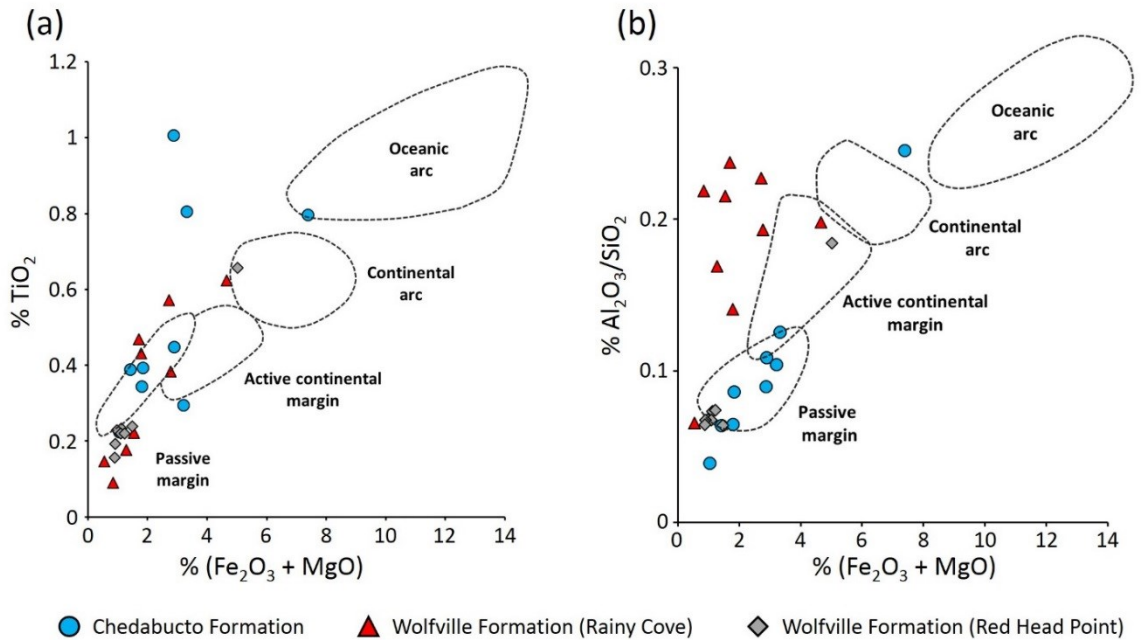


Figure 3.16: Major element composition plots of sands from the Wolfville and Chedabucto formations used for tectonic setting discrimination (after Bhatia, 1983). Each plot discriminates between passive margin, active continental margin, continental arc, and oceanic arc tectonic settings which are shown by the dotted black lines. Average values for each formation is shown by an X (a) Plot of TiO₂ versus Fe₂O₃ + MgO. Points from the Chedabucto Formation are generally clustered in or near the passive margin tectonic field. Points from the Wolfville Formation (Red Head) are tightly clustered below the passive margin tectonic field, with one point near the continental arc field. Points from the Wolfville Formation (Rainy Cove) are spread within the active continental margin tectonic field and below both the passive margin and active continental margin tectonic fields. Average value plots below the active continental margin field. (b) Plot of Al₂O₃/SiO₂ versus Fe₂O₃ + MgO. Points from the Chedabucto Formation plot in, beneath, or beside the passive margin tectonic field. Average value is near the passive margin tectonic field. Points from the Wolfville Formation (Red Head) are tightly clustered beneath the passive margin tectonic field. Average value plots near the passive margin tectonic field. Points from the Wolfville Formation (Rainy Cove) generally plot in and around the active continental margin tectonic field but are also present with and beneath the passive margin tectonic field. Average value plots between the active continental margin and passive margin fields.

3.4.2 Diagenesis

Petrographic analysis of the Chedabucto and Wolfville formation sandstones reveals that these units have undergone some degree of diagenesis, including mechanical and chemical compaction. The precipitation of iron oxide, carbonates, clays, and quartz, dissolution of K-feldspar, the formation of secondary minerals, the fracturing of brittle grains (quartz), and the grain supported textures are all indications of the diagenetic changes occurring within these sandstones.

Mechanical compaction is indicated by the formation of grain-supported textures (Figure 3.17 h and n), whereas the lack (or lesser extent) of mechanical compaction is indicated by cement-supported textures (Figure 3.17 i and j). Other indications of mechanical compaction include kink-banding of elongate muscovite minerals and fracturing of brittle minerals such as quartz and feldspars. In the Chedabucto Formation, quartz grains are often found in tangential contact with each other suggesting limited mechanical compaction (Figure 3.17 e to h). This is supported by the presence of microfractured quartz (Figure 3.17 k) and the presence of bending detrital micas (muscovite). However, these features are not common in all examined thin sections suggesting that mechanical compaction of these units may have been rather mild. The same features are found in the aeolian successions of the Wolfville Formation. The fluvial successions show a cement-supported texture, suggesting less mechanical compaction of these units and early cementation. There is a clear variation in the mechanical compaction, with the fluvial Wolfville Formation undergoing less compaction compared to the aeolian successions and those from the Wolfville Formation.

The chemical compaction and diagenesis are indicated as cementation, alteration, replacement and dissolution. Each of the three study locations has some degree of chemical

compaction. Iron cement is present in each of the samples and is found coating the grain boundaries as a thin layer (Figure 3.17 h, i, and n). The iron cement originated from the hydration of detrital iron oxides (magnetite and hematite), which are found in abundance as heavy minerals in each of these sandstones. Iron, silica, and calcite cements dominate the Chedabucto Formation sandstones, while only iron and calcite cements are prevalent in the aeolian and fluvial Wolfville Formation sandstones. Clays, forming through the alteration of feldspars, are most abundant in the Chedabucto Formation and least abundant in the aeolian successions of the Wolfville Formation (Figure 3.17 h and l). However, due to the sorting and mechanical abrasion of grains in wind derived successions, many of the chemically altered (or already weakened) feldspars would be removed from the framework grain fraction first. Calcite cement deposited from interstitial pore fluids was deposited and recrystallized during burial and filled much of the open spaces between grains in the sandstones from Rainy Cove (Figure 3.17 i and j). Silica cement within the Chedabucto Formations sandstones occurred through the partial dissolution of silica from quartz (and other minerals) and was deposited and recrystallized in the interstitial pore space between sand grains and as authigenic overgrowths on boundaries of some quartz grains.

Primary porosity is abundant in the Chedabucto Formation and aeolian Wolfville Formation (Figure 3.17 g, h, o, and p) but very poor to completely absent in the fluvial Wolfville Formation. Secondary porosity is present in all three locations and is typically found as microporosity from the alteration/dissolution of minerals (typically feldspar) (Figure 3.17 l), as microfractures in quartz and feldspar grains (Figure 3.17 k and o), and along irregular grain boundaries. These secondary microporosities formed through both mechanical and chemical diagenesis. As mentioned by Kettanah et al. (2013), the dissolution of these minerals in the

subsurface sandstones has not resulted in an overall net gain of porosity because of the counter action of effective burial compaction.

3.4.3 Reservoir Quality

Hydrocarbon source rocks forming during Mesozoic synrift deposition have been speculated in both the Fundy Basin (Wade et al., 1996; Brown, 2014) and the Scotian margin (Kettanah et al., 2013). The fluvial and aeolian successions of the Wolfville and Chedabucto formations could offer potential reservoirs to a working petroleum system if present.

TinyPerm values were collected on each rock sample gathered from the studied formations with results summarized in Table 3.10. Recent investigations into the permeability of materials have shown the increased interest, speed of use, and in situ (field work) capability of the handheld TinyPerm (Torabi and Alikarami, 2012; Haffen et al., 2013). De Boever et al. (2016) have shown that values produced from the handheld permeameter (TinyPerm) compare quite well to the widely used Lattice-Boltzmann method for measuring permeability.

The aeolian successions from the Wolfville Formation show the highest permeability values from, ranging from 849.57 mD to 31711.63 mD. Porosity in these successions has an average of 20.00%, with values ranging between 16.33 and 23.33%. These sandstones also comprised variable quantities of cements and were typically found to be grain-supported. The Chedabucto Formation sandstones has permeability values which range from 7.11 mD to 1971.44 mD. Porosity in these successions had an average of 10.78%, with values ranging between 2.00 and 20.75 %. The successions are typically well cemented but can also be completely cement free. The fluvial successions of the Wolfville Formation have permeability values which range between 17.19 mD to 497.42 mD. Porosity in these successions have an average of 7.06%, with values ranging between 3.50 and 14.00 %. These successions are typically

completely cemented. There is no apparent porosity in the Eurydice Formation and a single permeability value of 10.18 mD reveals very low permeability in the formation reflecting the fine grain size. A comparison of permeability versus porosity for each sample is shown in Figure 3.18. Samples from the Wolfville Formation (Rainy Cove) show low permeability and low to moderate porosity. Samples from the Chedabucto Formation show low to moderate permeability and porosity. Samples from the Wolfville Formation (Red Head) show moderate to high permeability and porosity. Typically, samples with higher porosity tend to have relatively higher permeability.

From this data it is obvious that the aeolian successions would be the highest quality reservoir (both high permeability and porosity, with little cementation). The Chedabucto and Wolfville formation fluvial sandstones would be considered medium to poor reservoirs respectively due to their lower average porosity and permeability. The Eurydice Formation shows poor porosity and permeability, and would be considered a very-poor reservoir. If speculative lacustrine source rocks are present (Wade et al., 1996; Kettanah et al., 2013; Brown, 2014) then the fluvial and aeolian successions offer potential presalt reservoirs in the subsurface offshore.

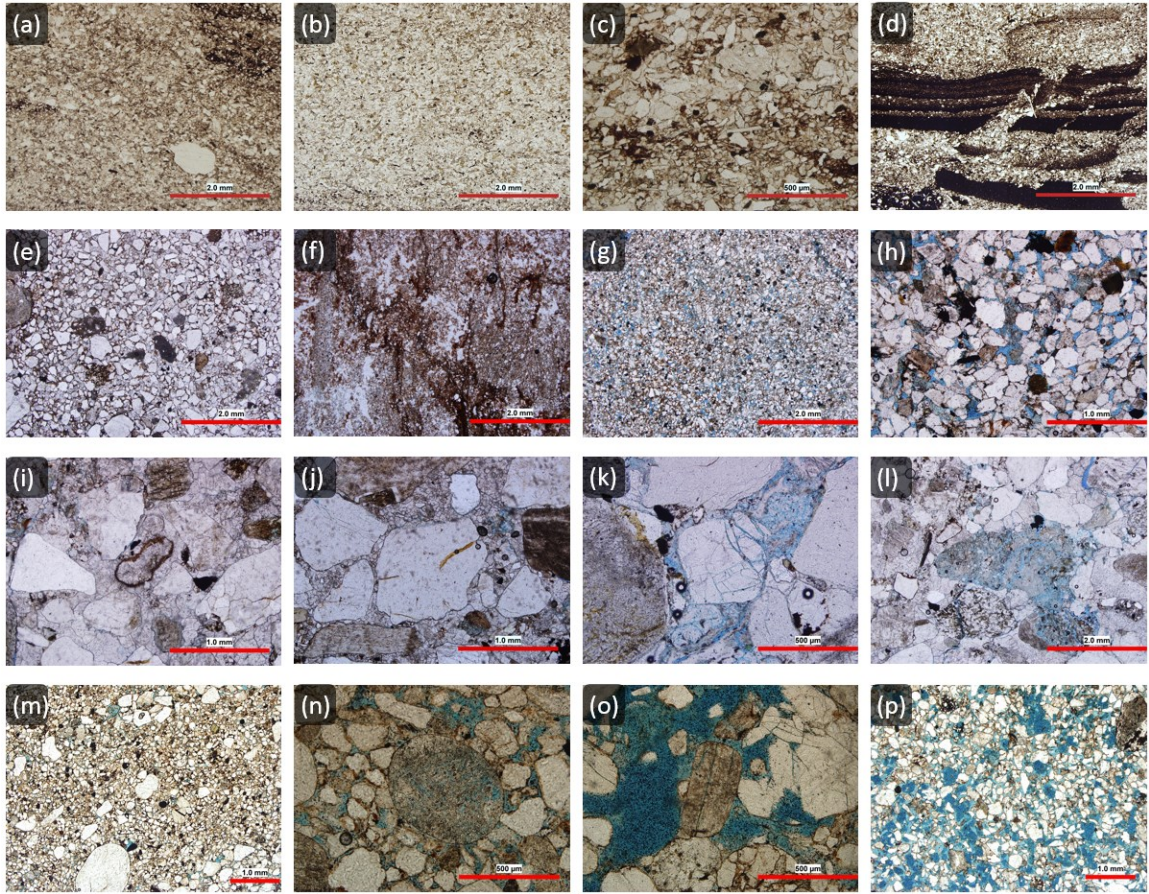


Figure 3.17: Thin section microphotographs highlighting porosity from each of the study areas. (a – d: Eurydice Formation) All four images show well cemented sandy siltstone and are generally fine-grained with occasional grain (a) or rip-up (d) clasts. (e – h): Chedabucto Formation) (e and f) Well cemented sections showing little to no primary porosity. (g) Primary porosity in a well sorted, very fine-grained sandstone. (h) Mixed primary and secondary porosity. Secondary porosity appears to be from alteration of feldspar grains. (i – l: Wolfville Formation at Rainy Cove) (i and j) Well cemented coarse-grained fraction of the conglomeratic facies showing no porosity. (k) secondary microfracture microporosity. (l) secondary porosity from alteration of feldspar. (m – p): Wolfville Formation at Red Head) (m) Well cemented, bimodal grained sandstone. (n) Secondary microporosity from the alteration of feldspar. (o) Primary and secondary porosity. Secondary porosity present as microfracture microporosity. (p) Primary porosity in a very fine to fine-grained sandstone

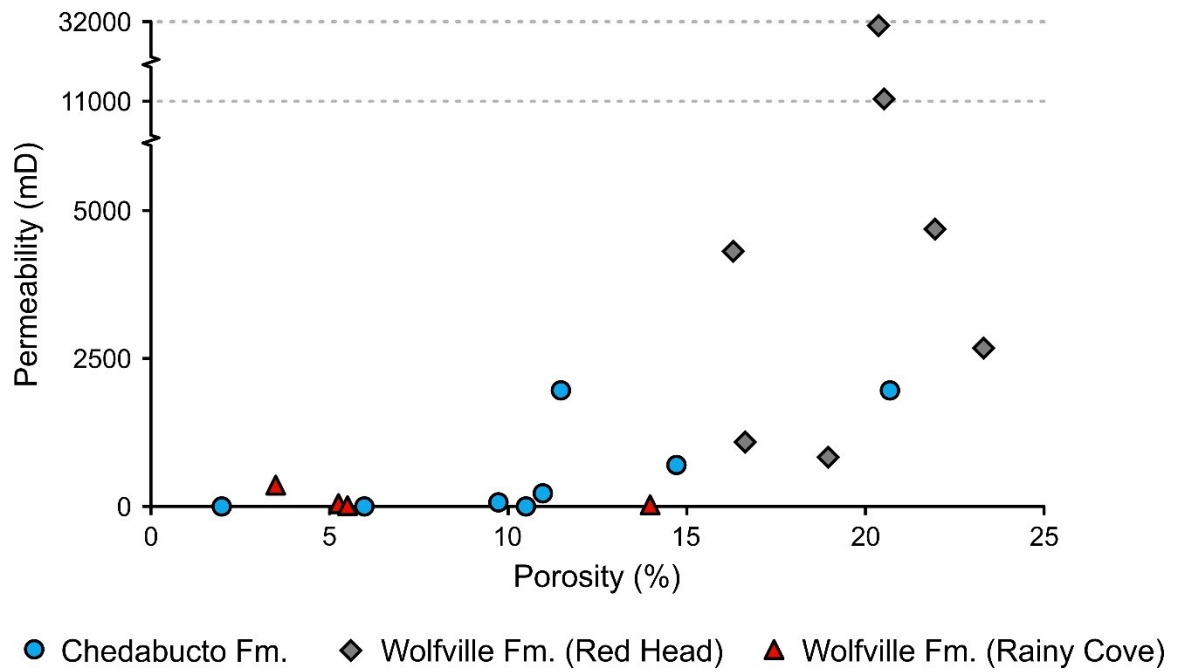


Figure 3.18: Permeability versus porosity of samples collected from the Chedabucto Formation (McCaul Island) and the Wolfville Formation (Red Head and Rainy Cove).

3.5 Conclusions

This study examines the reservoir characteristics of Late Triassic synrift successions from outcrops in the Minas Basin and Chedabucto Bay areas, and conventional drill core from the offshore Scotian Shelf using thin section petrography, X-ray fluorescence, and handheld permeability and gamma ray (radioactivity) tools. The objective of this research was to provide a new insight (or new insights) into the petroleum system elements of synrift successions of the Scotian margin.

Point count analyses from the fluvial Wolfville and Chedabucto formations shows that all of the sandstones are dominated by quartz > lithics > feldspars, with few volcanics and abundant heavy minerals such as garnets, tourmalines, and opaque minerals. The fluvial Wolfville Formation successions are highly cemented with calcite and are typically cement-supported. The Chedabucto Formation fluvial sandstones can be cement free or have some combination of silica, calcite, and iron oxide cement. The aeolian Wolfville Formation successions are dominated by quartz > lithics > feldspars, with some volcanics and fewer garnets and opaques relative to the fluvial successions. These successions may or may be weakly to non-cemented but, when present, is typically found at patchy calcite cement.

Classification of sandstones was completed using the Folk (1968) QtFL ternary plot and the Herron (1988) geochemical SandClass discrimination chart. For both classifications, the Chedabucto Formation and aeolian Wolfville Formation sandstones were found to be litharenites and sublitharenites respectively, and according to Dott (1964) were deposited in a cratonic (i.e. Pangean) fluvial to aeolian environment. The fluvial Wolfville Formation has variation between classifications of Folk and Herron. The point count QtFL ternary plot suggests

the samples are feldspathic litharenite or litharenites. The Herron geochemical classification shows that these sandstones are typically wackes.

The aeolian Wolfville Formation has a 'recycled orogenic provenance' of 'collision tectonic and arc orogen' setting. The fluvial Wolfville and Chedabucto formations dominantly plot in the 'recycled orogenic provenance' of a 'collision tectonic' setting. However, both sandstones have a scattered set of points which plot through the transitional recycled, quartzose recycled, and mixed provenance fields. The spread for the fluvial Wolfville Formation could be due to a 'transitional continental' environment during early rifting with uplift and exposure of varying basement terranes, but with time the tectonic conditions were changing towards a 'recycled orogenic environment.' Variation and scatter in the Chedabucto Formation may be due to changes in fluvial catchment areas, with possible catchment from the northern Avalon Terrane, the southern Meguma Terrane, or the same terranes but from 200 km to the west in the Minas Subbasin.

Geochemical classification using discrimination plots from Bhatia (1983) suggests that the aeolian Wolfville Formation deposited in a passive margin setting, the Chedabucto Formation deposited in a mixture between the passive margin and active continental margin settings, and the fluvial Wolfville Formation deposited in an active continental margin setting.

Results on reservoir quality show that, if present, the aeolian successions of the Wolfville Formation would be best suited as a potential presalt reservoir in the offshore subsurface. These successions have permeability values of up to 31711.63 mD, average porosity of 20.00%, and typically have only small amounts of patchy calcite cement. The fluvial Wolfville and Chedabucto formation sandstones would be fair to poor reservoirs with maximum permeability values of 497.42 mD and 1971.44 mD and average porosity of 7.06% and 10.78%

respectively. The limited study of the Eurydice Formation reveals that the core samples have an average permeability of 10.18 mD and negligible porosity, and thus would have no reservoir potential. The aeolian successions would therefore be best potential reservoirs and, depending on the amount of cement present, the fluvial successions from the Wolfville and Chedabucto formations could also produce acceptable reservoirs.

Chapter 4: Conclusions and Summary

4.1 Conclusions and Summary

This thesis described the facies, sedimentary architecture, provenance and reservoir quality of Mesozoic synrift successions from the Wolfville, Chedabucto, and Eurydice formations through cliff exposures and core lithology identification and recorded sections from outcrop along the southern (Rainy Cove) margin of the Minas Basin, along the western margin of the Orpheus Graben at Chedabucto Bay (McCaul Island), and from the Eurydice P-36 exploratory well from the Orpheus Graben offshore. A summary of findings from this study can be found in Table 4.1 and Table 4.2.

4.2 Facies and Architectural Elements

4.2.1 Lithology

Using handheld XRF data, sandstone chemical classification for the Wolfville and Chedabucto formations plotted on the SandClass scheme of Herron (1988) show the Chedabucto Formation with most points plotting in the litharenite and sublitharenite fields. Average values for all samples plot in the sublitharenite field. Classification of the Wolfville Formation (Red Head) aeolian succession has most points plotting in the sublitharenite field, including the average for all samples. Classification of the fluvial and alluvial strata of the Wolfville Formation (Rainy Cove) show most points plotting in the wacke and Fe-sand fields. The average value for these points plot in the litharenite field.

4.2.2 Facies

The facies and architectural elements from Triassic synrift successions were characterized. Facies from the Wolfville and Chedabucto formations were classified using a

modified version of Miall's (1977) facies classification system. Facies from the Eurydice Formation were described and were classified using the clastic coastal ternary diagram from Ainsworth et al. (2011).

Five facies are recognised in the lowermost part of the Wolfville Formation which form two facies associations (alluvial fan and fluvial). Four facies are recognized in the Chedabucto Formation which form two facies associations (alluvial fan and fluvial). The Eurydice Formation from the Eurydice P-36 well in the Orpheus Graben comprises three facies (cross-stratified sandstone, heterolithic sandstone and siltstone, poorly stratified to featureless sandy-siltstone) forming two facies associations (tide and wave influenced).

4.2.3 Architectural Elements

The lowermost section of the Wolfville Formation at Rainy Cove demonstrates five architectural elements, which are: GB, SB, DA, SG, and LS. The Chedabucto Formation near McCaul Island shows four architectural elements which are: GB, SB/CH, and FF.

Table 4.1: Summary table of interpreted facies, architectural elements, and paleoenvironments from the areas of Rainy Cove, McCaul Island, and the offshore Orpheus Graben.

	Rainy Cove	McCaul Island	Offshore Orpheus Graben
Facies	5 facies with 2 facies associations (fluvial and alluvial fan)	4 facies with 1 facies associations (fluvial)	3 facies with 2 facies associations (tide and wave)
Architectural Elements	Dominated by gravel (GB) but also comprises (SG), (SB), (DA), and (LS) elements	Dominated by fluvial fines (FF) but also significant channel (CH) and sandy bedform (SB) elements	-
Paleoenvironment	Fluvial – high energy, seasonally controlled, tectonically active	Fluvial – moderate to low energy, seasonally controlled, possibly tectonically active	Estuarine – tide dominated, possible vertical repetition?

4.3 Provenance, Diagenesis, and Reservoir Quality

The provenance, diagenesis, and reservoir quality of the early Mesozoic synrift infill were examined from the Wolfville, Chedabucto, and Eurydice formations using thin section petrography, X-ray fluorescence, and handheld permeability and gamma ray (radioactivity) tools. Samples were taken from outcrop along the western margin of the Orpheus Graben at Chedabucto Bay (McCaul Island), along the northern (Red Head) and the southern (Rainy Cove) margins of the Minas Basin, and from core of the Eurydice P-36 well (Orpheus Graben).

4.3.1 Provenance

Distribution of major framework mineral groups for the Wolfville and Chedabucto formations were plotted on provenance indicator ternary diagrams of Dickinson & Suczek (1979), Dickinson et al. (1982, 1983), Dickinson (1985), and Folk (1968). Sandstones from all three study locations fall into the field of ‘recycled orogenic provenance (quartzose recycled and mixed)’. Some samples from the Chedabucto Formation and aeolian Wolfville Formation

successions from Red Head fall into the 'cratonic interior'. All sandstones fall in the field of 'increasing maturity or stability from continental block provenances'. Fluvial samples from the Chedabucto and Wolfville formations all fall into the field of 'collision orogen sources'. Samples from the aeolian Wolfville Formation successions at Red Head are mixed and fall into the field of 'collision orogen sources' and 'arc orogen sources'.

Major element composition plots of sands discriminate between passive margin, active continental margin, continental arc, and oceanic arc tectonic setting (after Bhatia, 1983). In relation to TiO_2 versus $Fe_2O_3 + MgO$, average value plots between the active continental margin and passive margin tectonic fields. Points from the aeolian Wolfville Formation (Red Head) are tightly clustered below the passive margin tectonic field, with one point near the continental arc field. Points from the fluvial lowermost Wolfville Formation (Rainy Cove) are scattered within the active continental margin field and below the passive margin and active continental margin tectonic fields. The Chedabucto Formation points cluster near the passive margin tectonic field.

4.3.2 Reservoir Quality

Results on reservoir quality show that the aeolian successions of the Wolfville Formation would be best suited as a potential reservoir in the offshore subsurface. These successions had permeability values of up to 31711.63 mD, average porosity of 20.00%, and is typically found with only small amounts of patchy calcite cement. The fluvial Wolfville and Chedabucto formations have max permeability values of 497.42 mD and 1971.44 mD and average porosity of 7.06% and 10.78%. The Eurydice Formation has an average permeability of 10.18 mD and negligible porosity.

Thin section photomicrographs show porosity and reservoir quality for samples from each of the study areas. Secondary porosity is from alteration of feldspar grains in the fluvial

Wolfville Formation. The well cemented coarse-grained fraction of the conglomeratic facies shows no porosity. There is secondary microfracture microporosity and secondary porosity from alteration of feldspar. The aeolian Wolfville Formation shows well cemented, bimodal grained sandstone with secondary microporosity from the alteration of feldspar. The Chedabucto Formation thin sections are well cemented showing little to no primary porosity. The Eurydice Formation has well cemented fine grained sandy siltstone with occasional rip-up clasts.

4.3.3 Paleocurrents and Basin Analysis

Paleocurrents of the fluvial sediments of the Wolfville Formation at Rainy Cove along the Minas Basin show flow to the north. The fluvial strata from the younger Chedabucto Formation on Chedabucto Bay, indicate easterly flow towards the Orpheus Graben and may represent the eastern, onshore edge of the basin.

Table 4.2: Summary table of the sandstone classification, tectonic framework, tectonic setting, diagenesis, and reservoir quality of Mesozoic synrift successions from the areas of Rainy Cove, Red Head, McCaul Island, and the offshore Orpheus Graben.

	Rainy Cove	Red Head	McCaul Island	Offshore Orpheus Graben
Sandstone Classification	Litharenite and feldspathic litharenites	Sublitharenite	Litharenite and sublitharenite	-
Tectonic Setting (framework grain analysis)	Recycled orogen provenance	Recycled orogen provenance	Recycled orogen provenance	-
Tectonic setting (geochemical analysis)	Active continental margin	Passive margin	Passive margin	-
Diagenesis	Mechanical: mild Chemical: moderate to high	Mechanical: mild Chemical: moderate	Mechanical: moderate Chemical: moderate to high	Mechanical: mild Chemical: mild
Reservoir Quality	Mixed porosity and permeability	High porosity and permeability	Mixed porosity and permeability	Low/None porosity and permeability

References

- Ainsworth, R. B., Vakarelov, B. K., & Nanson, R. A. (2011). "Dynamic spatial and temporal prediction of changes in depositional processes on clastic shorelines: Toward improved subsurface uncertainty reduction and management." *American Association of Petroleum Geologists Bulletin*, 95(2): 267-297.
- Allen, J. (1983). "Studies in fluvial sedimentation: bars, bar-complexes and sandstone sheets (low-sinuosity braided streams) in the Brownstones (L. Devonian), Welsh Borders." *Sedimentary Geology* 33(4): 237-293.
- Armstrong-Altrin, J., Y.I. Lee, S. P. Verma, and S. Ramasamy, (2004). "Geochemistry of sandstones from the upper Miocene Kudankulam Formation, southern India: Implications for provenance, weathering, and tectonic setting." *Journal of Sedimentary Research* 74(2): 285-297.
- Barss, J. S., J. P. Bujak, J. A. Wade and G. L. Williams (1980). "Age, stratigraphy, organic matter type and color, and hydrocarbon occurrences in forty-seven wells offshore eastern Canada." *Geological Survey of Canada Open File Report No.714*: 6p.
- Bell, W. A. (1958). "Possibility for Occurrence of Petroleum in Nova Scotia." *Department of Mines, Province of Nova Scotia*: 177.
- Bhatia, M. R. (1983). "Plate tectonics and geochemical composition of sandstones." *The Journal of Geology*: 611-627.
- Bjørlykke, K., Ramm, M., & Saigal, G. C. (1989). "Sandstone diagenesis and porosity modification during basin evolution." *Geologische Rundschau*, 78(1), 243-268.
- Blair, T. C., and J. G. McPherson (1994). "Alluvial fans and their natural distinction from rivers based on morphology, hydraulic processes, sedimentary processes, and facies assemblages." *Journal of Sedimentary Research* 64(3).
- Blodgett, R. H. (1988). "Calcareous paleosols in the Triassic Dolores formation, southwestern Colorado." *Geological Society of America Special Papers* 216: 103-122.
- Broom, L. (2015). "The diversity of life in braided river systems during the Late Triassic at Burntcoat Head, Nova Scotia." *Earth Sciences, Dalhousie University. Bachelor of Science (Hons) thesis*: 73.
- Brouwer, P., 2006. *Theory of XRF*. PANalytical B.V, Almelo, Netherlands.
- Brown, D. E. (2014). "Lacustrine source rock potential in the Middle Triassic – Early Jurassic Chignecto Subbasin, offshore Eastern Canada". *Geological Association of Canada / Mineralogical Association of Canada Annual Meeting, University of New Brunswick, Fredericton, New Brunswick*.
- Canada, G. S.-O., et al. (1979). *Geology, Eastern Canada and Adjacent Areas*, Geological Survey of Canada.

- Chenin, P., and C. Beaumont (2013). "Influence of offset weak zones on the development of rift basins: Activation and abandonment during continental extension and breakup." *Journal of Geophysical Research: Solid Earth* 118(4): 1698-1720.
- De Boever, W., Bultreys, T., Derluyn, H., Van Hoorebeke, L., & Cnudde, V. (2016). "Comparison between traditional laboratory tests, permeability measurements and CT-based fluid flow modelling for cultural heritage applications." *Science of the Total Environment*, 554: 102-112.
- Dickinson, W.R., 1970, "Interpreting detrital modes of graywacke and arkose," *Journal of Sedimentary Petrology*, 40: 695–707.
- Dickinson, W. R. (1982). "Compositions of sandstones in Circum-Pacific subduction complexes and fore-arc basins." *American Association of Petroleum Geologists Bulletin* 66(2): 121-137.
- Dickinson, W. R. (1985). "Interpreting provenance relations from detrital modes of sandstones. Provenance of arenites," Springer: 333-361.
- Dickinson, W.R., Beard, L.S., Brakenridge, G.R., Erjavec, J.L., Ferguson, R.C., Inman, K.F., Knepp, R.A., Lindberg, F.A. and Ryberg, P.T., (1983). "Provenance of North American Phanerozoic sandstones in relation to tectonic setting." *Geological Society of America Bulletin* 94(2): 222-235.
- Dickinson, W. R. and C. A. Suczek (1979). "Plate tectonics and sandstone compositions." *American Association of Petroleum Geologists Bulletin* 63(12): 2164-2182.
- Fenies, H., and J.-P. Tastet (1998). "Facies and architecture of an estuarine tidal bar (the Trompeloup bar, Gironde Estuary, SW France)." *Marine Geology* 150(1): 149-169.
- Folk, R. L. (1968). "Petrology of Sedimentary Rocks." Austin, Texas, Hemphill Publishing Company.
- Gazzi, P., (1966). "Le arenarie del flysch sopracretaceo dell'Appennino modense: Correlazioni con il flysch di Monghidoro." *Mineralogica et Petrographica Acta*, 12: 69–97.
- Haffen, S., Géraud, Y., Diraison, M., & Dezayes, C. (2013). "Determination of fluid-flow zones in a geothermal sandstone reservoir using thermal conductivity and temperature logs." *Geothermics*, 46: 32-41.
- Herron, M. M. (1988). "Geochemical classification of terrigenous sands and shales from core or log data." *Journal of Sedimentary Research* 58(5): .
- Hovikoski, J., et al. (2008). "Tidal and seasonal controls in the formation of Late Miocene inclined heterolithic stratification deposits, western Amazonian foreland basin." *Sedimentology* 55(3): 499-530.
- Hubert, J. F., and Forlenza, M. F., (1988). "Sedimentology of Braided River Deposits in the Upper Triassic Wolfville Redbeds, Southern Shore of Cobequid Bay, Nova Scotia, Canada." In: Warren Manspiezer (Ed.) "Triassic-Jurassic Rifting: Continental Break-up and the Origin of the Atlantic Ocean and Passive Margins, Part A." Elsevier, New York: 231-247.
- Hubert, J. F., and K. A. Mertz Jr. (1980). "Eolian dune field of Late Triassic age, Fundy Basin, Nova Scotia." *Geology* 8(11): 516-519.

- Hubert, J. F., and K. A. Mertz Jr. (1984). "Eolian sandstones in Upper Triassic-Lower Jurassic red beds of the Fundy Basin, Nova Scotia." *Journal of Sedimentary Research* 54(3): 798-810.
- Jansa, L. F., and J. A. Wade (1975). "Paleogeography and sedimentation in the Mesozoic and Cenozoic, southeastern Canada." In: C. J. Yorath, E. R. Parker and D. J. Glass (Eds.) "Canada's Offshore Margins and Petroleum Exploration." Canadian Society of Petroleum Geologists, Memoir 4: 79-102.
- Keppie, J. D. (1982). "The Minas Geofracture." In: P. St. Julian and J. Beland (Eds.) "Major Structural Zones and Faults of the Northern Appalachians." Geological Association of Canada, Special Paper 24: 263-280.
- Kettanah, Y. A. (2013). "Hydrocarbon fluid inclusions in the Argo salt, offshore Canadian Atlantic margin." *Canadian Journal of Earth Sciences*, 50(6): 607-635.
- Kettanah, Yawooz A., Muhammad Y. Kettanah, and Grant D. Wach. "Provenance, diagenesis and reservoir quality of the Upper Triassic Wolfville Formation, Bay of Fundy, Nova Scotia, Canada." Geological Society, London, Special Publications 386 (2013): SP386-18
- Klein, G. D. (1962). "Triassic sedimentation, Maritime Provinces, Canada." *Geological Society of America Bulletin* 73(9): 1127-1146.
- Kent, D. V., and L. Tauxe (2005). "Corrected Late Triassic latitudes for continents adjacent to the North Atlantic. *Science*, 307: 240-244.
- Kent, D. V., P. E. Olsen, and W. K. Witte (1995). "Late Triassic-earliest Jurassic geomagnetic polarity sequence and paleolatitudes from drill cores in the Newark rift basin, eastern North America." *Journal of Geophysical Research – Solid Earth*, 100 (B8): 14,965-014,998.
- Leleu, S., and A. J. Hartley (2010). "Controls on the stratigraphic development of the Triassic Fundy Basin, Nova Scotia: implications for the tectonostratigraphic evolution of Triassic Atlantic rift basins." *Journal of the Geological Society* 167(3): 437-454.
- Leleu, S., A. J. Hartley, and B. P. J. Williams (2009). "Large-scale alluvial architecture and correlation in a Triassic pebbly braided river system, lower Wolfville Formation (Fundy Basin, Nova Scotia, Canada)." *Journal of Sedimentary Research* 79(5): 265-286.
- MacEachern, J., G. Pemberton, M. Gingras, and K. Bann (2010). "Ichnology and facies models." In: N. P. James and R. W. Dalrymple (Eds.) "Facies Models 4", Geological Association of Canada: 19-58.
- MacLean, B. C., and J. A. Wade (1993). "Seismic Markers and Stratigraphic Picks in the Scotian Basin Wells. "East Coast Basin Atlas Series, Geological Survey of Canada: 276.
- Miall, A. D. (1978). "Lithofacies types and vertical profile models in braided river deposits: a summary." In: A. D. Miall (Ed.) *Fluvial Sedimentology*." Canadian Society of Petroleum Geologists Memoir 5: 597-604.
- Miall, A. D. (1985). "Architectural-element analysis: a new method of facies analysis applied to fluvial deposits." *Earth Science Reviews*, 22 (4): 261-308.

- Miall, A. D. (1996). "The Geology of Fluvial Deposits." *Sedimentary Facies, Basin Analysis, and Petroleum Geology.* Springer-Verlag: 582.
- Miall, A. D. (2016). "Facies Models." In: A. D. Miall, "Stratigraphy: A Modern Synthesis." Springer: 161-214.
- Murphy, J. B., J.W. Waldron, D. J. Kontak, G. Pe-Piper, and D. J. W. Piper (2011). "Minas Fault Zone: Late Paleozoic history of an intra-continental orogenic transform fault in the Canadian Appalachians." *Journal of Structural Geology*, 33(3), 312-328.
- Olsen, P. E. (1997). "Stratigraphic record of the early Mesozoic breakup of Pangea in the Laurasia-Gondwana rift system." *Annual Review of Earth and Planetary Sciences* 25(1): 337-401.
- Olsen, P. E., and P. J. W. Gore (1989). "Tectonic, Depositional, and Paleontological History of Early Mesozoic Rift Basins, Eastern North America." 28th International Geological Congress, Field Trip Guidebook T351: 174.
- Olsen, P. E., and R. W. Schlische (1990). "Transtensional arm of the early Mesozoic Fundy rift basin: penecontemporaneous faulting and sedimentation." *Geology* 18(8): 695-698.
- Olsen, P. E., D. V. Kent, S. J. Fowell, R. W. Schlische, M. O. Withjack, and P. M. LeTourneau (2000). "Implications of a comparison of the stratigraphy and depositional environments of the Argana (Morocco) and Fundy (Nova Scotia, Canada) Permian-Jurassic basins." In: M. Oujidi and M. Et-Touhani (Eds.), "Le Permian et le Trias du Maroc, Actes de la Premier Reunion du Groupe Marocain de Permian et du le Trias." Hilal Impression, Oudja, Maroc: 165-183.
- Olsen, P. E., D. V. Kent, and M. Et-Touhami, M. (2003). "Chronology and stratigraphy of the Fundy and related Nova Scotia offshore basins and Morocco based on core and outcrop." In: Conventional Core Workshop, Geological Society of America (NE Section) and Atlantic Geoscience Society Conference, Halifax: 51-63.
- Ramos, A., and A. Sopeña (1983). "Gravel bars in low-sinuosity streams (Permian and Triassic, central Spain)."
- Reading, H. G., & Levell, B. K. (1996). "Controls on the sedimentary rock record." In: Reading, H. G. (Ed.), *Sedimentary environments: processes, facies and stratigraphy*, 3, 5-36.
- Roberts, D. G., and A. W. Bally (2012). *Regional geology and tectonics: Phanerozoic rift systems and sedimentary basins.* Elsevier.
- Russell, I. C. (1880). "On the former extent of the Triassic formation of the Atlantic states." *American Naturalist* 14: 703-712.
- Saigal, G. C., and K. Bjørlykke, (1987). "Carbonate cements in clastic reservoir rocks from offshore Norway—relationships between isotopic composition, textural development and burial depth." *Geological Society, London, Special Publications*, 36(1): 313-324.
- Schlische, R. W. (2003). "Progress in understanding the structural geology, basin evolution, and tectonic history of the eastern North American rift system." In: P. M. LeTourneau, and P. E. Olsen

- (Eds.) "The Great Rift Valleys of Pangea in Eastern North America 1. Columbia University Press, New York: 21-64.
- Smalley, P. C., et al. (2008). "Handling risk and uncertainty in petroleum exploration and asset management: An overview." *American Association of Petroleum Geologists Bulletin*, 92(10): 1251-1261.
- Smith, D. G. (1991). "Clastic tidal sedimentology." *Canadian Society of Petroleum Geologists Memoir* 16: 387.
- Steel, R., and D. Thompson (1983). "Structures and textures in Triassic braided stream conglomerates ('Bunter' pebble beds) in the Sherwood Sandstone Group, North Staffordshire, England." *Sedimentology* 30(3): 341-367.
- Sues, H.-D., and P. E. Olsen (2015). "Stratigraphic and temporal context and faunal diversity of Permian-Jurassic continental tetrapod assemblages from the Fundy rift basin, eastern Canada." *Atlantic Geology*, 51: 139-205.
- Swanson, M. T. (1986). "Pre-existing fault control for Mesozoic basin formation in eastern North America." *Geology* 14(5): 419-422.
- Tanner, L. H., and D. E. Brown (1999). "The Upper Triassic Chedabucto Formation, Guysborough County, Nova Scotia: depositional and tectonic context." *Atlantic Geology* 35: 129-138.
- Tillman, R. W., and W. R. Almon, (1979). "Diagenesis of Frontier Formation offshore bar sandstone, Spearhead Ranch Field, Wyoming." In: P.A. Scholle & P. R. Schluger (Eds.): "Aspects of diagenesis." *Soc. Econ. Paleontol. Mineral. Spec. Publ.* 26: 337-378.
- Torabi, A., and R. Alikarami, (2012). "Heterogeneity within deformation bands in sandstone reservoirs." In: 46th US Rock Mechanics/Geomechanics Symposium. American Rock Mechanics Association.
- Wade, J. A., and B. C. MacLean (1990). "The geology of the southeastern margin of Canada." *Geology of the continental margin of eastern Canada: Geological Survey of Canada, Geology of Canada* 2: 167-238.
- Wade, J. A., Brown, D. E., Fensome, R. A., and Traverse, A. (1996). "The Triassic-Jurassic Fundy Basin, Eastern Canada: regional setting, stratigraphy and hydrocarbon potential." *Atlantic Geology*, 32(3): 189-231.
- Williams, G. L., L. R. Fyffe, R. J. Wardle, S. P. Colman-Sadd, and R. C. Boehner (Eds.) (1985). "Lexicon of Canadian Stratigraphy Volume VI - Atlantic Region." *Canadian Society of Petroleum Geologists, Calgary*, 572p.
- Withjack, M. O., and R. W. Schlische (2005). A review of tectonic events on the passive margin of eastern North America. *Petroleum Systems of Divergent Continental Margin Basins: 25th Bob S. Perkins Research Conference, Gulf Coast Section of SEPM, SEPM.*

Withjack, M. O., P. E. Olsen, and R. W. Schlische (1995). "Tectonic evolution of the Fundy rift basin, Canada: evidence of extension and shortening during passive margin development." *Tectonics* 14(2): 390-405.

Withjack, M. O., R. W. Schlische, and M. S. Baum (2009). "Extensional development of the Fundy rift basin, southeastern Canada." *Geological Journal* 44(6): 631-651.

Withjack, M. O., R. W. Schlische, and P. E. Olsen (1998). "Diachronous rifting, drifting and inversion on the passive margin of Central Eastern North America: an analog for other passive margins." *American Association of Petroleum Geologists Bulletin*, 82(5A): 817-835.

Appendix A

Sample Description Overview

Sample: GW-02-RC

Hand sample:

- Colour: Reddish-Brown
- Grain Size: coarse to very-coarse (0.5 to 2 mm)
- Visible minerals: quartzite
- Sedimentary features: N/A



Thin section:

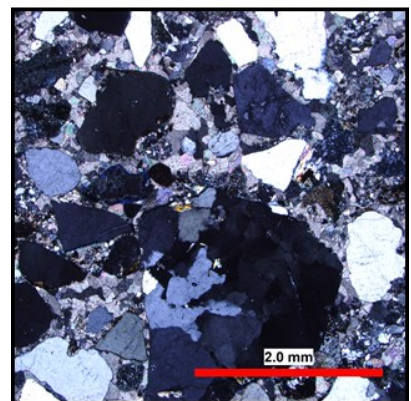
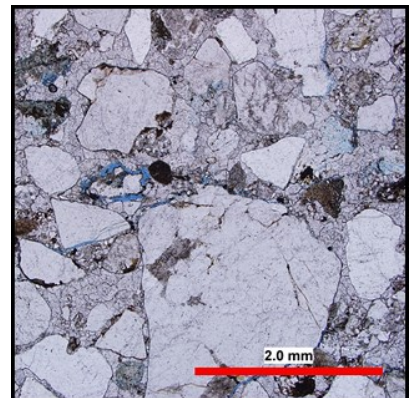
- Grain Size: coarse to very-coarse (0.5 to 2 mm)
- Grain Shape: Subangular to subrounded
- Grain Sorting: Poorly to very-poorly sorted
- Grain Packing: loosely packed with framework grains rarely in contact
- Pore space:
 - Primary found around few grain boundaries
 - Secondary found in vacuolized feldspars

Petrography:

- Framework Grains:
 - Quartz (70%)
 - Lithic fragments (15%)
 - Alkali Feldspar (10%)
 - Plagioclase (3%)
 - Opaques (1%)
 - Muscovite (1%)
- Matrix: Calcite cement
- Accessory minerals:
 - Garnet
 - Tourmaline

Notes:

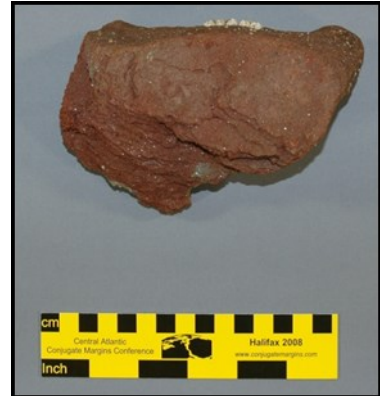
- Feldspars: highly altered and comprise internal quartz, tourmaline, lithic, and muscovite grains
- Feldspars: secondary porosity (vacuolized)
- Quartz: cracked grains are common
- Quartz: overgrowth on some grains



Sample: GW-03-RC

Hand sample:

- Colour: Reddish-Brown
- Grain Size: very-fine to fine
- Visible minerals: none
- Sedimentary features: mm-scale laminations



Thin section:

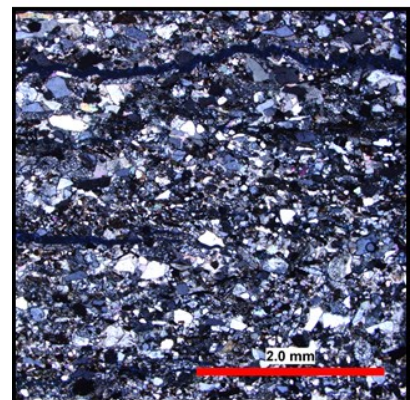
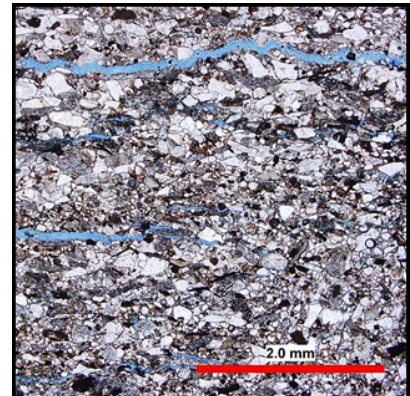
- Grain Size: very-fine to med. (0.062 to 0.5 mm)
- Grain Shape: Angular to subrounded
- Grain Sorting: Poor to moderate sorting
- Grain Packing: tightly packed and elongate grains are aligned parallel to laminations
- Pore space:
 - Primary: along lamination boundaries
 - Secondary: vacuolized feldspars and along margins of muscovite grains

Petrography:

- Framework Grains:
 - Quartz (70%)
 - Lithic fragments (20%)
 - Alkali Feldspar (5%)
 - Plagioclase (3%)
 - Opaques (1%)
 - Muscovite (1%)
 - Chlorite/Biotite (<1%)
- Matrix: Calcite cement
- Accessory minerals:
 - Garnet
 - Tourmaline

Notes:

- Grains are relatively tightly packed: porosity occurs along the boundaries between laminations.
- Clay minerals (chlorite, biotite, muscovite) rarely found either crushed or bending around detrital grains.
- Feldspars are altered (appear dirty) and comprise secondary porosity (vacuolized feldspars)
- Calcite cement after feldspar secondary porosity.



Sample: GW-04-RC

Hand sample:

- Colour: Reddish-Brown
- Grain Size: lower medium to upper very-coarse
- Visible minerals: quartz (possibly quartzite), calcite cement, feldspars
- Sedimentary features: N/A
- Name: Poorly sorted, very-coarse grained pebble conglomerate



Thin section:

- No thin section made

N/A

Sample: GW-05-RC

Hand sample:

- Colour: Reddish-Brown
- Grain Size: lower medium to upper very-coarse
- Visible minerals: quartz (possibly quartzite)
- Sedimentary features: mild imbrication?
- Name: Poorly sorted, very-coarse grained pebble conglomerate



Thin section:

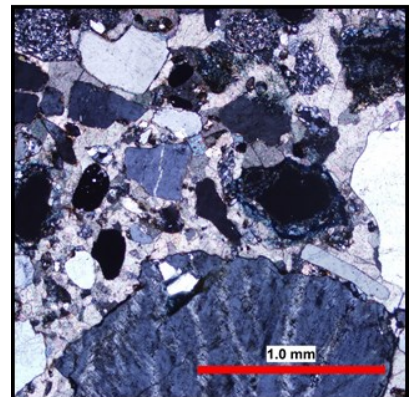
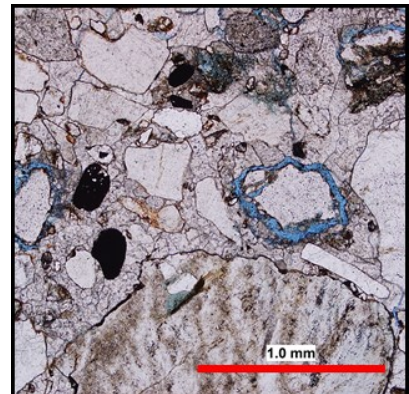
- Grain Size: silt to pebbles (0.031 to 64 mm)
- Grain Shape: subangular to rounded
- Grain Sorting: Very poorly sorted
- Grain Packing: Loosely packed, rarely in contact
- Pore space:
 - Primary: Primary along grain boundaries and within matrix
 - Secondary found in vacuolized feldspars and surrounding alteration rims of an unknown isotropic mineral

Petrography:

- Framework Grains:
 - Quartz (65%)
 - Lithic fragments (20%)
 - Alkali Feldspar (dominantly orthoclase) (8%)
 - Plagioclase (4%)
 - Opaques (2%)
 - Muscovite (1%)
- Matrix: Calcite cement
- Accessory minerals:
 - Tourmaline
 - Garnet

Notes:

- Feldspars: altered, could be related to unknown isotropic mineral, comprise secondary porosity (vacuolized)
- Smashed quarts are present
- Quarts overgrowth along rims of other detrital grains
- Calcite cementing after smashed quartz and alteration of feldspar



Sample: GW-06-RC

Hand sample:

- Colour: Reddish-Brown
- Grain Size: lower medium to upper very-coarse
- Visible minerals: quartz (possibly quartzite), calcite cement, feldspars
- Sedimentary features: N/A
- Name: Poorly sorted, very-coarse grained pebble conglomerate



Thin section:

- No thin section made

N/A

Sample: GW-07-RC

Hand sample:

- Colour: Reddish-Brown
- Grain Size: lower medium to upper very-coarse
- Visible minerals: quartz (possibly quartzite), calcite cement, feldspars
- Sedimentary features: N/A
- Name: Poorly sorted, very-coarse grained pebble conglomerate



Thin section:

- No thin section made

N/A

Sample: GW-08-RC

Hand sample:

- Colour: Reddish-Brown
- Grain Size: lower coarse to upper very-coarse
- Visible minerals: quartz (possibly quartzite), calcite cement
- Sedimentary features: mild imbrication?
- Name: Poorly sorted, very-coarse grained boulder conglomerate



Thin section:

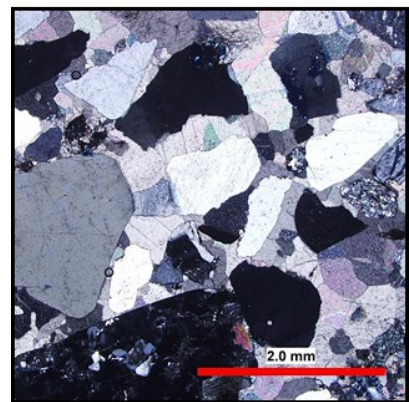
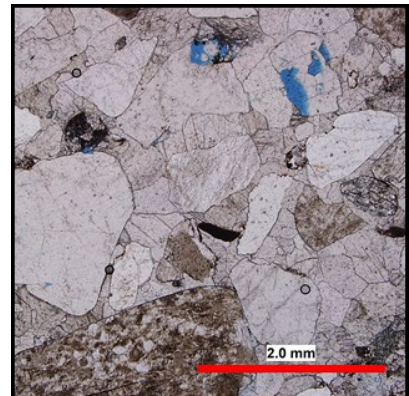
- Grain Size: coarse sand to boulder clasts (0.5 to 256+ mm)
- Grain Shape: subangular to rounded
- Grain Sorting: Poorly to moderately sorted
- Grain Packing: Loosely packed with framework grains rarely in contact
- Pore space:
 - Primary: Primary along grain boundaries and within matrix
 - Secondary: vacuolized feldspar

Petrography:

- Framework Grains:
 - Quartz (60%)
 - Lithic fragments (18%)
 - Alkali Feldspar (orthoclase) (10%)
 - Plagioclase (10%)
 - Opaques (1%)
 - Muscovite (1%)
- Matrix: Calcite cement
- Accessory minerals: None

Notes:

- Feldspars are lightly altered (appear dirty) relative to other samples
 - Feldspars also comprise secondary porosity (vacuolized feldspars)
- Calcite cement timing must have been after alteration of feldspar forming secondary porosity.
- Although alteration of minerals (muscovite and feldspars) is still present, the sample overall is much less altered relative to other samples



Sample: GW-09-RC

Hand sample:

- Colour: Brownish-red
- Grain Size: very-fine to fine grained sand
- Visible minerals: clasts (quartzite?)
- Sedimentary features: visible angular clasts
- Name: Fine grained pebble breccia



Thin section:

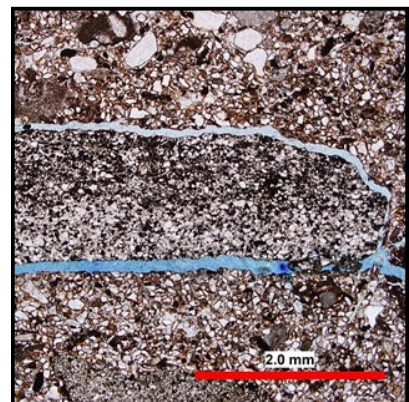
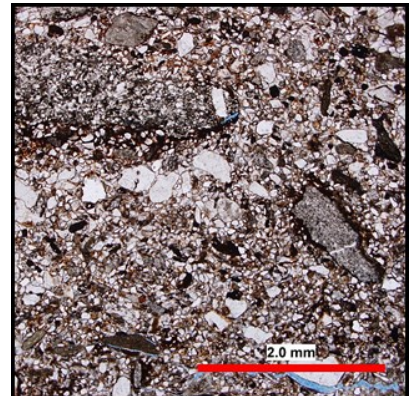
- Grain Size: very fine to coarse grained (0.062 to 1 mm)
- Grain Shape: Subangular to rounded
- Grain Sorting: Poorly sorted
- Grain Packing: Moderately to tightly packed
- Bimodal distribution of grains (coarse grains and fine to very-fine grains)
- Pore space:
 - Primary along larger breccia clasts boundaries
 - Minor secondary porosity within altered breccia clasts

Petrography:

- Framework Grains:
 - Quartz (75%)
 - Lithic fragments (10%)
 - Alkali Feldspar (dominantly orthoclase) (5%)
 - Plagioclase (5%)
 - Opaques (3%)
 - Muscovite (2%)
- Matrix: Calcite cement
- Accessory minerals:

Notes:

- Most of the framework clasts are comprised of quartz (with the coarser fraction being almost entirely quartz)
- Feldspars are altered (appear dirty) and comprise secondary porosity (vacuolized feldspars)
- Calcite cement timing must have been after alteration of feldspar forming secondary porosity.
- Sample appears relatively fresh compared to other samples



Sample: RHP-1

Hand sample:

- Colour: Red
- Grain Size: coarse to very-coarse
- Visible minerals: quartz (possibly quartzite), calcite cement
- Sedimentary features: N/A
- Name: Poorly sorted, very-coarse grained sandstone



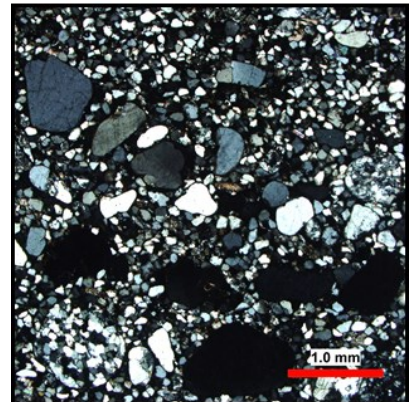
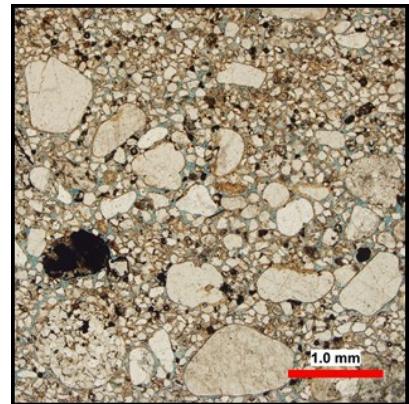
Thin section:

- Grain Size: Fine to very coarse-grained
- Grain Shape: Rounded
- Grain Sorting: Bimodal (well sorted)
- Grain Packing: Tight to moderate
- Pore space:
 - Primary

Petrography:

- Framework Grains:
 - Quartz (65%)
 - Lithic fragments (20%)
 - Alkali Feldspar (orthoclase) (5%)
 - Plagioclase (3%)
 - Opaques (5%)
 - Muscovite (2%)
- Matrix: some clays, calcite cement
- Accessory minerals:

Notes:



Sample: RHP-2

Hand sample:

- Colour: Red
- Grain Size: coarse to very-coarse
- Visible minerals: N/A
- Sedimentary features: Unconsolidated
- Name: Poorly sorted, coarse to very coarse-grained sandstone



Thin section:

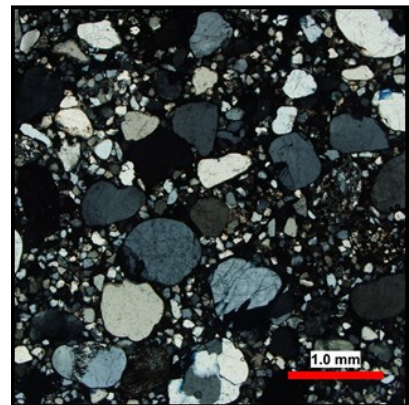
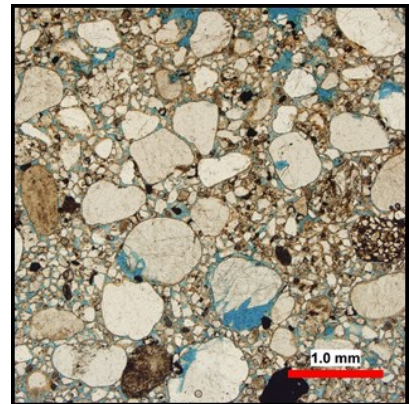
- Grain Size: Very fine to very coarse-grained
- Grain Shape: Round
- Grain Sorting: Bimodal (well sorted)
- Grain Packing: Moderate
- Pore space:
 - Primary: matrix space
 - Secondary: vacuolized feldspar, microfractured quartz

Petrography:

- Framework Grains:
 - Quartz (65%)
 - Lithic fragments (20%)
 - Alkali Feldspar (orthoclase) (5%)
 - Plagioclase (3%)
 - Opaques (5%)
 - Muscovite (2%)
- Matrix: clays, patchy calcite cement
- Accessory minerals:
 - Zircon
 - Garnet

Notes:

- Patchy calcite cementation
- Alteration of feldspars of different stages (little to no alteration to complete alteration)



Sample: RHP-3

Hand sample:

- Colour: Red
- Grain Size: medium to coarse
- Visible minerals: Quartz
- Sedimentary features: N/A
- Name: Poorly sorted, medium to coarse-grained, pebbly sandstone



Thin section:

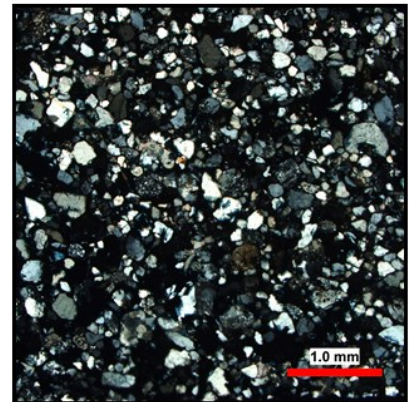
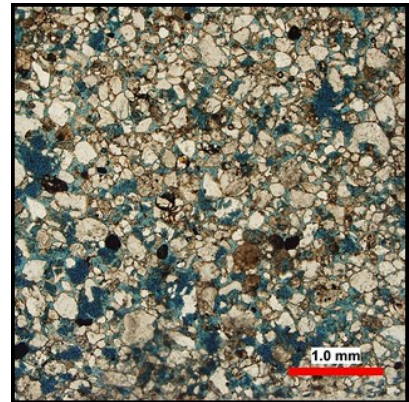
- Grain Size: Fine to medium-grained
- Grain Shape: subround to round
- Grain Sorting: Bimodal (well sorted)
- Grain Packing: Moderate to loose
- Pore space:
 - Primary: matrix space
 - Secondary: vacuolized feldspar, microfractured quartz

Petrography:

- Framework Grains:
 - Quartz (68%)
 - Lithic fragments (17%)
 - Alkali Feldspar (orthoclase) (5%)
 - Plagioclase (4%)
 - Opaques (4%)
 - Muscovite (2%)
- Matrix: clays, patchy calcite cement
- Accessory minerals:
 - Zircon
 - Garnet

Notes:

- Patchy calcite cementation
- Mild alteration of feldspars



Sample: RHP-4

Hand sample:

- Colour: Red
- Grain Size: silt to very fine-grained
- Visible minerals: N/A
- Sedimentary features: N/A
- Name: Well rounded, very fine-grained silty sandstone



Thin section:

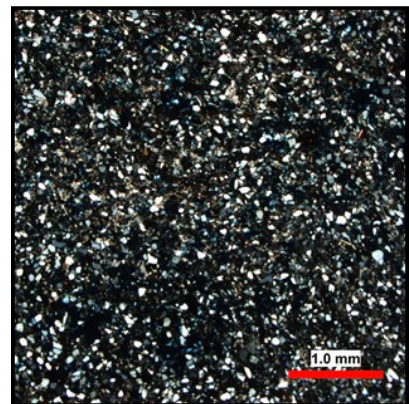
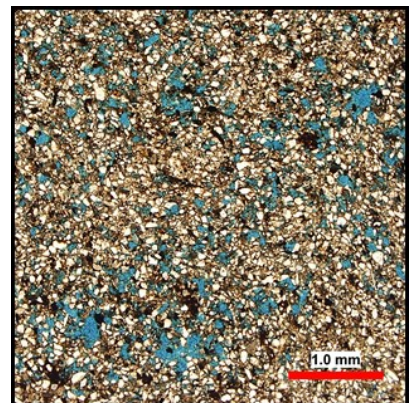
- Grain Size: Very fine to fine-grained
- Grain Shape: subround
- Grain Sorting: Well sorted
- Grain Packing: Moderate to loose
- Pore space:
 - Primary: matrix space
 - Secondary: vacuolized feldspar (rare)

Petrography:

- Framework Grains:
 - Quartz (60%)
 - Lithic fragments (23%)
 - Alkali Feldspar (orthoclase) (5%)
 - Plagioclase (5%)
 - Opaques (5%)
 - Muscovite (2%)
- Matrix: clays, patchy calcite cement
- Accessory minerals:
 - Zircon

Notes:

- Patchy calcite cementation
- Mild alteration of feldspars



Sample: RHP-5

Hand sample:

- Colour: Red
- Grain Size: silt to very fine-grained
- Visible minerals: N/A
- Sedimentary features: N/A
- Name: Well rounded, very fine-grained silty sandstone



Thin section:

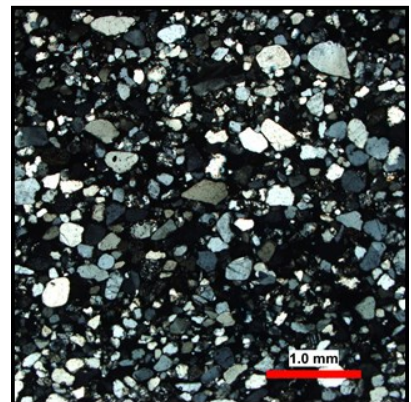
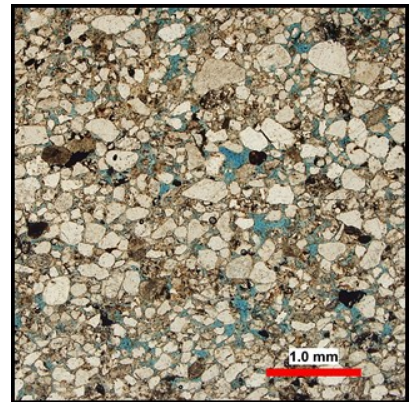
- Grain Size: Very fine to coarse-grained
- Grain Shape: Subround
- Grain Sorting: Bimodal (well sorted)
- Grain Packing: Tight to moderate
- Pore space:
 - Primary: matrix space
 - Secondary: vacuolized feldspar, microfractured quartz (rare)

Petrography:

- Framework Grains:
 - Quartz (65%)
 - Lithic fragments (18%)
 - Alkali Feldspar (orthoclase) (5%)
 - Plagioclase (5%)
 - Opaques (5%)
 - Muscovite (2%)
- Matrix: clays, patchy calcite cement
- Accessory minerals:
 - Zircon

Notes:

- Patchy calcite cementation
- Alteration of feldspars forming secondary porosity



Sample: RHP-7

Hand sample:

- Colour: Red
- Grain Size: medium to coarse-grained
- Visible minerals: Quartz pebbles
- Sedimentary features: N/A
- Name: Well rounded, medium to coarse-grained sandstone



Thin section:

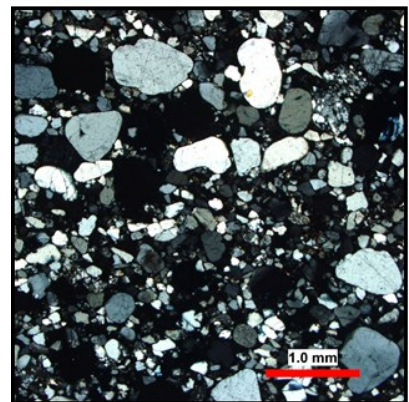
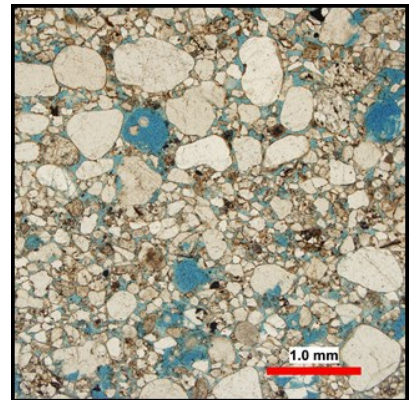
- Grain Size: Fine to very coarse-grained
- Grain Shape: Subround to round
- Grain Sorting: Bimodal (well sorted)
- Grain Packing: Tight to moderate
- Pore space:
 - Primary: matrix space
 - Secondary: vacuolized feldspar, microfractured quartz (rare)

Petrography:

- Framework Grains:
 - Quartz (75%)
 - Lithic fragments (17%)
 - Alkali Feldspar (3%)
 - Plagioclase (2%)
 - Opaques (2%)
 - Muscovite (1%)
- Matrix: clays, patchy calcite cement
- Accessory minerals:
 - Zircon
 - Garnet
 - Tourmaline

Notes:

- Patchy calcite cementation



Sample: RHP-8

Hand sample:

- Colour: Red
- Grain Size: medium to coarse-grained
- Visible minerals: Quartz pebbles
- Sedimentary features: N/A
- Name: Well rounded, medium to coarse-grained sandstone



Thin section:

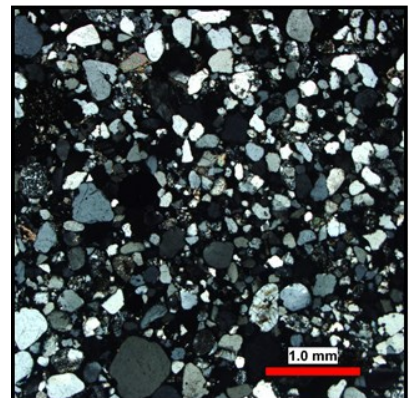
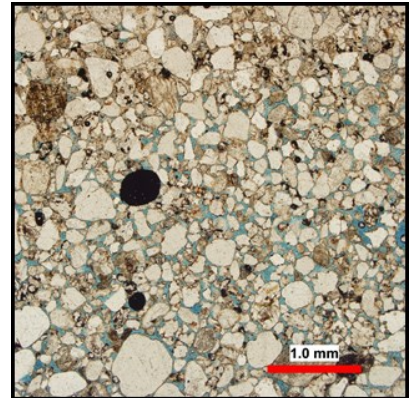
- Grain Size: Fine to very coarse-grained
- Grain Shape: Subround to round
- Grain Sorting: Bimodal (moderately sorted)
- Grain Packing: Tight
- Pore space:
 - Primary: matrix space
 - Secondary: vacuolized feldspar

Petrography:

- Framework Grains:
 - Quartz (75%)
 - Lithic fragments (15%)
 - Alkali Feldspar (5%)
 - Plagioclase (2%)
 - Opaques (2%)
 - Muscovite (1%)
- Matrix: clays, patchy calcite cement
- Accessory minerals:
 - Zircon
 - Garnet
 - Tourmaline

Notes:

- Patchy calcite cementation



Sample: RHP-Base

Hand sample:

- Colour: Red
- Grain Size: coarse to very coarse-grained
- Visible minerals: Quartz pebbles
- Sedimentary features: N/A
- Name: Medium to coarse-grained, massive sandstone



Thin section:

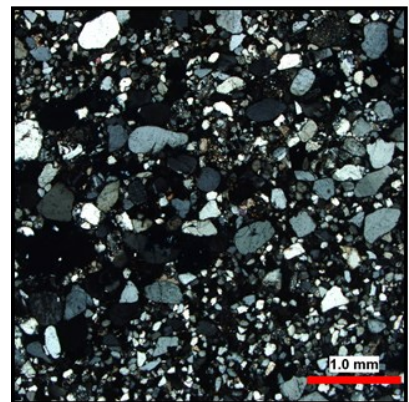
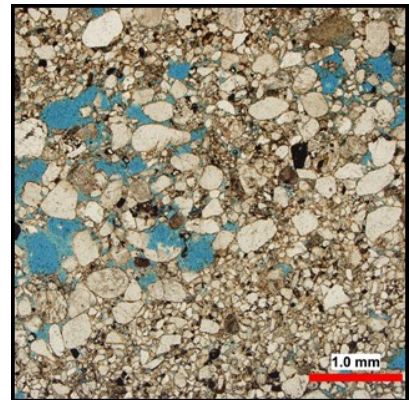
- Grain Size: Very fine to coarse-grained
- Grain Shape: Subround
- Grain Sorting: Bimodal (well sorted)
- Grain Packing: Tight to moderate
- Pore space:
 - Primary: matrix space
 - Secondary: vacuolized feldspar, microfractured quartz (rare)

Petrography:

- Framework Grains:
 - Quartz (65%)
 - Lithic fragments (18%)
 - Alkali Feldspar (orthoclase) (5%)
 - Plagioclase (5%)
 - Opaques (5%)
 - Muscovite (2%)
- Matrix: clays, patchy calcite cement
- Accessory minerals:
 - Zircon

Notes:

- Patchy calcite cementation
- Alteration of feldspars forming secondary porosity



Sample: GW-301

Hand sample:

- Colour: Red-gray
- Grain Size: very fine to medium-grained
- Visible minerals: N/A
- Sedimentary features: Redox spots/marks
- Name: Moderately sorted, very fine to medium-grained sandstone

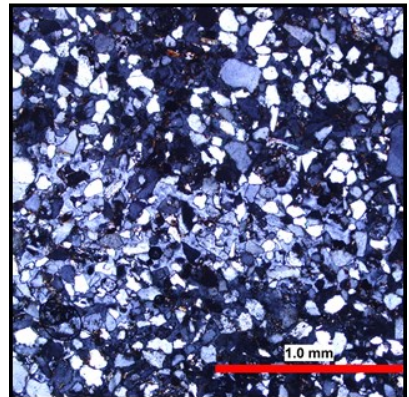
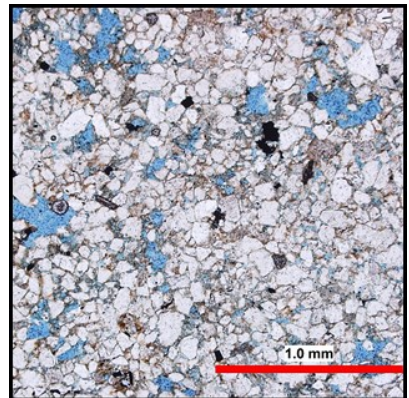


Thin section:

- Grain Size: very-fine lower to medium lower (0.0625 to 0.35 mm)
- Grain Shape: Subangular to rounded
- Grain Sorting: moderately to well sorted
- Grain Packing: moderate to tight packing

Petrography:

- Framework Grains:
 - Quartz: 80 %
 - Lithics: 10%
 - Alkali feldspar: 4%
 - Plagioclase: 4%
 - Muscovite: (<1%)
 - Opaques: (<1%)
 - Biotite: (<1%)
- Matrix:
 - Silica
 - Calcite
 - Iron oxide
- Accessory minerals:
 - Garnet
 - Tourmaline
 - Zircon



Sample: GW-302

Hand sample:

- Colour: Red-gray
- Grain Size: medium to coarse-grained
- Visible minerals: N/A
- Sedimentary features: N/A
- Name: Well sorted, medium to coarse-grained sandstone



Thin section:

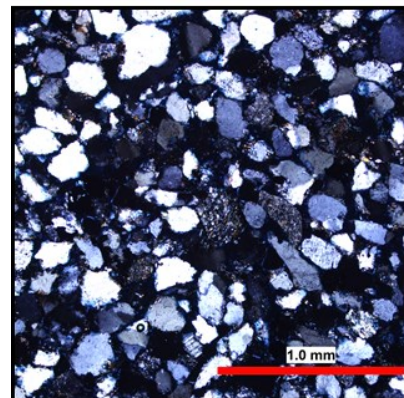
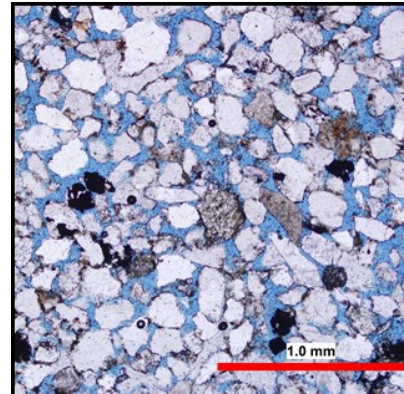
- Grain Size: very-fine lower to medium upper (0.0625 to 0.5 mm)
- Grain Shape: subangular to rounded
- Grain Sorting: Well sorted
- Grain Packing: Tightly packed
- Pore space:
 - Primary: between grains
 - Secondary: grain dissolution, grain boundary, intragranular (lithics)

Petrography:

- Framework Grains:
 - Quartz: 90%
 - Lithics: 3%
 - Alkali feldspar: 2%
 - Plagioclase: 3%
 - Muscovite: (<1%)
 - Opaques: 2%
 - Biotite: (<1%)
 - Muscovite: (<1%)
- Matrix: None
- Accessory minerals:
 - Garnet
 - Zircon
 - Tourmaline

Notes:

- Little to no alteration of minerals.
 - Some alteration of feldspars
- Little amounts of iron oxide cementation
- Sample is well sorted and comprises mostly quartz as a framework grain



Sample: GW-303

Hand sample:

- Colour: Red
- Grain Size: very fine-grained
- Visible minerals: N/A
- Sedimentary features: N/A
- Name: Well sorted, very fine-grained sandstone



Thin section:

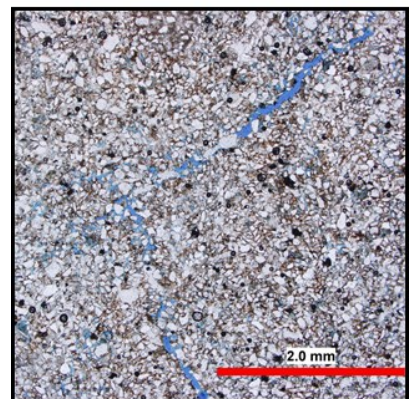
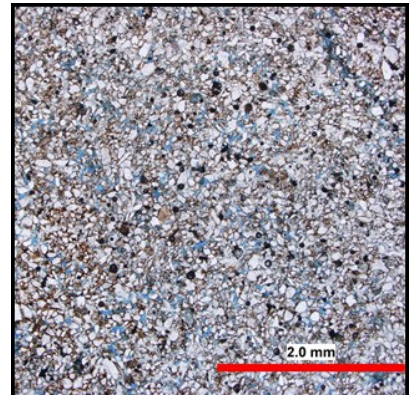
- Grain Size: silt to fine upper sands (0.002 to 0.025 mm)
- Grain Shape: subangular to subrounded
- Grain Sorting: well sorted
- Grain Packing: moderately packing
- Pore space:
 - Primary: Present, largely occurs in fractures
 - Secondary: Grain dissolution

Petrography:

- Framework Grains:
 - Quartz: major
 - Lithics: medium
 - Alkali feldspar: minor
 - Plagioclase: minor
 - Muscovite: minor
 - Opaques: minor
 - Biotite: minor
- Matrix:
 - Calcite cement
 - Iron oxide cement
- Accessory minerals:
 - Garnet
 - Tourmaline

Notes:

- Mostly silt and clay minerals with few detrital grains of quartz and feldspar



Sample: GW-304

Hand sample:

- Colour: Gray
- Grain Size: very fine-grained
- Visible minerals: N/A
- Sedimentary features: N/A
- Name: Moderately sorted, very fine-grained sandstone



Thin section:

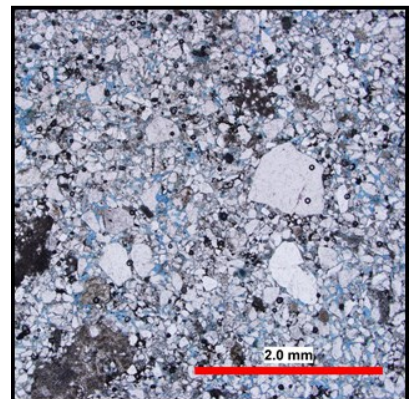
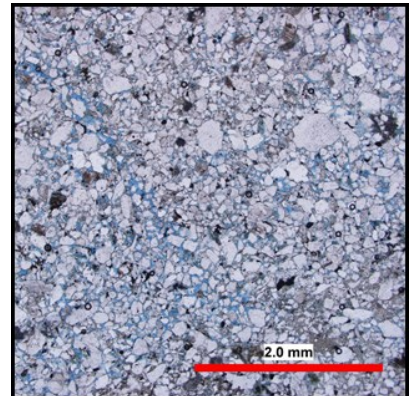
- Grain Size: silt to coarse upper sands (0.002 to 1.0 mm)
- Grain Shape: angular to rounded
- Grain Sorting: Very poor
- Grain Packing: Moderately to tightly packed
- Pore space:
 - Primary: Present (between grains and in fractures)
 - Secondary: Grain dissolution

Petrography:

- Framework Grains:
 - Quartz: 80%
 - Lithics: 10%
 - Alkali feldspar: 3%
 - Plagioclase: 5%
 - Muscovite: <1%
 - Opaques: 1%
- Matrix:
 - Calcite cement (major)
 - Silica cement (minor)
- Accessory minerals:
 - Garnet
 - Tourmaline
 - Zircon

Notes:

- Alteration of feldspar into secondary pore space



Sample: GW-305

Hand sample:

- Colour: Gray
- Grain Size: very fine to medium-grained
- Visible minerals: N/A
- Sedimentary features: Black, soft mm sized spots (possible organic material?)
- Name: Moderately sorted, very fine to medium-grained sandstone



Thin section:

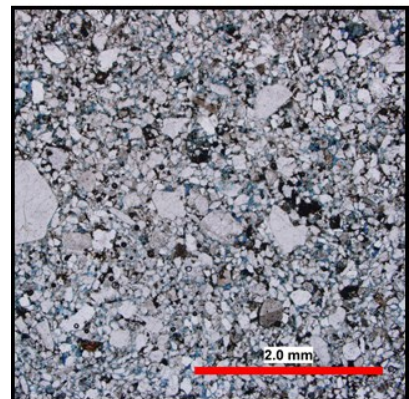
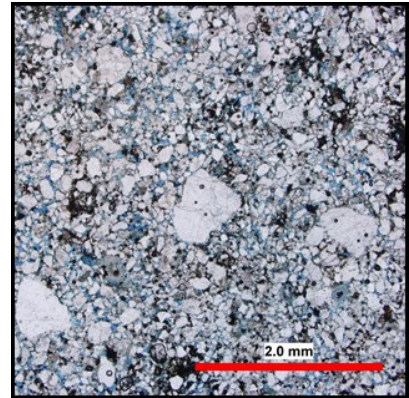
- Grain Size: silt to coarse upper sands (0.002 to 1.0 mm)
- Grain Shape: angular to rounded
- Grain Sorting: Very poor
- Grain Packing: Moderately to tightly packed
- Pore space:
 - Primary: Present
 - Secondary: Grain dissolution

Petrography:

- Framework Grains:
 - Quartz: 80%
 - Lithics: 10%
 - Alkali feldspar: 3%
 - Plagioclase: 5%
 - Opaques: 1%
 - Muscovite: <1%
- Matrix:
 - Calcite cement (patchy)
 - Iron oxide (coating detrital grains)
- Accessory minerals:
 - Garnet
 - Zircon?

Notes:

- Alteration of feldspar into secondary pore space



Sample: GW-306

Hand sample:

- Colour: Red/gray
- Grain Size: very fine-grained
- Visible minerals: N/A
- Sedimentary features: Redox spotting
- Name: Well sorted, very fine-grained sandstone



Thin section:

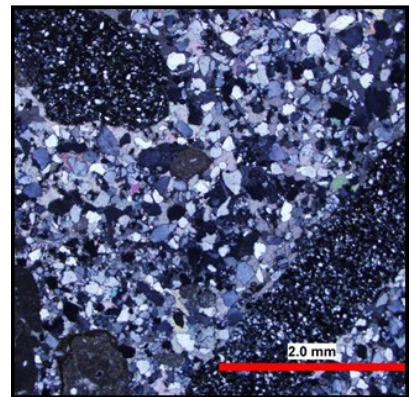
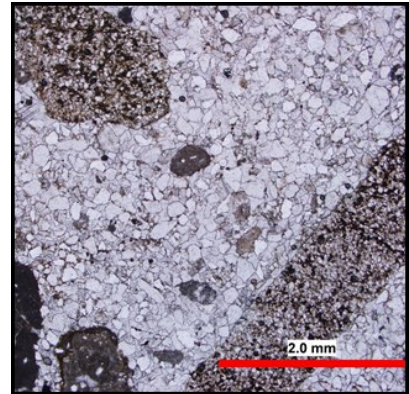
- Grain Size: silt to coarse upper sands (0.002 to 1.0 mm)
- Grain Shape: angular to rounded
- Grain Sorting: Very poor
- Grain Packing: Moderately to tightly packed
- Pore space:
 - Primary: Present
 - Secondary: Grain dissolution

Petrography:

- Framework Grains:
 - Quartz: 80%
 - Lithics: 10%
 - Alkali feldspar: ~1%
 - Plagioclase: 3%
 - Opaques: 2%
- Matrix:
 - Calcite cement
 - Iron oxide (coating detrital grains - minor)
- Accessory minerals:
 - Garnet
 - Zircon

Notes:

- Near completely cemented
- Variable size in framework grain size (lithics dominantly comprise shale and siltstone/sandstone)



Sample: GW-307

Hand sample:

- Colour: Red/gray
- Grain Size: very fine-grained
- Visible minerals: N/A
- Sedimentary features: Redox spotting
- Name: Well sorted, very fine-grained sandstone



Thin section:

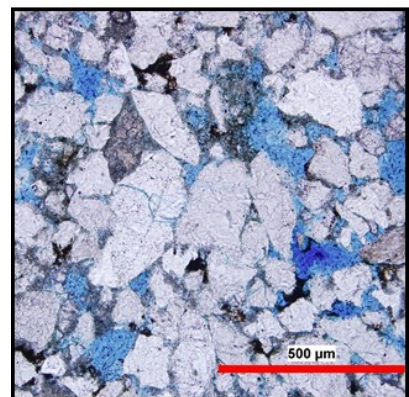
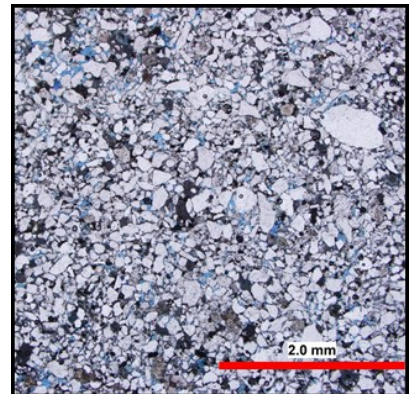
- Grain Size: very-fine lower to coarse lower (0.0625 to 0.71 mm)
- Grain Shape: angular to subrounded
- Grain Sorting: Moderate to poor
- Grain Packing: Tightly packed
- Pore space:
 - Primary: Present
 - Secondary: Intergranular, grain dissolution, microfracture of quartz

Petrography:

- Framework Grains:
 - Quartz: 85%
 - Lithics: 8%
 - Alkali feldspar: 3%
 - Plagioclase: 3%
 - Opaques: 1%
- Matrix:
 - Intragranular mix of clays
- Accessory minerals:
 - Garnet
 - Zircon

Notes:

- Few accessory minerals
- Poor porosity
- Tightly packed detrital grains



Sample: GW-308

Hand sample:

- Colour: Red-gray
- Grain Size: medium to coarse-grained
- Visible minerals: mm sized pebbles (quartzite?)
- Sedimentary features: N/A
- Name: Well sorted, medium to coarse-grained sandstone



Thin section:

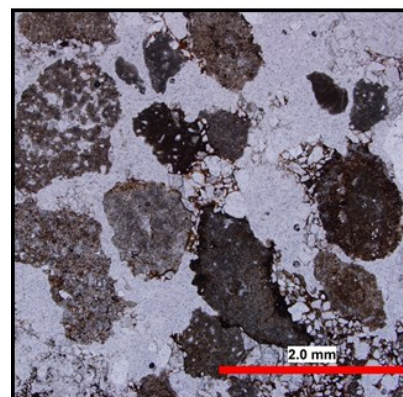
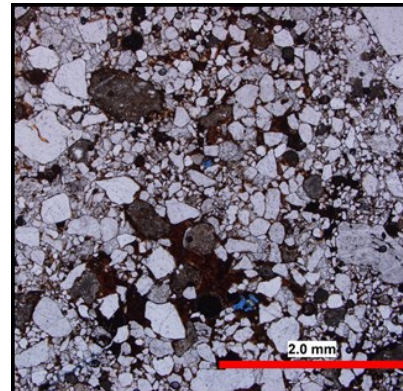
- Grain Size: Very-fine upper to very-coarse upper (0.088 to 2.0 mm)
- Grain Shape: Angular to subangular
- Grain Sorting: Poorly sorted
- Grain Packing: Tightly packed
- Pore space:
 - Primary: None
 - Secondary: Negligible (microfractures in quartz)

Petrography:

- Framework Grains:
 - Quartz: 60%
 - Lithics: 35%
 - Alkali feldspar: 2%
 - Plagioclase: 3%
- Matrix:
 - Calcite cement
 - Iron oxide (coating detrital grains)
- Accessory minerals:
 - Tourmaline
 - Zircon

Notes:

- Bimodal distribution of framework grains
 - Very-coarse upper quartz and lithics (1.41 to 2.0 mm)
 - Very-fine upper to coarse lower (0.088 to 0.71 mm)



Sample: GW-309

Hand sample:

- Colour: Red/gray
- Grain Size: very fine-grained
- Visible minerals: N/A
- Sedimentary features: Redox spotting
- Name: Well sorted, very fine-grained sandstone



Thin section:

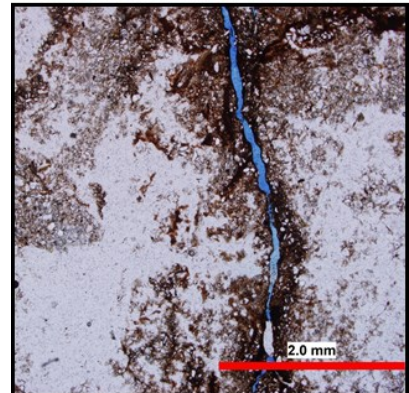
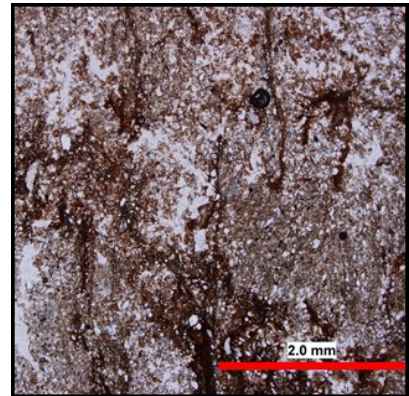
- Grain Size: Silt
- Grain Shape: Angular to subangular
- Grain Sorting: N/A
- Grain Packing: N/A
- Pore space:
 - Primary: Along fractures (negligible)
 - Secondary: Negligible

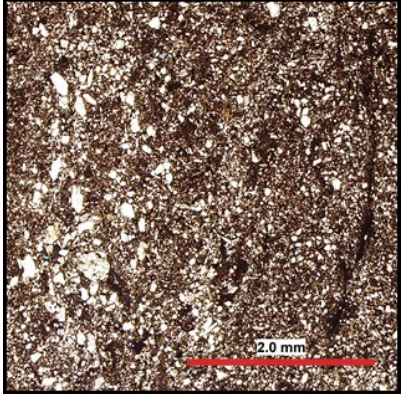
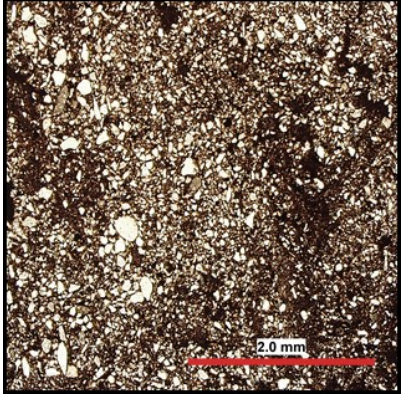
Petrography:

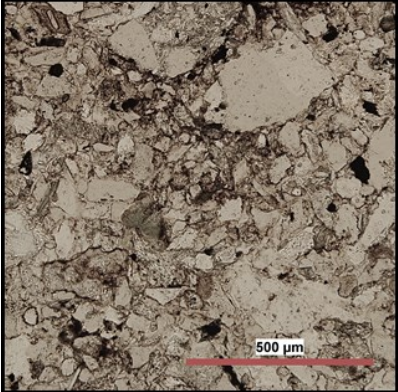
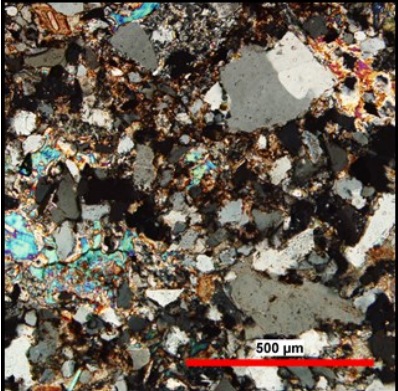
- Framework Grains: N/A
- Matrix:
 - Calcite cement
 - Iron oxide (dominant)
- Accessory minerals:
 - Zircon (0.005 to 0.01 mm)

Notes:

- Siltstone
- Clasts comprised of dominantly angular quartz grains



Sample: TSEC 427	
<p>Hand sample:</p> <ul style="list-style-type: none"> • N/A 	N/A
<p>Thin section:</p> <ul style="list-style-type: none"> • Grain Size: Silt to fine-grained • Grain Shape: angular to round • Grain Sorting: Moderate to poor • Grain Packing: Tight • Pore space: <ul style="list-style-type: none"> ○ Primary: N/A ○ Secondary: N/A <p>Petrography:</p> <ul style="list-style-type: none"> • Framework Grains: <ul style="list-style-type: none"> ○ Quartz, alkali feldspar, plagioclase • Matrix: <ul style="list-style-type: none"> ○ Clays, calcite and silica cement • Accessory minerals: N/A <p>Notes:</p> <ul style="list-style-type: none"> • Dominated by clay minerals (silts) with few detrital sand sized grains. 	 

Sample: TSEC 428	
<p>Hand sample:</p> <ul style="list-style-type: none"> • N/A 	N/A
<p>Thin section:</p> <ul style="list-style-type: none"> • Grain Size: Silt to coarse-grained • Grain Shape: Angular to round • Grain Sorting: Poor • Grain Packing: Tight • Pore space: <ul style="list-style-type: none"> ○ Primary: Negligible ○ Secondary: Negligible <p>Petrography:</p> <ul style="list-style-type: none"> • Framework Grains: <ul style="list-style-type: none"> ○ Quartz, alkali feldspar, plagioclase • Matrix: <ul style="list-style-type: none"> ○ Clays, calcite, silica, and other cement • Accessory minerals: N/A <p>Notes:</p> <ul style="list-style-type: none"> • Dominated by clay minerals (silts) with few detrital sand sized grains. 	 

Sample: TSEC 429

Hand sample:

- N/A

N/A

Thin section:

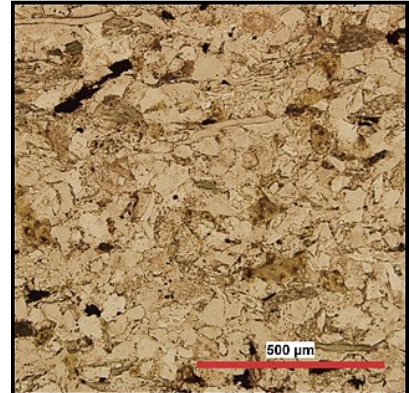
- Grain Size: Silt to fine-grained
- Grain Shape: angular to round
- Grain Sorting: Moderate to poor
- Grain Packing: Tight
- Pore space:
 - Primary: N/A
 - Secondary: N/A

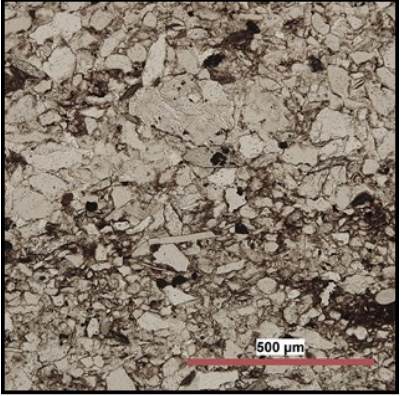
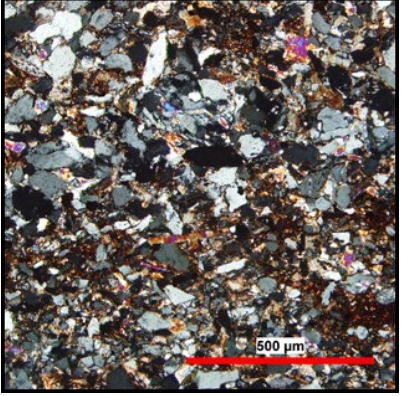
Petrography:

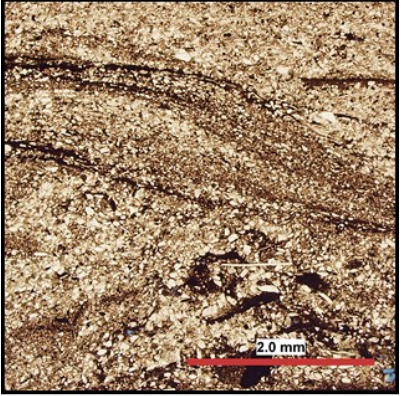
- Framework Grains:
 - Quartz, alkali feldspar, plagioclase
- Matrix:
 - Clays, calcite and silica cement
- Accessory minerals: N/A

Notes:

- Dominated by clay minerals (silts) with few detrital sand sized grains.



Sample: TSEC 430	
<p>Hand sample:</p> <ul style="list-style-type: none"> • N/A 	N/A
<p>Thin section:</p> <ul style="list-style-type: none"> • Grain Size: Silt to medium-grained • Grain Shape: Angular to round • Grain Sorting: Poor • Grain Packing: Tight • Pore space: <ul style="list-style-type: none"> ○ Primary: Negligible ○ Secondary: Negligible <p>Petrography:</p> <ul style="list-style-type: none"> • Framework Grains: <ul style="list-style-type: none"> ○ Quartz, alkali feldspar, plagioclase • Matrix: <ul style="list-style-type: none"> ○ Clays, calcite, silica, and other cement • Accessory minerals: N/A <p>Notes:</p> <ul style="list-style-type: none"> • Dominated by clay minerals (silts) with few detrital sand sized grains. 	 

Sample: TSEC 431	
<p>Hand sample:</p> <ul style="list-style-type: none"> • N/A 	N/A
<p>Thin section:</p> <ul style="list-style-type: none"> • Grain Size: Silt to fine-grained • Grain Shape: angular to round • Grain Sorting: Moderate to poor • Grain Packing: Tight • Pore space: <ul style="list-style-type: none"> ○ Primary: N/A ○ Secondary: N/A <p>Petrography:</p> <ul style="list-style-type: none"> • Framework Grains: <ul style="list-style-type: none"> ○ Quartz, alkali feldspar, plagioclase • Matrix: <ul style="list-style-type: none"> ○ Clays, calcite and silica cement • Accessory minerals: N/A <p>Notes:</p> <ul style="list-style-type: none"> • Dominated by clay minerals (silts) with few detrital sand sized grains. 	 

Appendix B

Palynological Report from Robert Fensome

Report No. M.R.G.-PAL.6-2013RAF

Palynological analysis of four grab samples from Guysborough County, onshore Chedabucto Bay

“This report has restricted internal circulation, is not reviewed and must not be cited as a publication. Reference to data or interpretations in the report may be made only with prior approval from the author of the Marine Resources Geoscience Subdivision, Geologic Survey of Canada (Atlantic), P.O. Box 1006, Dartmouth, Nova Scotia, B2Y 4A2, Tel. (902) 426-2740. If approval is granted, reference should be as a personal communication with the author.”

G.S.C. Locality No.: D-4313

Locations:

GSC sample number P41815 (GW 305) - N45.39344 W61.47403 Altitude: 8m

GSC sample number P41816 (GW 309) - N45.39354 W61.47411 Altitude: 1m

GSC sample number P41817 (GW 303) - N45.39241 W61.47584 Altitude: 5m

GSC sample number P41818 (GW 304) - N45.39241 W61.47584 Altitude: 5m

Grab samples from onshore section

Samples were collected from a red bed sequence on the shores of Chedabucto Bay in Guysborough County by Darragh O’Connor and Grant Wach, four of which were submitted for palynological analysis. The small exposures of red beds in this area have been assumed to be equivalent to the Fundy Group of the Bay of Fundy and the deeper deposits in the offshore Orpheus graben, although their age has not been confirmed to date biostratigraphically or otherwise as far as I am aware.

Sample P41815 is barren

Sample P41816 contained black kerogen fragments and probably contaminants from the modern environment of an undetermined affinity

Sample P41817 contained material of undetermined affinity that again almost certainly contamination

Sample P41818 contained contaminants (angiosperm and conifer pollen, as well as plant cuticle), but also a fungal body whose body colour suggests that it is in situ, and a single pollen grain that could be identified as *Classopollis* with reasonable confidence.

The genus *Classopollis* has a range from Triassic (Norian) to middle Cretaceous. Although this range is broad, assuming that the lithology is akin to similar strata in the Fundy Basin, this would indicate a Triassic (post-Norian) to earliest Jurassic age for sample P41818 and, by extension, the “Chedabucto Bay” red beds. These strata could thus be equivalent to the Blomidon or McCoy Brook formations of the Fundy Basin, but not to the Wolfville Formation.

16 April 2013 – Robert A Fensome

Marine Resources Geoscience Subdivision

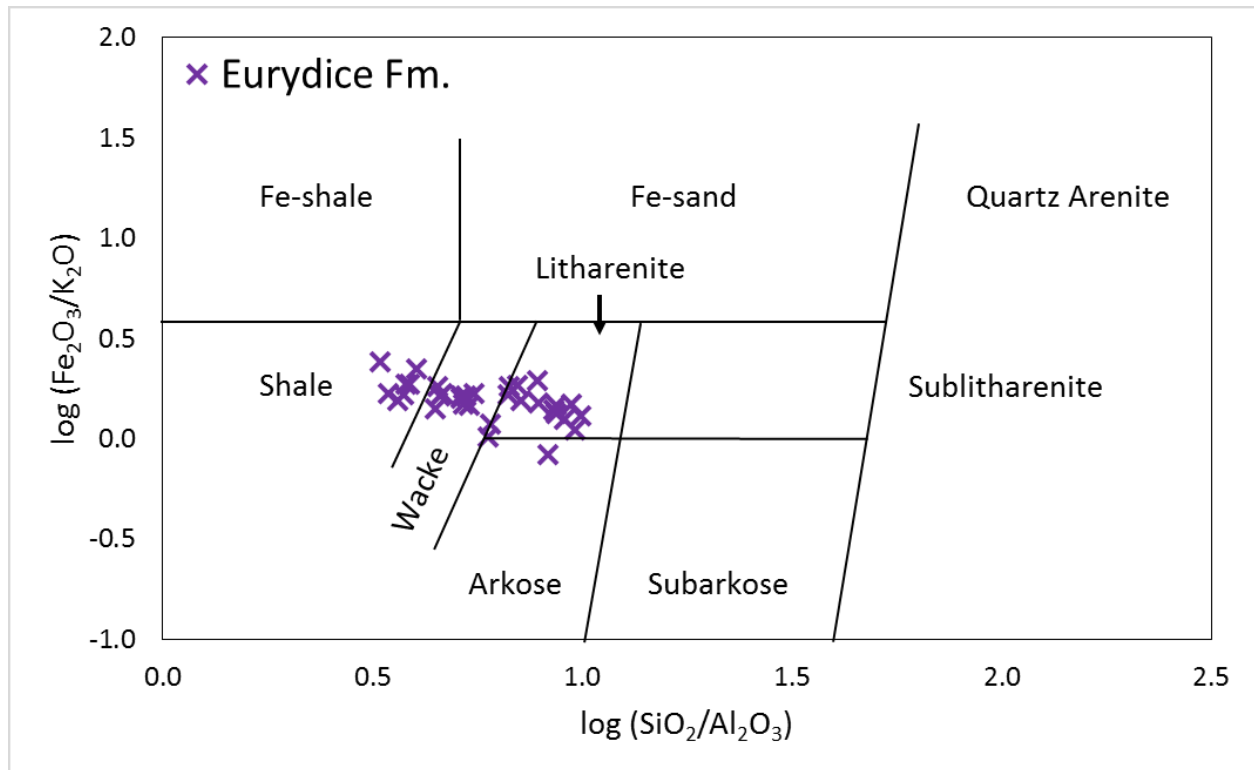
Appendix C

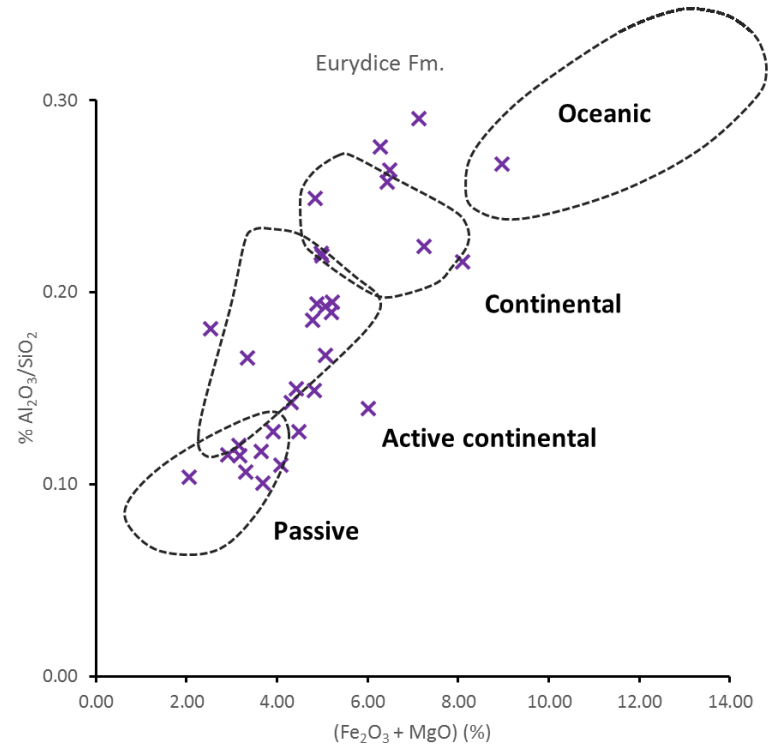
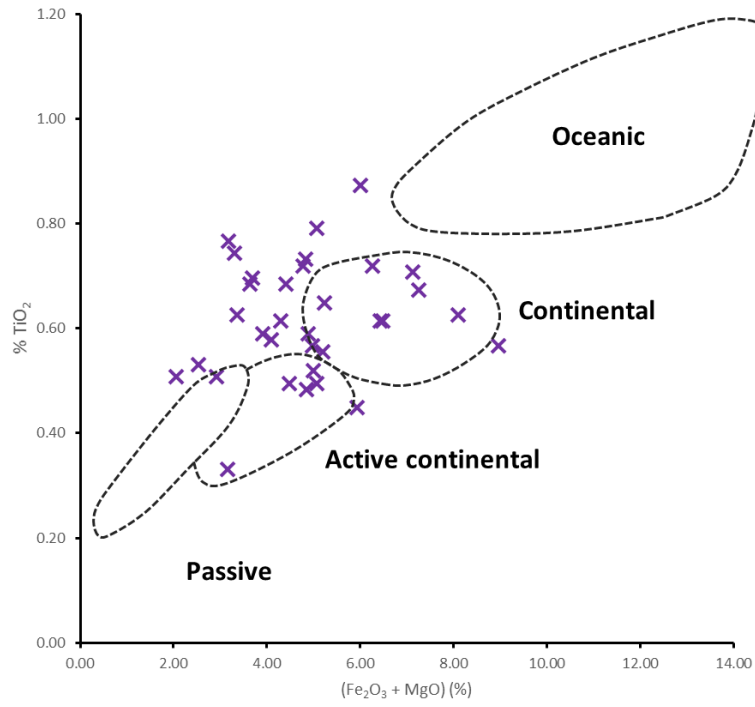
Eurydice Formation – major elemental composition and discrimination plots

Major elemental composition of sands and sandstones of the Eurydice Formation, Eurydice P-36 well from the Orpheus Graben.

		Elemental concentrations from XRF analysis of the Eurydice Formation (Eurydice P-36 well)												
Core Box:	Depth (ft):	SiO ₂	TiO ₂	Al ₂ O ₃	Fe ₂ O ₃ *	MnO	MgO	CaO	K ₂ O	P ₂ O ₅	Fe ₂ O ₃ */K ₂ O	SiO ₂ /Al ₂ O ₃	Fe ₂ O ₃ * + MgO	Al ₂ O ₃ /SiO ₂
Box #1	9698	24.85	0.61	6.56	6.49	0.13	-	1.35	3.47	-	1.87	3.79	6.49	0.26
Box #1	9698	36.96	0.55	7.01	5.20	0.18	-	1.33	3.19	-	1.63	5.27	5.20	0.19
Box #1	9701	36.55	0.71	10.62	7.12	0.12	-	0.31	4.25	-	1.68	3.44	7.12	0.29
Box #1	9701	57.62	0.50	9.64	3.57	0.07	1.50	0.35	3.49	-	1.02	5.98	5.07	0.17
Box #2	9703	73.70	0.51	7.66	2.06	0.25	-	6.39	1.86	-	1.11	9.62	2.06	0.10
Box #2	9703	63.32	0.33	7.62	1.54	0.07	1.61	9.27	1.84	-	0.84	8.30	3.16	0.12
Box #2	9704	48.49	0.73	7.22	4.82	0.26	-	3.73	2.65	-	1.82	6.71	4.82	0.15
Box #2	9704	66.45	0.77	7.64	3.18	0.37	-	6.83	2.16	0.05	1.47	8.70	3.18	0.11
Box #3	9706	70.08	0.51	8.09	2.92	0.26	-	5.61	2.18	-	1.34	8.66	2.92	0.12
Box #3	9707	38.45	0.61	5.48	4.30	0.20	-	2.88	2.33	-	1.85	7.02	4.30	0.14
Box #3	9707.5	26.77	0.61	6.89	6.43	0.12	-	0.89	3.43	-	1.87	3.88	6.43	0.26
Box #3	9707.5	25.21	0.57	5.56	4.97	0.12	-	2.25	2.73	-	1.82	4.53	4.97	0.22
Box #4	9709.4	31.50	0.57	8.41	5.30	0.11	3.66	1.84	3.19	-	1.66	3.75	8.97	0.27
Box #4	9709.4	39.90	0.72	11.00	6.27	0.13	-	1.99	4.04	-	1.55	3.63	6.27	0.28
Box #4	9713.1	30.60	0.53	5.54	2.53	0.09	-	18.59	1.50	-	1.69	5.52	2.53	0.18
Box #4	-	62.36	0.74	6.63	3.31	0.14	-	2.34	2.23	0.06	1.48	9.41	3.31	0.11
Box #5	9713.9	51.77	0.72	9.61	4.78	0.21	-	3.47	3.26	-	1.47	5.39	4.78	0.19
Box #5	-	61.09	0.63	10.12	3.35	0.26	-	5.71	2.84	0.06	1.18	6.04	3.35	0.17
-	-	53.11	0.79	10.22	5.06	0.21	-	3.22	3.41	0.04	1.49	5.20	5.06	0.19
Box #5	9715	63.02	0.87	8.79	4.42	0.18	1.59	2.90	2.85	0.08	1.55	7.17	6.01	0.14

Box #5	-	41.61	0.65	8.11	5.23	0.18	-	2.93	3.20	-	1.63	5.13	5.23	0.19
Box #6	9719	81.90	0.58	9.02	3.22	0.20	0.87	1.80	2.58	0.07	1.25	9.08	4.09	0.11
Box #6	-	76.04	0.70	7.66	2.69	0.20	1.01	3.40	2.06	0.06	1.30	9.93	3.69	0.10
Box #6	9720.8	49.31	0.59	6.28	3.92	0.12	-	0.54	2.58	-	1.52	7.86	3.92	0.13
Box #6	-	60.44	0.68	7.07	3.65	0.08	-	1.93	2.61	-	1.39	8.54	3.65	0.12
Box #7	9721	32.74	0.50	4.18	4.49	0.12	-	2.38	2.29	-	1.96	7.84	4.49	0.13
Box #7	-	34.38	0.59	6.68	4.88	0.20	-	3.04	3.08	-	1.58	5.15	4.88	0.19
Box #7	9723	12.03	0.45	3.65	5.94	0.11	-	1.35	2.45	-	2.43	3.30	5.94	0.30
Box #7	-	21.00	0.52	4.59	5.00	0.18	-	2.60	3.05	-	1.64	4.57	5.00	0.22
Box #8	9727.3	45.39	0.67	10.17	5.41	0.17	1.84	2.35	3.83	-	1.41	4.46	7.25	0.22
Box #8	9728	19.65	0.48	4.89	4.84	0.13	-	1.22	2.17	-	2.23	4.02	4.84	0.25
Box #8	9728.1	33.33	0.63	7.19	5.36	0.17	2.73	2.04	3.17	-	1.69	4.63	8.10	0.22
Box #8	9728.3	51.17	0.68	7.67	4.42	0.29	-	4.38	2.66	-	1.66	6.67	4.42	0.15





Appendix D

Core Description Analysis

Methodology – Core description analysis

Step	Description
1	<ul style="list-style-type: none">• Describe all available core and identify the lithofacies (e.g., rippled sandstone) by examining the following:<ul style="list-style-type: none">• grain size• lithology• physical sedimentary structures• biogenic sedimentary structures• all surfaces (laminam beds, bed sets, parasequences/sequences)
2	<ul style="list-style-type: none">• Group lithofacies into lithofacies associations. A lithofacies association is a repetitive group of lithofacies that occur in a vertical arrangement (e.g., burrowed siltstone, wave-rippled siltstone, and hummocky cross-bedded sandstone = lithofacies association).
3	<ul style="list-style-type: none">• Interpret depositional environments and sub-environments e.g. (1) sub-environment = lower shoreface; environment = wave dominated shoreline; (2) sub-environment = sand shoal; environment = outer estuarine.
4	<ul style="list-style-type: none">• Identify parasequence boundaries (if possible) and identify parasequence sets using the lithofacies associations.
5	<ul style="list-style-type: none">• Integrate any additional data that can be utilized to interpret depositional environments, such as well-log data, seismic data (distribution of sequences, seismic facies), paleontologic data (palynology, micro and macro fossils, environmental indicators).
6	<ul style="list-style-type: none">• Describe the vertical stacking pattern of the parasequence sets (e.g., retrogradational, progradational or aggradational), as noted in the well logs and core.
7	<ul style="list-style-type: none">• Use the parasequences and stacking patterns to develop a model of the distribution of depositional environments, thereby providing a tool to predict and interpret the distribution of source, reservoir and seal facies.

Note*

- In siliciclastic reservoirs, abrupt changes in depositional environments and reservoir properties commonly mark flooding surfaces or sequence boundaries.
- Seismic stratigraphy and 3-D seismic interpretation can be used to constrain the geometry, distribution and depositional environments of reservoir and seal facies.

Methods – Clastic Core

Described by noting:

- surfaces
- grain size
- lithology
- sedimentary structures
- trace fossils
- depositional environments
- fractures and/or micro faults
- oil staining
- diagenesis
- potential sequences and parasequences

Grant Wach
2012